PONTIFICIA UNIVERSIDAD CATÓLICA DE CHILE
SCHOOL OF ENGINEERING

PHOTOPRODUCTION OF HYDROGEN USING NANOPARTICLES OF TITANIUM DIOXIDE

FELIPE JOSÉ VARAS CONCHA

Thesis submitted to the Office of Research and Graduate Studies in partial fulfillment of the requirements for the Degree of Doctor of Science in Engineering

Supervisor:
CÉSAR ANTONIO SÁEZ NAVARRETE

Santiago de Chile, April 2018

PONTIFICIA UNIVERSIDAD CATÓLICA DE CHILE
SCHOOL OF ENGINEERING

PHOTOPRODUCTION OF HYDROGEN USING NANOPARTICLES OF TITANIUM DIOXIDE

FELIPE JOSÉ VARAS CONCHA

Members of the Committee:

CÉSAR SÁEZ

BLANCA ANTÍZAR

RODRIGO ESCOBAR

VÍCTOR FUENZALIDA

LEANDRO HERRERA

MAURICIO ISAACS A

JUAN DE DIOS ORTÚZAR

Thesis submitted to the Office of Research and Graduate Studies in partial fulfillment of the requirements for the Degree of Doctor of Science in Engineering

Santiago de Chile, April 2018

To my beloved parents…

ACKNOWLEDGEMENT

I want to thank my family for their support. To my parents Marfilda and Mariano, for being an example of sacrifice, effort and good-hearted people. To Mariana, Ignacio and María Jesús for understanding my long absences meanwhile I was following this goal.

To César, my supervisor, for sharing his expertise in research, for his support when I choose this non-traditional topic, and for showing me that it is possible to be a good person in the competitive academic world. To all my friends from Sáez' Lab: Germán and Cristián, my μalgae friends; Catalina, my H_2-partner; Leonardo, the leader and road-opener friend; and especially to my friend and doctoral partner, Sebastián, who was my company, technical opinion and fun in this very demanding PhD experience.

To Prof. Isaacs, who guided me in the world of nanoscience, for opening his lab to this engineer entering into a chemist's world. To Diego, my nanoworld mate, for all his help, patience and friendship. To the whole MAIC lab team, especially to Quezada, Jessica, Esteban and Natalia for their help and nice moments.

Thanks to Kipus from U. Talca, especially to Carlos, boss and friend, for giving me a parallel R+D route to follow, and for helping me finish this process. To Rachael and the Academic Writting Center, for their support in using correct English in my writing.

Finally, thanks to CONICYT for its financial support via a doctoral grant, number 21100026. This would not be possible without its important role.

CONTENTS INDEX

TABLE OF FIGURES

TABLE OF TABLES

ABSTRACT

The current global energy scenario has led scientists to look for more sustainable fuels. Hydrogen is an option, but it implies big challenges like changing the current dominant fossil fuel based production system. In this context, hydrogen production via photocatalytic routes is an interesting option. However, the reported yields have been disappointingly low, so it is crucial to focus research on improving these processes.

This doctoral thesis seeks to identify the operational conditions with highest effect on the production of hydrogen and valuable by-products via photoreforming of alcohols using TiO_2 nanoparticles, among five factors and their interactions: presence of gold as a co-catalyst, type of alcohol, intensity of light, concentration of alcohol and concentration of nanoparticles. Special focus was given to exploring the influence of these factors in a low range of catalyst concentrations. TiO_2-Au nanoparticles synthesized via sol-gel method were fully characterized (UV-Vis, SEM-EDS, ICP-AES, DLS, TEM). Hydrogen, formaldehyde and formic acid were produced. The presence of gold as a co-catalyst, the intensity of UV light and their interaction showed the highest effect. The best configuration allowed reaching a catalyst productivity of 2,900 $\mu mol \cdot g^{-1} \cdot h^{-1}$.

Keywords: Photocatalysis • Hydrogen • Photo-reforming of organic compounds • Titanium dioxide nanoparticles • Gold nanoparticles • Formaldehyde • Formic acid

RESUMEN

El actual escenario energético mundial ha llevado a los científicos a buscar combustibles más sustentables. El hidrógeno destaca como alternativa, pero implica grandes desafíos como el cambio del actual sistema de producción a partir de combustibles fósiles. La producción de hidrógeno vía fotocatálisis destaca como opción, pero los rendimientos reportados han sido bajos, siendo crucial enfocar esfuerzos en mejorar estos procesos. Esta tesis doctoral busca identificar las condiciones operacionales con mayor efecto en la producción de hidrógeno y de subproductos valiosos, a través del fotorreformado de alcoholes utilizando nanopartículas de TiO_2, entre cinco condiciones y sus interacciones: presencia de oro como cocatalizador, tipo de alcohol, intensidad de la luz, concentración de alcohol y concentración de nanopartículas. Se prestó especial atención a explorar la influencia de estos factores en un rango de bajas concentraciones de catalizador. Las nanopartículas de TiO_2-Au sintetizadas mediante un método sol-gel fueron completamente caracterizadas (UV-Vis, SEM-EDS, ICP-AES, DLS, TEM). Se logró generar H_2, CH_2O y CH_2O_2. La presencia de oro como cocatalizador, la intensidad de la luz UV y su interacción fueron los factores de mayor peso. La mejor configuración permitió alcanzar una productividad de catalizador de 2,900 $\mu mol \cdot g^{-1} \cdot h^{-1}$.

Palabras clave: Fotocatálisis • Hidrógeno • Fotorreformado de compuestos orgánicos • Nanopartículas de dióxido de titanio • Nanopartículas de oro • Formaldehído • Ácido fórmico

1 CONCEPTUAL FRAMEWORK

1.1 Problematic and selected approach

1.1.1 Energy needs and hydrogen as an option

Humanity faces a huge challenge: to deal with and fight climate change. Even when there is not total agreement about its origin, the scientific community considers greenhouse gases (GHG) accumulation as the main cause behind this phenomenon, especially those with anthropogenic source, linked to the use of fossil fuels.

The problem is complex considering that: 81% of the world's primary energy matrix is based on fossil fuels (IEA, 2017a), 65% of anthropogenic GHG emissions come from energy consumption (Stern, 2006), and the strong signs of a growing oil shortage (IEA, 2017b).

In this scenario, hydrogen has a relevant role as a sustainable fuel with several positive features, such as its high energy content per mass unit (IEA, 2007) (141,850 $kJ \cdot kg^{-1}$ H_2 gas, standard), and its clean usage, which just generates water as by-product. These virtues make hydrogen an interesting choice in the technology road to a more sustainable society.

However, the current scenario does not have the necessary conditions for massive production of hydrogen for energy purposes: 96% worldwide hydrogen production is based on fossil fuels (IEA, 2007); almost 100% of global production is used as raw material for the petrochemical industry (C. A. Grimes, Varghese, & Ranjan, 2008); the

current electrolytic hydrogen costs twice as much as the cost goal of 2-3 USD kg^{-1}, which does not make it competitive (Turner et al., 2008); its productive chain has important technological barriers; it requires a profound technological and social transformation, and a renewal of the existing infrastructure.

Despite all these challenges, leading countries have developed a roadmap to make hydrogen a competitive fuel against traditional the fossil fuels (IEA, 2015; US DOE, 2002). In this plan, the development of production technologies is crucial, and it is required to expand the understanding of the phenomena involved in hydrogen generation. So, experimental and mechanistic studies are key factors in this route to a sustainable hydrogen based system.

1.1.2 Technologies for hydrogen production

Hydrogen production technologies can be classified according to the raw material used in the process: fossil fuels, water or biomass (Balat, 2008; IEA, 2006; Turner et al., 2008). Among the technologies based on fossil hydrocarbons, methane steam reforming (SMR) is the dominant technology, followed by partial oxidation (POX), autothermal reforming (ATR) and coal gasification. However, they have high carbon, water and energy footprints. In the case of biomass, thermochemical and biological processes are used. This is the least mature technology and is mostly at laboratory level. Water-based methods are considered a more sustainable option, but electrolysis is the only industrial-scale technology commercially available. Other systems under development with good

projections are the thermochemical cycles and those that use solar energy such as photoelectrolysis and photocatalysis.

There are currently many challenges in the development of technologies for the production of hydrogen. The efficiency of production plants must be improved and the capital costs reduced. In processes based on fossil fuels and biomass, the main limitation is related to its CO_2 emissions and the intensive use of energy (Balat, 2008; Brentner, Peccia, & Zimmerman, 2010; Janusz Nowotny & Veziroglu, 2011). In the case of electrolytic processes, the problem is the high cost of electricity and the intensive use of energy (Zeng & Zhang, 2010). Biological processes and those that use solar energy must face various challenges before being able to scale-up, due to their low production rates and low efficiencies (Dincer & Acar, 2015; H.-S. Lee, Vermaas, & Rittmann, 2010).

1.1.3 Hydrogen production by photocatalysis using nanosized semiconductors

Water-splitting, the generation of hydrogen using solar energy based on water as raw material and semiconductive catalysts has become the Holy Grail process (Serpone et al., 2016). Therefore, many researchers have focused their efforts on photocatalysis using particulate systems, becoming one of the most promising energy solutions in the near future. This method relies on the photoelectric effect, which was discovered in the 70s by Fujishima and Honda (Fujishima & Honda, 1972). When a semiconductor suspended in water is excited by light, the electrons of its valence band receive enough energy to overcome its band gap and pass to the conduction band, generating electron-hole (e^-/h^+)

pairs, also called charge carriers. Therefore, the photogenerated holes oxidize water molecules in the surface forming O_2, and the electrons reduce protons to H_2, without changing the semiconductor composition (Osterloh & Parkinson, 2011). Unfortunately, although this method may seem technically simple, it involves a complex reaction where inverse reactions are involved, and usually good photocatalysts for H_2 production are good catalysts for their recombination too (Osterloh & Parkinson, 2011).

An alternative approach for solar hydrogen generation is photoreforming of aqueous solutions containing oxygenated organic compounds. Photoreforming could be viewed as an intermediate process between photocatalytic water splitting and photooxidation. Compared to pure water splitting, photocatalytic reforming has emerged as a more efficient light-promoted hydrogen production. Kawai and Sakata first achieved photocatalytic hydrogen production from a liquid mixture of methanol and water in 1980 (Kawai & Sakata, 1980). It has been reported that the oxygenated organic compounds such as hole scavengers are capable of reacting with the photogenerated holes to inhibit charge carrier recombination and preventing oxygen production to suppress the back-reaction between H_2 and O_2, in turn enhancing H_2 production (Carraro et al., 2014; Chao Wang et al., 2017). Photoreforming can even be a sustainable method, and many biomass-derived compounds as renewable sources have been proposed for photoreforming hydrogen production (Gallo et al., 2012; Puga, 2016; Chao Wang et al., 2017).

The advances in nanosized materials have contributed to the technological development of applications in photocatalysis. It is more effective to work at nanometric scale, increasing

the photoefficiency of the systems where the transfer of charges is the limiting step (S. Gupta & Tripathi, 2011), because in small sized particles, the charge carriers are always near the surface, where the reactions take place (Osterloh & Parkinson, 2011).

1.1.4 Photocatalysts: Titanium dioxide

The photocatalysis is generally defined as the catalysis of a photochemical reaction on a solid surface, usually a semiconductor. There must be at least two reactions occurring at the same time in a balanced way: oxidation and reduction. If such a balance does not exist its composition would change, and one of the basic requirements of any catalyst would not be fulfilled (Fujishima, Zhang, & Tryk, 2008).

The basic criterion for defining a good photocatalyst to produce H_2 is to have an appropriate band gap, where the lowest energy level of the conduction band, also called LUMO (lowest unoccupied molecular orbital), must be more negative than the redox potential for H^+/H_2 (-0.41 V), and that the highest energy level of the valence band, also called HOMO (highest occupied molecular orbital), should be more positive than the redox potential for the oxidation reaction. In case of water-splitting, it should be more positive than O_2/H_2O (+0.82 V) (Kudo, 2007). Moreover, an ideal semiconductor should be simple to produce and use, cost-effective, photostable, harmless for the health of people and the environment, respond to sunlight, and be able to catalyze the reaction effectively (Carp, Huisman, & Reller, 2004; S. Gupta & Tripathi, 2011). However, most photocatalysts have limitations. For example, Ge, GaAs, PbS and CdS are not stable

enough for catalysis in aqueous media, suffering photocorrosion and in some cases presenting toxicity; ZnO dissolves in water; and Fe_2O_3, SnO_2 and WO_3 have incompatible conduction bands with H_2 generation (Fujishima et al., 2008; S. Gupta & Tripathi, 2011).

Titanium dioxide (TiO_2) stands out for several reasons: its 3.2 eV gap satisfies the basic requirement in relation to the redox potentials; it is photostable in aqueous environments; it is not toxic; its holes are strongly oxidizing and selective; and it is more abundant than other photosensitive materials; and it has a high refractive index resulting in an efficient dispersion of diffuse light through the pores of the material (S. Gupta & Tripathi, 2011; J. Nowotny, Bak, Nowotny, & Sheppard, 2007).

In spite of the mentioned virtues, the production rates of H_2 and the solar-to-hydrogen conversion efficiencies are still modest, due to mainly three reasons: i) the rapid recombination of its charge carriers; ii) the rapid reverse reaction of recombination of H_2 and O_2; and iii) that it only can capture UV light photons (4% of solar energy, while visible light represents 50%) (Ni, Leung, Leung, & Sumathy, 2007).

1.1.5 Improvement techniques and factors affecting H_2 production

The main problem affecting hydrogen productivity is that the time scale of the different reaction steps in photocatalytic hydrogen production is very different. The photoinduced generation of an electron-hole couple occurs in femtoseconds, meanwhile their recombination in 10–100 ns. Reduction reactions mediated by the excited electrons need a longer time, in the range of ms, whereas the oxidative reaction carried out by holes takes

ca. 100 ns. Therefore, electrons need to be preserved for a longer time by trapping them into a metal where they can migrate, or by making holes react with a suitable hole scavenger, also called electron donor or sacrificial agent (Hoffmann, Martin, Choi, & Bahnemann, 1995; Melo & Silva, 2011; Rossetti, 2012). This second technique is the reason behind the better results in photoreforming than water-splitting.

Regarding the metal deposition on the semiconductor surface, the Schottky barrier (B. Gupta, Melvin, Matthews, Dash, & Tyagi, 2016; Rajeshwar, Chenthamarakshan, Ming, & Sun, 2002) formed at the interface between metal and semiconductor can serve as an electron trap, increasing the lifetime of charge carriers and enhancing the efficiency of the photocatalytic reaction. The metal also serves as an active site to reduce protons to H_2 (Rossetti, 2012).

Other modification techniques are the ion-doping to reduce the band gap of the semiconductor and expand the captured spectrum of light, and the use of sensitizing dyes, which have the ability of injecting more electrons to the conduction band of the semiconductor.

Besides the already mentioned techniques, researchers have shown interest in how different factors affect hydrogen production. Most of them are operational conditions like concentration and type of electron donors, concentration and type of nanoparticles, geometry and size of nanoparticles, wavelength and intensity of light, among others.

However, most of these studies analyze the effect of these factors independently, skipping the possible joint effect when several of them interact.

1.2 Contribution of this research

Based on the necessity to develop new sources of clean energy and that we must move towards H_2 production methods that are neither dependent on fossil fuels nor intensive in energy use, this research seeks to contribute to the a better understanding of the effects of several operational conditions on the H_2 production via photoreforming of alcohols using TiO_2 and TiO_2-Au nanoparticles.

Many studies in this field provide valuable information about the effect of an isolated factor on hydrogen production, but as is typical in nanosized applications, there exists a long list of factors affecting it, with very different experimental conditions too. This makes it very difficult to compare the impact of different factors and identify which is the best route to higher productivities and higher efficiencies.

In this scenario, this work provides an evaluation and quantification of the combined effects of five factors on hydrogen production and its by-products, formaldehyde and formic acid, in particulate systems:

- The presence of gold as a co-catalyst
- The type of alcohol to be photoreformed
- The intensity of UV-light supplied to the photoreactor
- The concentration of alcohol

- The concentration of nanoparticles

Based on these analyses, statistical models are proposed for hydrogen, formaldehyde and formic acid production and their catalyst productivities estimations. This tool can help to estimate these responses when a change in these five factors is made.

As a secondary contribution, this work explores the photo-reforming of alcohols in a range of nanoparticle concentrations never reported before (below 0.1 $g \cdot L^{-1}$) under high levels of UV-light intensity (above 10 $mW \cdot cm^{-2}$), providing valuable experimental data, which could be used for validation of different theorical models and for comparing with isolated factors analyses.

1.3 Hypothesis and objectives

The hypothesis:

> Adding gold nanoparticles over the surface of titanium dioxide nanoparticles is the main factor affecting the production of hydrogen and by-products in the photoreforming of alcohol processes. The magnitude of this effect can be affected by the combined influence of changes in operational conditions, such as type of alcohol, intensity of light, concentration of alcohol and concentration of nanoparticles.

The general objective is:

To identify the operational conditions with the highest effect on the production of hydrogen and by-products via photoreforming of alcohols using TiO_2 nanoparticles among five factors and their interactions: presence of gold as a co-catalyst, type of alcohol, intensity of light, concentration of alcohol and concentration of nanoparticles.

The specific objectives are to:

1) synthesize and characterize nanoparticles of TiO_2 modified with gold as a co-catalyst.
2) produce hydrogen via photoreforming of alcohols using the synthesized TiO_2-Au nanoparticles.
3) quantify and prioritize the main and interaction effects of the selected operational conditions on the hydrogen production, on its catalyst productivity, and its alcohol productivity.
4) propose and validate a statistical model to predict the hydrogen production and its catalyst productivity.
5) quantify and prioritize the main and interaction effects of the selected operational conditions on the production of valuable by-products – formaldehyde and formic acid – and its catalyst productivity.
6) propose and validate a statistical model to predict the formaldehyde and formic acid production, and their catalyst productivities.

1.4 Outline of the thesis

This thesis is organized in six chapters. They contribute as follows:

- Chapter 1 is titled “CONCEPTUAL FRAMEWORK”, it presents the problematic and motivations behind this work, a brief status of art, the proposed hypothesis and objectives, and the general methodology used to achieve the objectives.
- Chapter 2 presents the article “Hydrogen productivity analysis using low concentration of TiO_2-Au nanoparticles on a UV-LED based photocatalytic reactor”. It covers the synthesis and full characterization of the nanomaterial and evaluates the feasibility of hydrogen production via photoreforming. It contributes to the achievement of the specific objectives 1) and 2).
- Chapter 3 presents the article “Operational conditions affecting hydrogen production via photo-reforming of organic compounds using TiO2-Au nanoparticles”. It is the main chapter of this work, directly related to the hypothesis verification. It contributes to the achievement of the specific objectives 3) and 4).
- Chapter 4 presents the article “Operational conditions affecting formaldehyde and formic acid formation as by-products of hydrogen production via photoreforming of methanol”. It analyzes four factors affecting the production of intermediaries. It contributes to the achievement of the specific objectives 5) and 6).
- Chapter 5 shows the Conclusions of doctoral work.
- Chapter 6 presents the Bibliography used in this document.

1.5 General methodology

The methodology used in this research consists of three analytical stages and six experimental stages. They follow the sequence showed by the diagram in Figure 1.

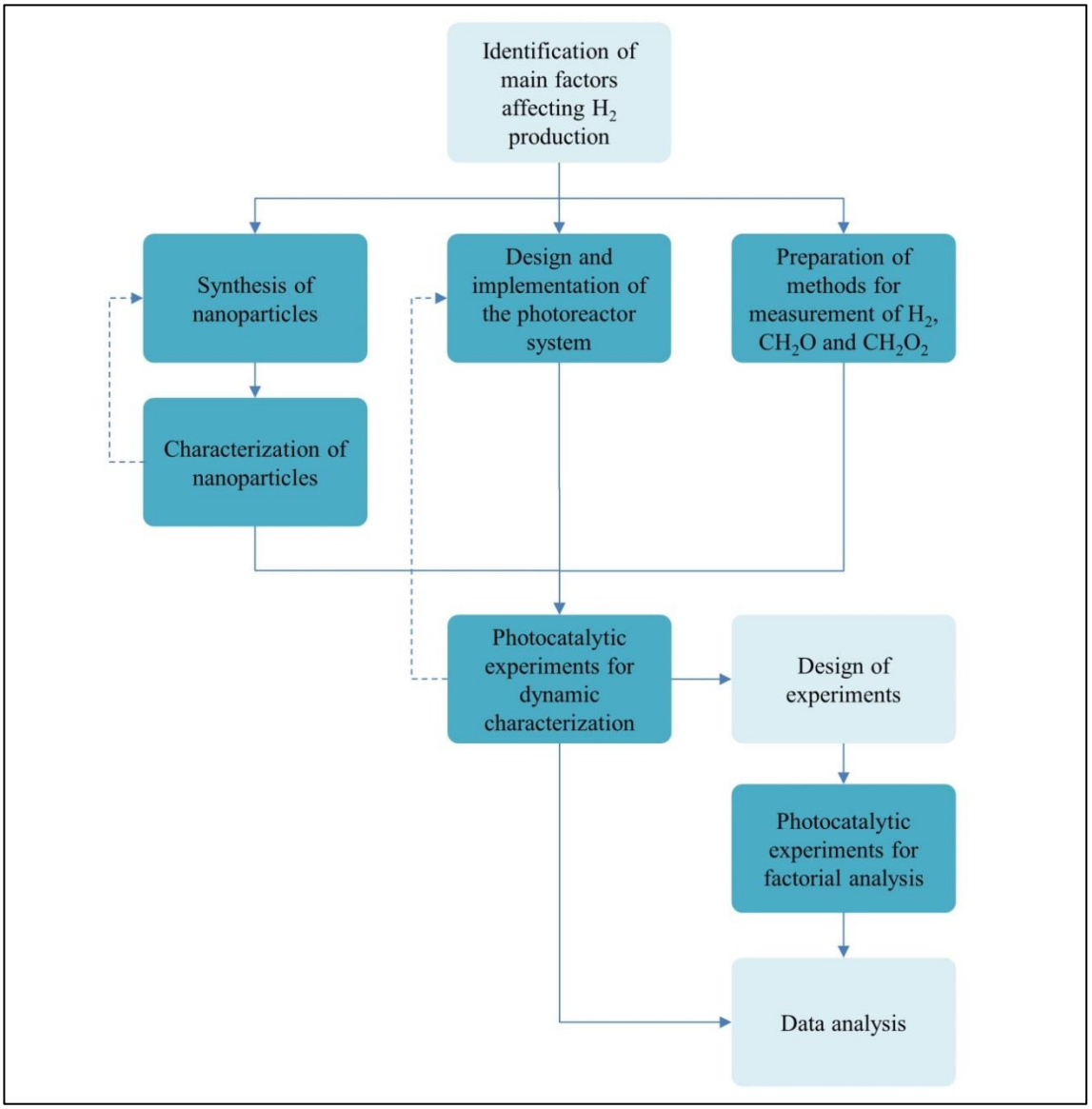

Figure 1. Flowchart with the general methodology. Blue: experimental stage; light blue: analytical stage.

The stages are briefly described as follows:

- Identification of main factors: the first stage considered a bibliographic review to identify the main factors affecting hydrogen production in photocatalytic processes, and a further selection of controllable factors to include in the study.
- Synthesis: commercial P25 TiO_2 nanoparticles were modified with gold using a sol-gel approach described in detail in section 2.2.3. The method was adjusted iteratively until gold deposition and nanometric scale were reached.
- Characterization: the resultant particles were analyzed by several techniques described in section 2.3.
    - UV-Vis spectroscopy to obtain the characteristic absorbance spectrum of the nanomaterial modified by gold.
    - Scanning electron microscopy + electron dispersive spectroscopy (SEM-EDS) to obtain the proportion of gold in the composite nanomaterial via elemental analysis.
    - Inductively coupled plasma - atomic emission spectrometry (ICP-AES) to verify the proportion of gold via elemental analysis.
    - Dynamic light scattering (DLS) to obtain the particle size distribution of the nanomaterial.
    - Transmission electron microscopy (TEM) to obtain nanoscale images of the nanomaterial.

  - Image processing analysis using software ImageJ (Rasband, n.d.) to obtain the particle size distribution of the gold nanoparticles over the titania surface.

- Design and implementation of the photoreactor system: the fourth stage was to design the experimental set-up for photocatalytic reactions. Batch photoreactors were selected as the particulate system; located within an environment with temperature control at known atmospheric pressure. They were illuminated by UV-LED lamps (375 nm) at known intensities. More details in sections 2.2.2.
- Preparation of methods for measurement of main products: Hydrogen production was measured using gas chromatography (GC) and a U-tube manometer to follow in time the changes of gas pressure in the headspace of the reactor. A calibration curve was prepared for H_2 production by GC and reported colourimetric methods were selected to measure the formaldehyde and formic acid production. Details about these methods are presented in sections 2.2.5 and 4.2.6.
- Photocatalytic experiments for characterization of the reaction dynamic: Photocatalytic hydrogen production was confirmed and monitored during 6 hour experiments. This stage considered evaluation of kinetic rates, productivities and efficiencies. More details in sections 2.2.4 and 2.3.6.
- Design of experiments (DOE) for factorial analysis: a half-fraction factorial completely randomized experimental design was selected to configure a set of possible combinations of factors to evaluate their influence on the hydrogen,

formaldehyde and formic acid production. Every factor had two levels (high and low) and the selection of factor's levels was based on literature review. More details in sections 3.2.4 and 4.2.4. Level selection and chosen combinations of factors are presented in sections 3.3.2 and 4.3.2.

- Photocatalytic experiments for factorial analysis: based on the set-up resulting from the previous stage, selected experimental combinations were run under UV illumination for 11 hours. After that, the main products were quantified. Summary of results are shown in sections 3.3.2 and 4.3.2.
- Data analysis: data analysis of the experimental results was made via statistical analyses such as linear regression, analysis of variance (ANOVA) and the specific DOE package of Minitab 17®.

2 HYDROGEN PRODUCTIVITY ANALYSIS USING LOW CONCENTRATION OF TiO_2-Au NANOPARTICLES ON A UV-LED BASED PHOTOCATALYTIC REACTOR

2.1 Introduction

The current global energy scenario has led the scientific community to look for more sustainable fuels as an attempt to decrease the anthropogenic CO_2 emissions. Hydrogen has a relevant role in this task, but it implies big challenges. One of these tasks is to develop a sustainable production system, from the current fossil fuel based system which dominates the world's hydrogen production. 95% (Balat, 2008) of hydrogen production is mainly based on gas steam reforming, oil reforming and coal gasification (Dincer & Acar, 2015).

The photocatalytic hydrogen production via semiconductor nanoparticles that use sunlight as an energy source is an interesting option. Literature reports in this field are focused on the synthesis, characterization of properties and testing of nanomaterials able to photocatalyze the degradation of pollutants (Bansal, Chaudhary, & Mehta, 2015; Ling et al., 2015; Majidnia & Idris, 2015; Saud et al., 2015), water splitting reaction (Ahmad, Kamarudin, Minggu, & Kassim, 2015; Ortega Méndez et al., 2014; Rosseler et al., 2010) or photo reforming reaction (Daskalaki & Kondarides, 2009; Gunlazuardi & Dewi, 2014; Ni, Leung, & Leung, 2007; Oros-Ruiz, Zanella, López, Hernández-Gordillo, & Gómez, 2013), but information about catalyst performance in a very low range of concentrations

($< 0.1\ g \cdot L^{-1}$) is scarce, which is a relevant factor to reduce costs in future real applications for hydrogen photo-production.

Among the photocatalysts, the most studied material is titanium dioxide (Bowker et al., 2014; Clarizia et al., 2014; B. Gupta et al., 2016; S. Gupta & Tripathi, 2011; Jose, Sorensen, Rayalu, Shrestha, & Klabunde, 2013; Linsebigler, Lu, & Yates, 1995; Y. Wang, He, Lai, & Fan, 2014) thanks to its availability, corrosion resistance, non-toxicity, low price, high photoactivity and stability (Taboada, Angurell, & Llorca, 2014a), however its photocatalytic activity is limited to the ultraviolet region (B. Gupta et al., 2016). Catalytic properties of titania are improved using sacrificial agents or modification techniques. Organic species, like alcohols (Al-Azri et al., 2015; D'Elia et al., 2011; Dosado, Chen, Chan, Sun-Waterhouse, & Waterhouse, 2015; Taboada, Angurell, & Llorca, 2014b) and glycerol (Chang, Huang, Chen, Chu, & Hsu, 2015; Fujita, Kawamori, Honda, Yoshida, & Arai, 2016; Lyubina, Markovskaya, Kozlova, & Parmon, 2013; Sadanandam, Lalitha, Kumari, Shankar, & Subrahmanyam, 2013), are typical sacrificial agents to be used as electron donors or hole scavengers. Between the usual modification techniques to improve the photocatalytic process, three of them stand out: combination with metals (Pt (Beltram, Romero-Ocaña, Josè Delgado Jaen, Montini, & Fornasiero, 2015; Jung et al., 2015; Lu et al., 2015), Pd (Gomathisankar, Yamamoto, Katsumata, Suzuki, & Kaneco, 2013; X. Liu, Zhao, Domen, & Takanabe, 2014; H. Yan et al., 2009), Cu (Clarizia et al., 2014; Gomathisankar, Hachisuka, et al., 2013; Jung et al., 2015), Ni (Balcerski, Ryu, & Hoffmann, 2015; Xiying Li, Wang, Chu, Li, & Mao, 2014; Melián et al., 2014; Y. Xu &

Xu, 2015), Rh (Gomathisankar, Hachisuka, et al., 2013; D. Wang et al., 2015; F. Zhang, Maeda, Takata, Hisatomi, & Domen, 2012), Ag (Ansari, Khan, Ansari, & Cho, 2015; S. Yang et al., 2016), Au (Al-Azri et al., 2015; Jovic, Chen, et al., 2013; Ortega Méndez et al., 2014; Sinatra et al., 2015), etc.), combination with other semiconductors (Cu oxides (J. Chen et al., 2014; Sinatra et al., 2015; Q. Wang et al., 2013), Ni oxides (Melián et al., 2014; Y. Xu & Xu, 2015), ZnO (Bel Hadjltaief, Ben Zina, Galvez, & Da Costa, 2016; Nsib, Naffati, Rayes, Moussa, & Houas, 2015; Roy, Lingampalli, Saha, & Rao, 2015), WO_3 (Bai et al., 2015; Lam, Sin, Abdullah, & Mohamed, 2015; Chao Wang et al., 2015)), and cation or anion doping (Fujita et al., 2016; R. Liu, Yoshida, Fujita, & Arai, 2014).

In recent years, gold nanoparticles have received great attention as co-catalysts due to their effectiveness in degrading and mineralizing organic compounds (Ayati et al., 2014) .They are comparatively cheaper than platinum, and their inherent plasmonic oscillation makes them photoactive in the visible region (B. Gupta et al., 2016). The gold loading, after deposition on semiconductor surfaces, exhibits movement of the Fermi level towards a more negative direction, which is a key factor for increasing the Schottky barrier effect or efficiency of charge-transfer, which in turn suppresses the e^--h^+ recombination (B. Gupta et al., 2016; Rajeshwar et al., 2002).

In addition to the materials, a non-energy intensive synthesis method is necessary to project real size applications of this process. Considering the low rates of hydrogen production in these kinds of processes, compared with mature technologies, the use of atmospheric pressure and room temperature to modify titania nanoparticles is relevant for

increasing the chance of economic feasibility and a positive net energy balance. Several methods are reported to synthesize gold supported catalysts. Some of them are impregnation, coprecipitation, deposition–precipitation, deposition–reduction, hydrothermal, photodeposition, gas phase grafting, solid grinding, physical vapor deposition, and cathodic arc plasma deposition (B. Gupta et al., 2016; Takei et al., 2012). Between this range of options, a conventional sol-gel chemistry approach was used, which was reported for antimicrobial coatings and surface-enhanced Raman scattering (SERS) tags (Fu, Vary, & Lin, 2005; W. Li, Guo, & Zhang, 2010a). This method stands out due to its low energy requirements, as opposed to methods with heat treatments, such as impregnation or hydrothermal treatments, high vacuum requirements, gas phase grafting or methods involving electrical demands, such as cathodic arc plasma deposition or sonochemical reduction (Mizukoshi et al., 2007; Takei et al., 2012).

In this context, the goal of this study is to prepare and characterize TiO_2 particles partially coated with gold nanoparticles synthesized with a conventional sol-gel method under mild conditions to explore the active mechanism of hydrogen photo-production via photo-reforming of organic compounds and the catalyst productivity using a low concentration of nanoparticles in a methanol-water solution. Elemental composition, agglomeration status, and shape and size analyses are reported. The photocatalytic experiments use a batch experimental setup with 375 nm UV-light supplied by a low-consumption LED light based system, which can deliver seven times the UV intensity of light supplied by the sun (considering 1 sun = 100 $mW \cdot cm^{-2}$ and 3% of the sun radiation on the UV range

(Chowdhury, Gomaa, & Ray, 2011)) to increase the performance of particles synthesized at routine level. Photocatalytic experiments under visible light irradiation from cold-white LED lights with different amounts of gold are also given for comparing and analyzing the active mechanism.

2.2 Experimental

2.2.1 Reagents

For TiO_2-Au synthesis, Aeroxide® P25 Titanium(IV) oxide nanopowder (TiO_2, 80% anatase, 20% rutile, Sigma Aldrich^{TM}), gold(III) chloride hydrate ($HAuCl_4 \cdot 3H_2O$, Sigma Aldrich^{TM}), sodium borohydride ($NaBH_4$, Merck^{TM}), and tri-sodium citrate dehydrate ($C_6H_5Na_3O_7 \cdot 2H_2O$, Merck^{TM}) were used as received without further purification. Hydrochloric acid fuming 37% for analysis (Merck^{TM}) was used in a solution 0.1 N. Also, for photocatalytic reactions, methanol (CH_3OH, Merck^{TM}, analytical grade ACS, ISO, Reag. Ph Eur) was used without further purification.

2.2.2 Instruments

Composites were characterized using an UV-VIS photodiode array spectrophotometer Shimadzu, model MultiSpec-1501. Particle size distribution was measured using dynamic light scattering (DLS) analysis on a Malvern Zetasizer Nano ZS instrument. Microscopic images were obtained using a Philips Tecnai 12 Biotwin transmission electron microscope (TEM). Elemental analysis was done using a LEO 1420VP scanning electron microscope

(SEM) with an electron dispersive spectroscopy (EDS) detector. The inductively coupled plasma - atomic emission spectrometry (ICP-AES) was made using a Varian Liberty Series II Axial. Image processing for determination of gold particle size distribution and morphological analysis was carried out using software ImageJ (Rasband, n.d.). The statistical analyses were conducted using software Minitab^{TM} 17. Radiation measurements were developed using a PCE Instruments UVA-UVB radiation sensor, model PCE-UV34 and a StellarNet Miniature UV-VIS Spectrometer, model Black Comet Super Range Concave Grating Series.

The photocatalytic reactor system was implemented within an incubator (Shin Saeng, model SBOD-201) as a controlled temperature chamber. The system is based on: two 50 mL Erlenmeyer flasks (total volume 68 mL) with GL18 screw caps with hole and septum of silicone as batch reactors; a humidity, temperature and barometric pressure USB datalogger Extech, RHT50; four 50 W UV-LED lights of 375 nm, Justar, model JX-50UV10X5G, each one with aluminum heatsink, fan of 12 V for cooling and a LED driver; and four 3 W cold-white LED lights, model JDRE27 (emission spectrums in Figure - S 1 in annex I).

Determination of hydrogen was made using a gas chromatograph DANI, model Master GC, equipped with a fused silica capillary column with molecular sieve of 5 A° Supelco, model Mol Sieve 5A PLOT, and a micro-volume thermal conductivity detector VICI, model TCD-NIFED-220DI. Evolution in real time of hydrogen concentration was calculated using a USB thermocouple datalogger Pico Technology, model TC-08, with

two type K thermocouples, and a U-tube manometer (Range 250-0-250 mm H_2O, resolution 1 mm H_2O) with water as fluid.

2.2.3 Synthesis method

An adjusted method for synthesizing TiO_2-Au nanoparticles was used, proposed by Fu (Fu et al., 2005) and Li (W. Li et al., 2010a). It is based on the chemical reduction of $[AuCl_4]^-$ over TiO_2 surface using $NaBH_4$ as a reducing agent. It works at room temperature and pressure. First, 100 mL of 0.2 mM TiO_2 and 0.2 mM $HAuCl_4$ colloidal suspension was prepared. $HAuCl_4$ works as a gold precursor giving $[AuCl_4]^-$ ions to the solution. After 5 minutes of an ultrasonic bath to avoid agglomeration, pH of the reaction media was adjusted to 2.2 by dropwise addition of 0.1 M HCl solution, to obtain a negative electric charge on the surface of TiO_2 particles. After 5 more minutes of the ultrasonic bath, 1 mL of a 25 mM sodium citrate solution was added to the colloidal suspension in a round-bottom flask. After stirring for 5 minutes, 3 mL of 25 mM citrate and 0.1 M $NaBH_4$ solution were added, showing a change of color from white to purple, and thus the reduced Au^0 over the TiO_2 particles surface was obtained, with a pH 4.5. After stirring for 10 minutes, the TiO_2-Au obtained was analyzed to check if the expected UV-vis spectroscopy pattern (Jovic, Chen, et al., 2013; W. Li et al., 2010a) was obtained. Finally, after 5 minutes of the ultrasonic bath, the colloidal suspension was stored in darkness at 4°C.

The described procedure leads to composites with TiO_2:Au molar ratio 1:1. The full procedure was repeated to obtain nanoparticles in a molar ratio 20:1, increasing the amount of TiO_2, keeping the amount of gold constant.

2.2.4 Photocatalytic experiments

The experimental unit was integrated by two batch reactors partially covered with aluminum foil with two 11 cm^2 square windows. Both were filled with 63 mL of 1.2 M methanol-water solution, with a 4 mL headspace filled with argon gas at barometric pressure of 950 kPa (see Figure 2-left).

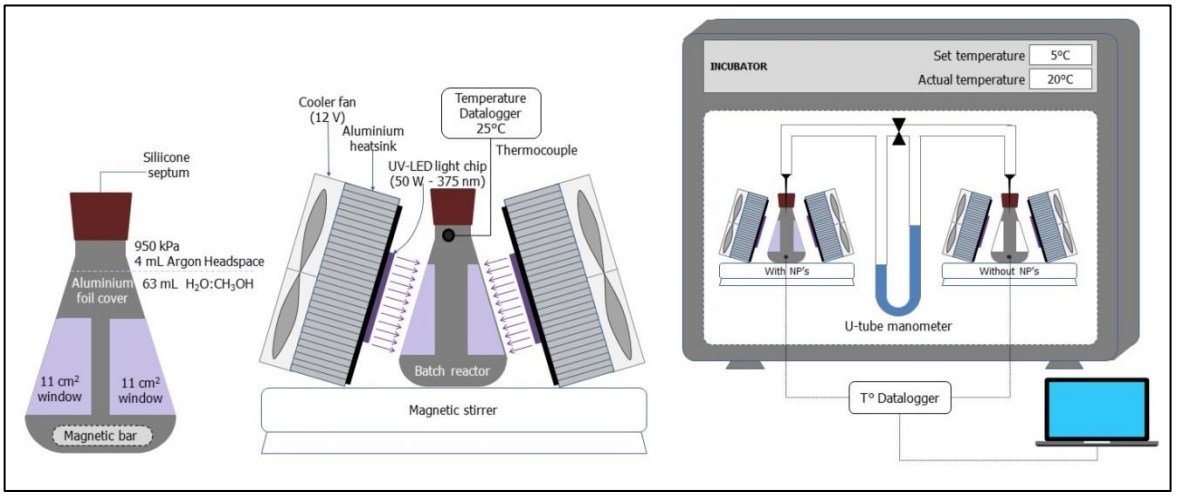

Figure 2. Experimental setup for hydrogen generation: (left) batch reactor; (center) UV-LED setting; (right) system configuration within the incubator

One of the reactors had a concentration of nanoparticles of 0.056 $g \cdot L^{-1}$ and the second one did not have nanoparticles to catalyze the reaction. Both reactors were illuminated with

two 375 nm UV-LED lights focusing on the windows, parallel to their surfaces, receiving an intensity of light of 20 $mW \cdot cm^{-2}$ ($3.78 \cdot 10^{16}$ $photons \cdot s^{-1} \cdot cm^{-2}$) during 6 hours under slow stirring (see Figure 2-center). The headspaces on both reactors were connected by a glass manifold with a U-tube manometer to measure the differential pressure produced by the generated gases on the reactor with nanoparticles, which under these conditions, is proportional to the gas concentration. The manifold also had a by-pass valve in the middle to set the same initial pressure on both reactors (see Figure 2-right). The experiment was performed within the incubator with a temperature set at 5°C to increase the radiation delivered by the UV-LED lamps. The heat released by the lamps raised the temperature of the chamber to 20°C, and the temperature of the reactors to an average of 25°C. Intensity of light was regulated by the distance between the surface and the LED lamp.

After 6 hours of reaction, the final hydrogen concentration was measured using gas chromatography in triplicate of 250 µL from the headspace of each reactor using the method described in next section. Evolution in real time of hydrogen concentration was calculated based on temperature and differential pressure.

The same procedure was repeated using cold-white visible light, just changing the light source, keeping the intensity of light constantly at 20 $mW \cdot cm^{-2}$.

2.2.5 Measurement of hydrogen

A gas chromatographic method was developed for determining the amount of hydrogen gas using argon as a carrier gas. It consists in: oven temperature at 40°C, isotherm during

13 minutes, injector temperature at 40°C, thermal conductivity detector at 60°C, column flow at 1 mL/min constant during 12 minutes, and 1 minute at 50 mL/min. The calibration curve is given by Equation 1.

$$n_{H_2} = 0.001576\ A_{GC} + 0.5460 \qquad \text{Equation 1}$$

Where n_{H2} is the amount of moles of hydrogen gas in μmol and A_{GC} is the area of the first peak obtained in the chromatogram, which appears at a retention time of 8.6 min. This method also allows the measurement of O_2, N_2 and CO. The concentration of H_2 gas in the headspace of the photocatalytic reactor is obtained dividing n_{H2} by the volume of the syringe used for sampling; in this case, 250 μL.

2.3 Results & discussion

2.3.1 Synthesis

Gold ions (Au^{3+}) can be deposited over the surface of TiO_2 particles by anionic adsorption. The amphoteric nature of TiO_2 allows changing its surface electric charge with the change of pH value. This method uses acidic pH (2.2) under the TiO_2 isoelectronic point (IEP), pH=6.0 (Zanella et al., 2002), as TiO_2 surface becomes positively charged (with $TiOH_2^+$ as main surface species). The positive charges over the TiO_2 induce the adsorption of $[AuCl_4]^-$ anions. When the reducing agent is added ($NaBH_4$), Au^{3+} from $[AuCl_4]^-$ anions is reduced to Au^0 over the TiO_2 (Gómez-de Pedro, Puyol, Izquierdo, Salinas, & Alonso, n.d.). The reaction is shown in Equation 2 and Equation 3.

Equation 2

$$TiO_2 + HAuCl_4 \rightarrow TiO_2\text{-}[AuCl_4]^- + H^+$$

Equation 3

$$TiO_2\text{-}[AuCl_4]^- + 4NaBH_4 + 12H_2O \rightarrow TiO_2\text{-}Au + 4NaCl + 4B(OH)_3 + 29H^+$$

2.3.2 UV-Vis Absorption spectroscopy

Figure 3 shows the absorption spectra for TiO_2 and TiO_2-Au composites synthesized using two different molar ratios for [TiO_2]:[Au]. Bare TiO_2 did not show peaks at visible light region, unlike Au nanoparticles which presented a peak at 540 nm (W. Li, Guo, & Zhang, 2010b). After reduction of gold ions over the TiO_2 surface, the TiO_2-Au absorption spectrum presented a peak at 530 nm. Composites with a higher proportion of gold nanoparticles showed a higher peak and higher maximum peak wavelength. This is explained by the size of the gold nanoparticles and its influence on the surface plasmon resonance effect (SPR).

As the size of gold nanoparticles increased, the maximum peak wavelength and its intensity also increased (Hong & Li, 2013), which agrees with the reported conclusion that the maximum peak wavelength red-shifts as the relative particle size increased (Cyrankiewicz, Wybranowski, & Kruszewski, 2007). The size of the gold nanoparticles is presented in the section about image processing analysis. These spectra are consistent with reported information in studies based in similar synthesis methods (Fu et al., 2005; W. Li et al., 2010b), being a first confirmation of metallic gold coating.

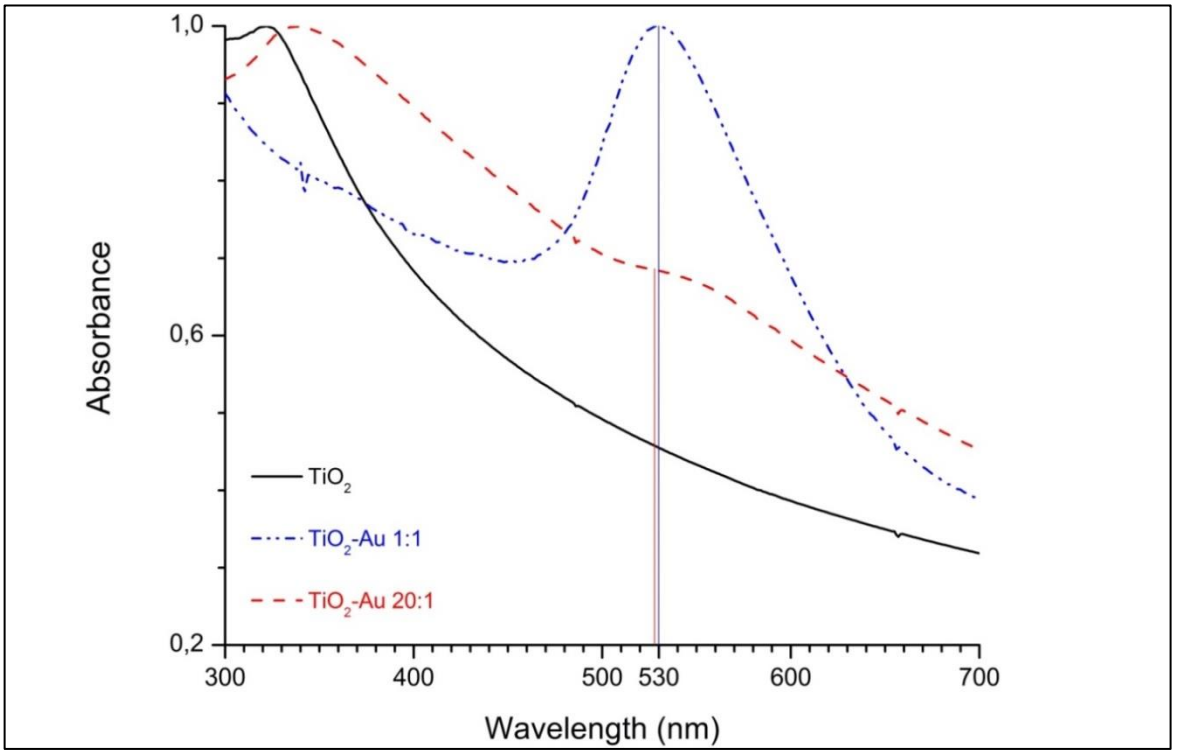

Figure 3. Normalized UV-visible absorption spectra of TiO_2, TiO_2-Au synthesized using molar ratio 1:1 ([TiO_2]=0.2 mM), and TiO_2-Au synthesized using molar ratio 20:1 ([TiO_2]=4 mM)

2.3.3 Elemental analysis via EDS and ICP-AES

Figure 4 shows the EDS spectra for a sample of TiO_2-Au synthesized in a molar ratio 20:1, ratifying the presence of Ti (46.54%wt), O (47.02%wt) and Au (6.45%wt). The results show that the measured content of Au was half the nominal value (12.3%wt) calculated with the quantities used during the synthesis. ICP-AES analysis indicates that in particles 20:1, 9.1%wt of the total mass is gold and 90.9%wt is TiO_2. For particles 1:1 69.5%wt is gold and 30.5%wt is TiO_2.

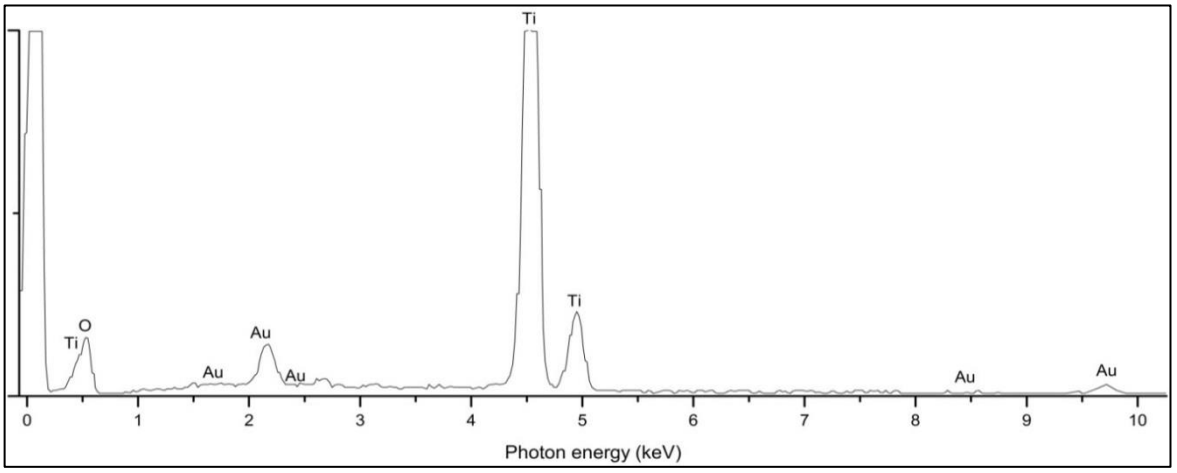

Figure 4. EDS spectra of TiO_2-Au 20:1, confirming presence of Ti, O and Au.

2.3.4 Particle size distribution of the aggregates by DLS analysis

Figure 5 shows the particle size distribution (as a function of the radius) from a DLS analysis on TiO_2-Au aggregates synthesized using two different molar ratios and pH values.

Results show that particle size of agglomerates increased with the amount of gold and pH. This supports the reported evidence which affirms that agglomerate size increases both with ionic strength and as the pH of the solution approached the IEP (H. H. Liu, Surawanvijit, Rallo, Orkoulas, & Cohen, 2011). This is because pH alters the colloidal stability of the nanoparticle system by modulating the protonation/deprotonation equilibrium and further altering the electrostatic repulsion (Dunphy Guzman, Finnegan, & Banfield, 2006; French et al., 2009; Zhou et al., 2013). For composites synthesized using a molar ratio 20:1, the peak in the particle size distribution shifted from 46 nm to 110 nm

when pH changed from 2.2 to 4.5, closer to the IEP of TiO_2. Synthesis using a lower molar ratio of 1:1 resulted in bigger agglomerates, with a peak at 71 nm when pH was 2.2, which shifted to 142 nm when pH was 4.5. Higher pH also increased the variability on the radius of agglomerates in a factor by 2.5, from 439 nm when pH was 2.2, to 1081 nm when pH was 4.5.

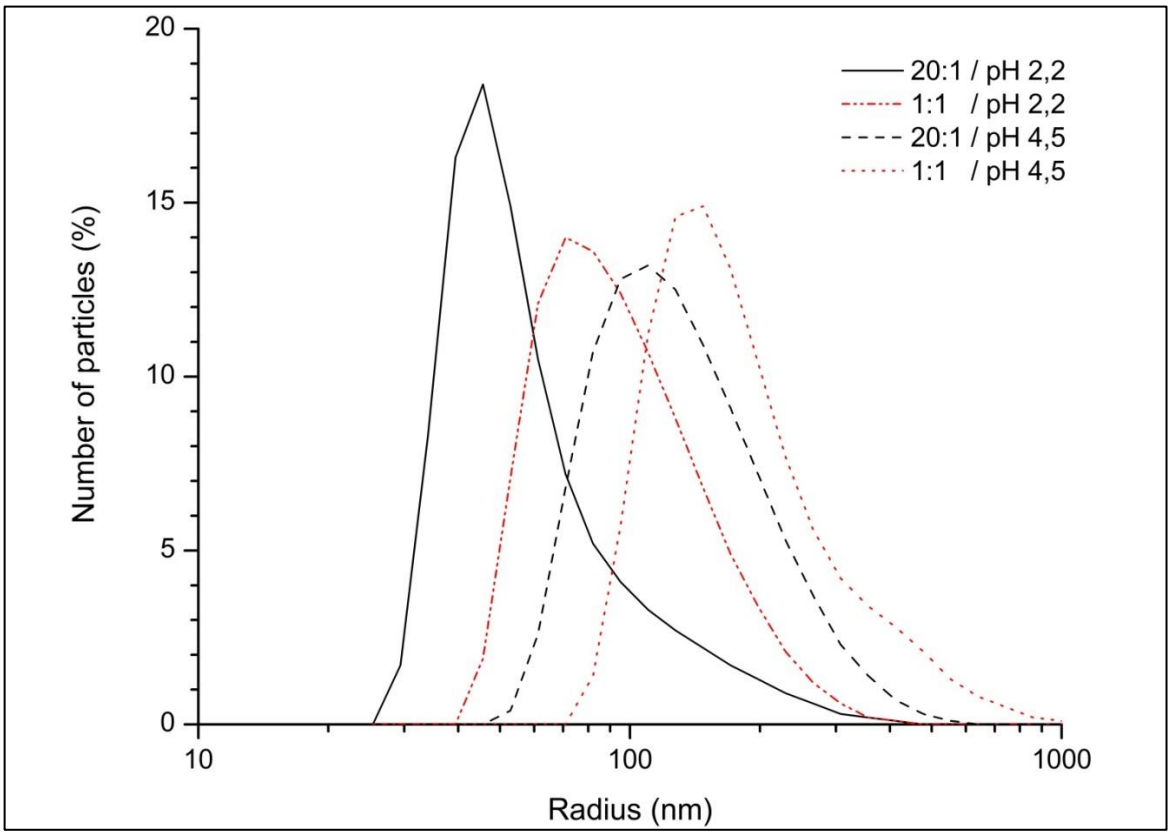

Figure 5. Particle size (radius) distribution results from DLS analysis for TiO_2-Au aggregates synthesized with molar ratios 20:1 and 1:1, with synthesis pH level adjusted to 2.2 and 4.5

2.3.5 Aggregates and gold coating characterization using TEM and image processing analysis

The TEM images in Figure 6 show TiO_2-Au aggregates synthesized using [TiO_2]:[Au] molar ratios 1:1 (left) and 20:1 (center) at pH 2.2 during the synthesis. It also shows an agglomerate of bare TiO_2 (right). The images highlight the gold nanoparticles detected by ImageJ, which can be recognized by a smaller and more rounded shape than bare TiO_2. Since particles are irregular, particle size is represented by the Feret's diameter, the longest distance between any two points along the selection boundary, also known as maximum caliper (Ferreira & Rasband, 2012). The aggregate using 20:1 molar ratio has a Feret's diameter of 175 nm and the one using 1:1 molar ratio, 362 nm, both within the range of values shown in Figure 5. In both cases, the shape analysis shows low circularity near 25% (1.0 indicates a perfect circle; 0.0 indicates an increasingly elongated shape), medium solidity around 80%, and high aspect ratio, highest in the case of 1:1 synthesis. Specific values of these descriptors are presented in Table 1. Image processing analysis showed similar TiO_2 area covered by gold nanoparticles, both around 14%. It is important to highlight that ImageJ gives an area that represents the projection of the three-dimensional particle over a plane, serving as an approximation to the actual percentage of surface covered by the gold particles.

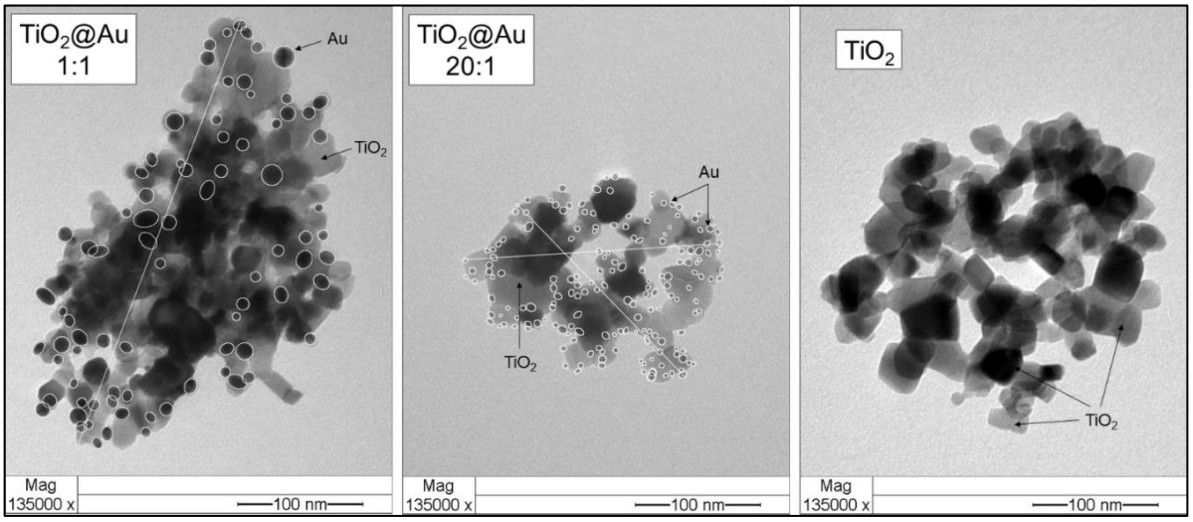

Figure 6. TEM images for agglomerates TiO_2-Au synthetized using a molar ratio [TiO_2]:[Au] 1:1 and 20:1, analyzed with ImageJ, and an agglomerate of bare TiO_2

Table 1. Size, area, and shape descriptors from image processing analysis

pH	2.2	
Molar ratio	20:1	1:1
Size and area descriptors		
Aggregate Feret's diameter (nm)	175	362
Equivalent spherical diameter (nm)	275	252
Total area (nm^2)	14,088	49,993
Area used by gold	13.2%	14.6%
Shape descriptors		
Circularity	0.285	0.253
Aspect ratio	1.38	1.71
Solidity	0.817	0.803

The images show a big difference between the sizes of gold particles deposited over the TiO_2 when different molar ratios are used in the synthesis method; when lower molar ratio was used, there were bigger nanoparticles and less dispersion over TiO_2 surface. Image processing analysis allowed dimensioning a sample of 180 nanoparticles in image type 20:1 and 280 nanoparticles in image type 1:1 to address a statistical analysis. The results are summarized on the histograms in Figure 7 and Table 2. The chart shows the particle size distribution for gold nanoparticles on the surface of TiO_2 with normal distribution in both cases, centered on mean values 3.9 nm and 11.5 nm, respectively. The statistical significance of this 7.6 nm of difference was corroborated by applying an independent 2 samples t-test with a 95% confidence level.

The fact that higher molar ratios resulted in smaller gold particles is consistent with earlier results from characterizations of gold coated TiO_2 where authors used the same gold precursor, varying the molar ratio, but in a different synthesis method (Iliev, Tomova, Bilyarska, & Tyuliev, 2007; Jovic, Chen, et al., 2013), or even using a different core material (Lkhagvadulam, Kim, Yoon, & Shim, 2013).

Also, in relation to the spreading of sizes in both distributions, it is clear that 20:1 synthesis ends in a much more homogeneous particle size than the 1:1 synthesis, which can be observed in the standard deviation ($\sigma_{1:1}$ = 4.0 nm ; $\sigma_{20:1}$ = 1.0 nm). The kurtosis near 0 is consistent with the normality of both distributions, and the not too flat, not too sharp peaks, and the positive but near to zero skewness, agree with the almost symmetrical shape of distributions.

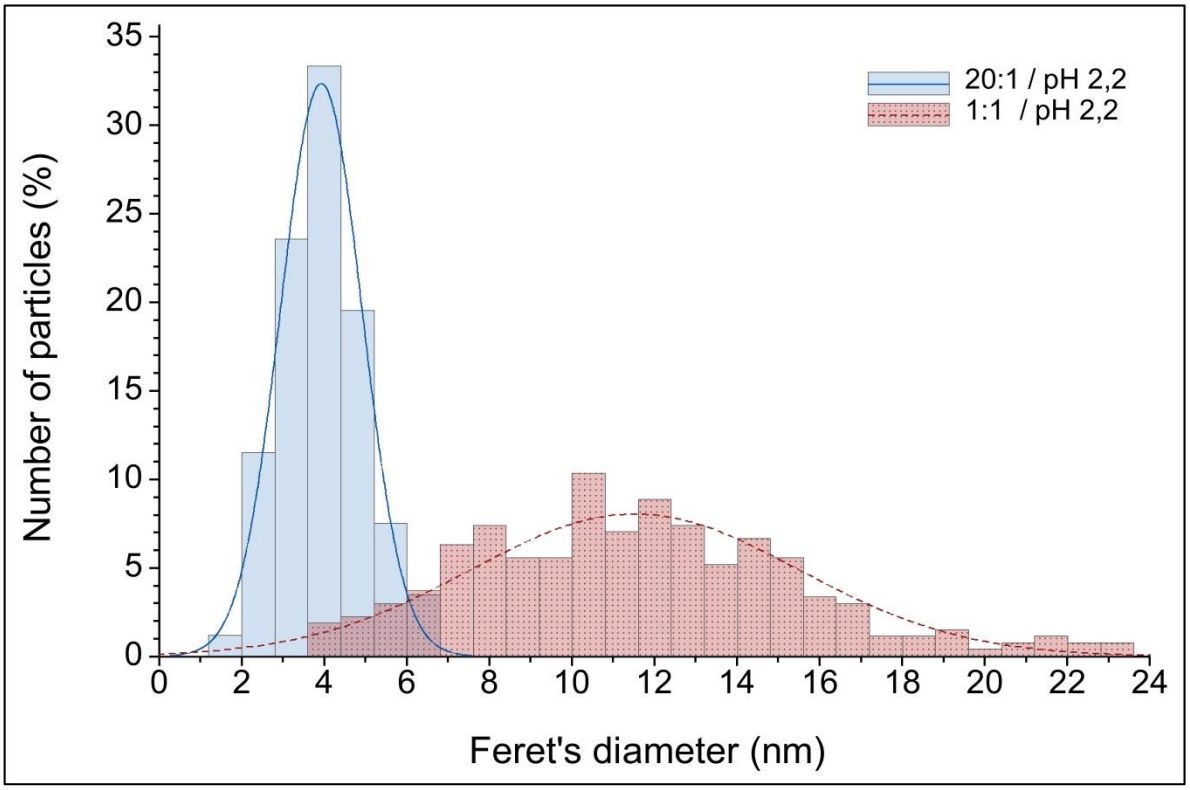

Figure 7. Particle size distribution for gold nanoparticles on the surface of TiO_2-Au synthesized using molar ratios 20:1 and 1:1, with fitted curves for normal distribution centered on 3.9 nm and 11.5, respectively.

Table 2. Measures of central tendency and dispersion for particle size distributions (Feret's diameter) of gold nanoparticles from ImageJ analysis.

Molar ratio	20:1	1:1		20:1	1:1
Mode/peak (nm)	3.8	10.4	Coefficient of variation (%)	25%	34%
Mean (nm)	3.9	11.5	Skewness	0.3	0.5
Median (nm)	3.9	11.3	Kurtosis	0	0.15
Standard deviation (nm)	1.0	4.0	Range (nm)	4.7 (1.9-6.6)	19.2 (3.7-22.9)

2.3.6 Photocatalytic hydrogen production

TiO_2-Au aggregates obtained with 20:1 and 1:1 molar ratios were tested in photocatalytic experiments (described in Figure 2) during 6 hours, by triplicate, under UV light and then under cold-white visible light. The H_2 generation profile is shown in Figure 8 with a linear fitting through linear regression and a ±95% confidence prediction band.

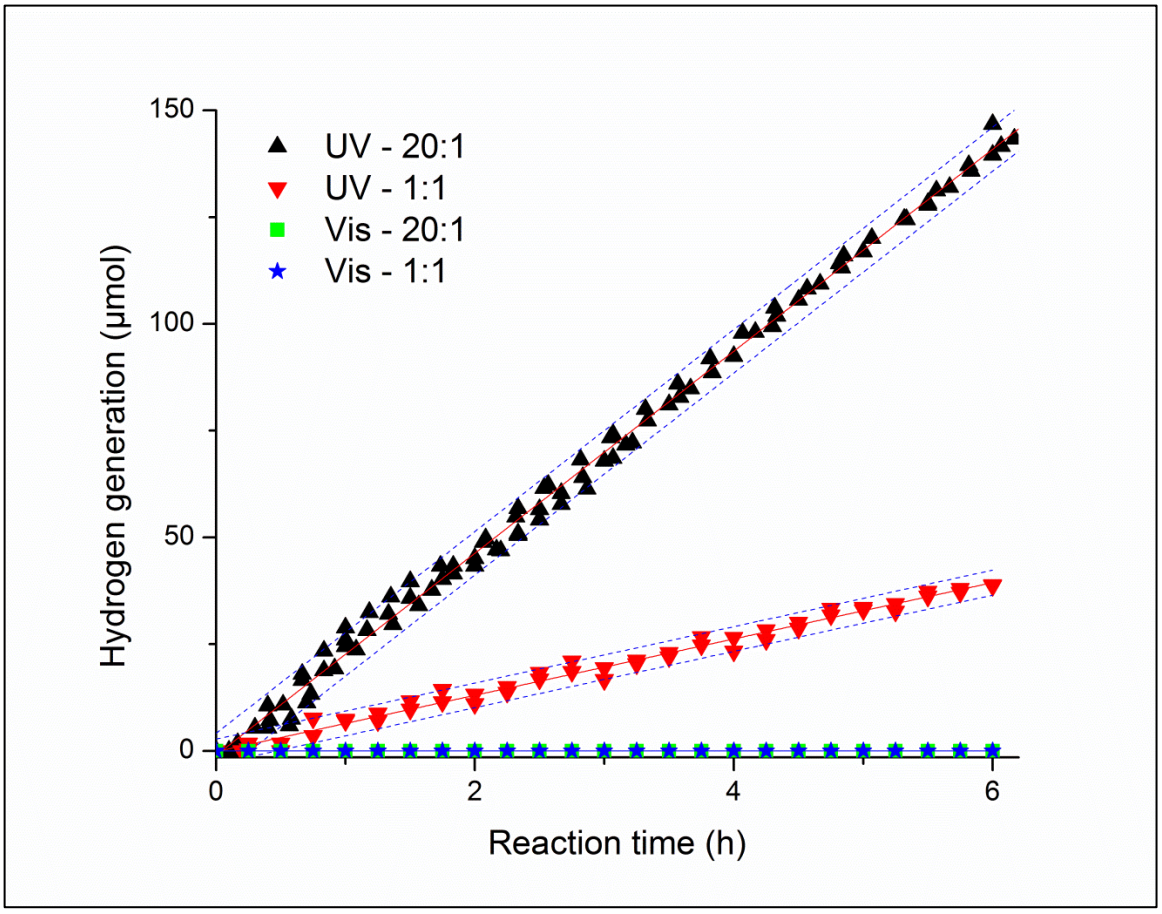

Figure 8. Cumulative hydrogen generation profile showing zero-order kinetics with respect to H_2 using UV-light for nanoparticles synthesized in ratios 20:1 and 1:1.

This linearity with time is indicative of high stability of the material related to the photocatalytic activity. UV-Vis absorption spectra for particles before (Figure 3) and after (Figure - S 2-S3) photocatalysis showed signs of a small degradation for the particles 20:1, decreasing the intensity of the Au-related peak, while a small shift toward lower energies was observed with the 1:1 nanoparticles This behavior can be sign of agglomeration too, but TEM images obtained after experiments (Figure - S 6 and S9) did not show big aggregation, only a reduction in gold presence.

The linear behavior indicates a zero order kinetics in relation to the H_2 production, which is consistent with a Langmuir-Hinshelwood mechanism, typical on heterogeneous catalytic systems (Dickinson, James, Perkins, Cassidy, & Bowker, 1999) where the photocatalytic reaction rate is independent of the reactants' adsorption coverage (Iliev et al., 2007). Equation 4 shows a Langmuir–Hinshelwood kinetic model, modified to describe reactions occurring on the solid–liquid interphase surface:

$$r_0 = \frac{dC}{dt} = \frac{k_r K C_{eq}}{1 + K C_{eq}} \qquad \text{Equation 4}$$

Where r_0 is the initial rate of appearance of the product, k_r is the limiting step rate constant of reaction at maximum coverage degree under the given experimental conditions, K is the reactant adsorption constant and C_{eq} is the equilibrium bulk-solute concentration. Independence of reactant adsorption means a $KC_{eq} \gg 1$, so the active center of the catalyst is almost saturated with the reactant, thus the adsorbed form is in equilibrium with the reactant in the solution (Dickinson et al., 1999).

For particles synthesized using molar ratio 20:1 under UV-light, the rate of hydrogen generation for the reactor was 24 $\mu mol \cdot h^{-1}$, which leads to an estimated reaction rate of 370 $\mu mol \cdot L^{-1} \cdot h^{-1}$. In terms of yields, the mass productivity of the catalyst (also called turnover rate (Maschmeyer & Che, 2010)) reached 6700 $\mu mol \cdot h^{-1} \cdot g^{-1}$. This value represents a fifth of the highest value reported in recent literature using a similar catalyst with ethanol as a sacrificial agent, but using 6 times higher catalyst concentration and 11 times higher alcohol concentration. Also, this result represents a third of the highest reported value using the same sacrificial agent, methanol, which used 18 times higher catalyst concentration, 5 times higher alcohol concentration, and a different type of titania as catalyst, 100% anatase and photoactive under visible light. The molar productivity of methanol was 310 $\mu mol \cdot h^{-1} \cdot mol^{-1}$. The overall energy conversion efficiency (Taboada et al., 2014a), defined as the energy stored as hydrogen divided by the incident photon energy was 0.5% and the apparent quantum yield (AQY) (Maschmeyer & Che, 2010) was 1.0% (formulas are shown in annex I). This low value could be tentatively ascribed to the high intensity of light supplied to the system, and to the high volume of free water within the reactor.

When the photocatalytic system used particles with a higher proportion of gold (1:1, under UV-light), hydrogen production decreased a 72%: rate of hydrogen generation was 7 $\mu mol \cdot h^{-1}$, estimated reaction rate was 100 $\mu mol \cdot L^{-1} \cdot h^{-1}$, mass productivity of the catalyst was 1900 $\mu mol \cdot h^{-1} \cdot g^{-1}$, molar productivity of the methanol was 90 $\mu mol \cdot h^{-1} \cdot mol^{-1}$, overall energy conversion efficiency was 0.1% and AQY was 0.3%.

For both types of particles, the cold-white visible light from the LED lamp source was not able to catalyze the reaction.

These results support a mechanism where the titanium dioxide is the one which captures the photons with enough energy to excite their valence electrons. Gold nanoparticles on the titania surface just helps to decrease the recombination of charge carriers, but they do not make the material photoactive under visible light. The observed gold loading dependence, with higher production rates on composites with smaller but more abundant gold particles (20:1), and the fact that both types of particles have similar TiO_2 area covered by gold, support the reported thesis (Bowker et al., 2014) that active sites are located on the perimeter length around the metallic nanoparticles, in the TiO_2-Au junction.

An extra test with particles 20:1 was run using a higher concentration of particles under the same experimental conditions. It showed that hydrogen production is not proportional to the catalyst amount. With 10 times higher concentration (0.56 $g \cdot L^{-1}$), the system generated only 6.9 times more hydrogen. The screening effect between particles led to a lower mass productivity of the catalyst (4,600 $\mu mol \cdot h^{-1} \cdot g^{-1}$). Nonetheless, the system used the same light supply in a better way: the overall energy conversion efficiency increased to 3.2% and the AQY to 7.2%.

Figure 9 and Table 3 compare the highest catalyst productivity obtained in this work, with reported data from recent literature about photocatalytic hydrogen generation using TiO_2-Au nanoparticles, distinguishing the type of sacrificial agent used in each experiment.

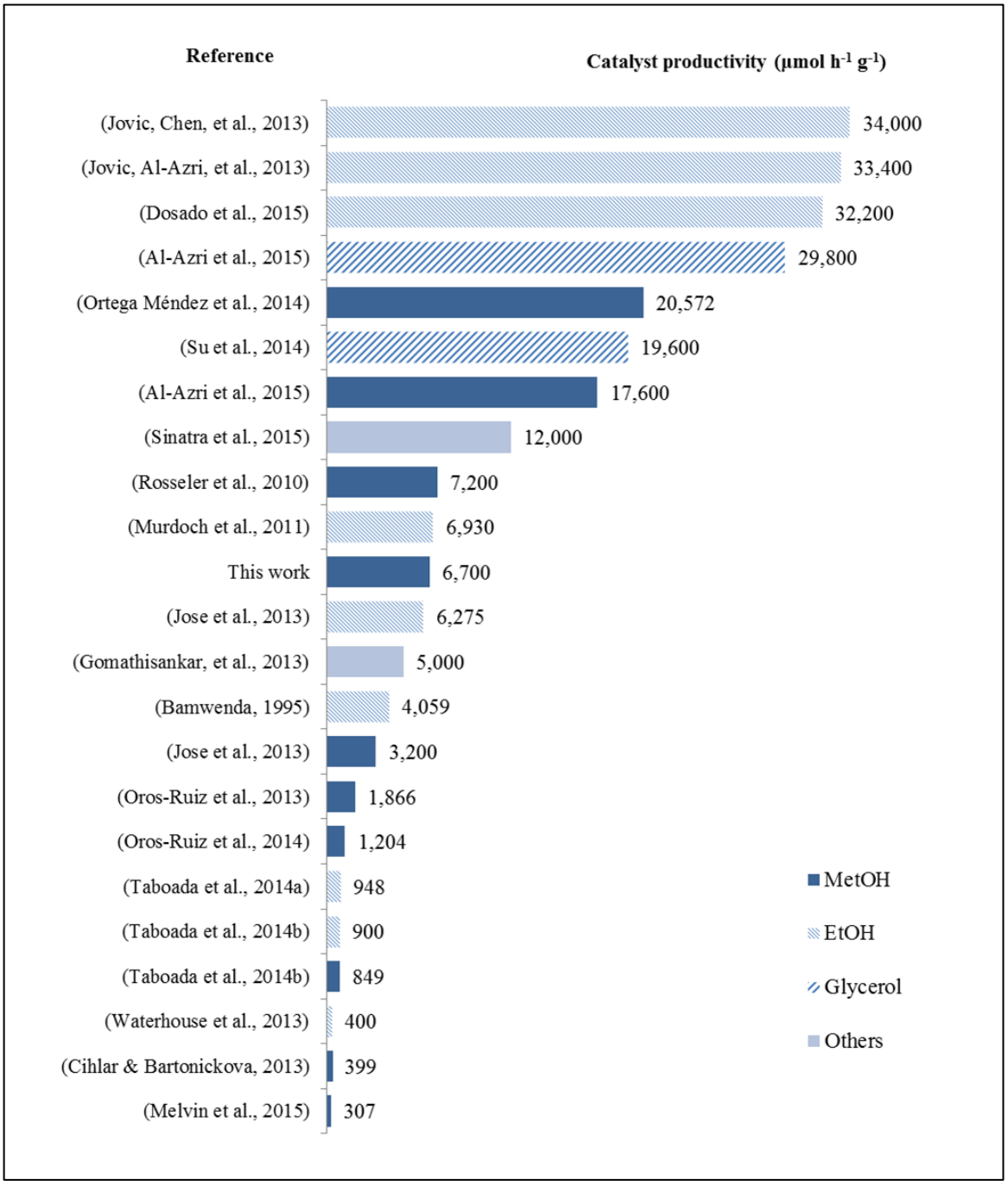

Figure 9. Catalyst productivity, also called turnover rate, reported in the literature for photocatalytic hydrogen generation using TiO_2-Au catalysts, compared to the results of this work.

Table 3. Comparative summary of experimental conditions and main results for recent literature reporting photocatalytic hydrogen generation using TiO_2-Au nanoparticles, organized by catalyst productivity.

Reference	Catalyst productivity	Sacrificial agent productivity	Sacrificial agent	Type of titania (Anatase/Rutile)	Sacrificial agent concentration	Catalyst concentration	Gold loading	Modification method	Primary wavelength	Light intensity	AQY ***
	$\mu mol \cdot h^{-1} \cdot g^{-1}$	$\mu mol \cdot h^{-1} \cdot mol^{-1}$			M / %vol.	$g \cdot L^{-1}$	%wt	**	ηm	$mW \cdot cm^{-2}$	%
(Jovic, Chen, et al., 2013)	34,000	860	EtOH	$P25_{Degussa}$ (85/15)	13.7 / 80%	0.347	1%	DPU+C	365	6.5	NR
(Jovic, Al-Azri, et al., 2013)	33,400	845	EtOH	$P25_{Degussa}$ (85/15)	13.7 / 80%	0.347	2%	DPU+C	365	6.5	NR
(Dosado et al., 2015)	32,200	764	EtOH	$P25_{Degussa}$ (85/15)	13.7 / 80%	0.325	1.5%	DPU+C	365	6.5	NR
(Al-Azri et al., 2015)	29,800	7,079	Glycerol	$P25_{Degussa}$ (85/15)	1.4 / 10%	0.325	1%	DPU+C	365	5	NR
(Ortega Méndez et al., 2014)	20,572	3,329	MetOH	$Anatase_{KronosVlp}$ (100/0)	6.2 / 25%	1	0.8%	PD+D	365	--	17.6%
(Su et al., 2014)	19,600	11,460	Glycerol	$P25_{Degussa}$ (--/--)	3.4 / 25%	2	1%[#]	SI+D	365	217	70%
(Al-Azri et al., 2015)	17,600	2,314	MetOH	$P25_{Degussa}$ (85/15)	2.5 / 10%	0.325	1%	DPU+C	365	5	NR
(Sinatra et al., 2015)	12,000	7,894	Ethylene glycol	$Anatase_{Synthesized}$ (100/0)	0.9 / 5%	0.56	2%[##]	GR	365	8	7%
(Rosseler et al., 2010)	7,200	29,127	MetOH	$P25_{Degussa}$ (80/20)	0.2 / 1%	1	2%	DAE+C	Vis	30	NR
(Murdoch et al., 2011)	6,930	234	EtOH	$Anatase_{Synthesized}$ (100/0)	3.9 / 23%	0.13	4%	DPU+C	350	1.5	NR
This work	6,700	310	MetOH	$P25_{SigmaAldrich}$ (80/20)	1.2 / 5%	0.056	9.1%	SG	375	20	1.0%
(Jose et al., 2013)	6,275	5,495	EtOH	$P25_{Degussa}$ (75/25)	0.9 / 5%	0.75	1%	SMAD+C	--	--	NR
(Gomathisankar, Yamamoto, et al., 2013)	5,000	2,500	Glucose	$P25_{Degussa}$ (75/25)	1.0 / --	0.5	5 ppm	PD	365	5	NR
(Bamwenda, Tsubota, Nakamura, & Haruta, 1995)	4,059	1,380	EtOH	$P25_{JapanAerosil}$ (--/--)	5.0 / 29%	1.7	1%	PD+VD	276-342	30	NR
(Jose et al., 2013)	3,200	1,942	MetOH	$P25_{Degussa}$ (75/25)	1.2 / 5%	0.75	1%	SMAD+C	--	--	NR
(Oros-Ruiz et al., 2013)	1,866	75	MetOH	$P25_{Degussa}$ (--/--)	12.4 / 50%	0.5	0.5%	DPU+C	254	2.2	NR
(Oros-Ruiz, Zanella, Collins, Hernández-Gordillo, & Gómez, 2014)	1,204	35	MetOH	$P25_{Degussa}$ (70/30)	17.1 / 69%	0.5	0.5%	DPU+VD	254	2.2	NR
(Taboada et al., 2014a)	948	36	EtOH	$Anatase_{Synthesized}$ (97/3)	13.1 / 76%	0.5	1%	IWI+C	365	0.2*	20.8%
(Taboada et al., 2014b)	900	103	EtOH	$Anatase_{Synthesized}$ (97/3)	13.1 / 76%	1.5	1%	IWI+C	365	0.2*	38%
(Taboada et al., 2014b)	849	74	MetOH	$Anatase_{Synthesized}$ (97/3)	17.1 / 69%	1.5	1%	IWI+C	365	0.2*	36%
(Waterhouse et al., 2013)	400	1,362	EtOH	Inverse opal (--/--)	0.1 / 1%	0.29	2%	DPU+C	UV+Vis	0.35	80%
(Cihlar & Bartonickova, 2013)	399	112	MetOH	$Anatase_{Synthesized}$ (82.6/17.4)	5.9 / 24%	1.67	0.02%	GAR+C	300-700	14.4	NR
(Melvin et al., 2015)	307	25	MetOH	$P25_{Degussa}$ (--/--)	6.2 / 25%	0.5	1%	PD+D	370-640	100	1.5%
(J.-J. Chen, Wu, Wu, & Tsai, 2011)	8	--	None	$P25_{Degussa}$ (--/--)	0 / 0%	1.43	3%	PD+VD	UV+Vis	$30_{(UV)}$ $1680_{(vis)}$	NR

(--) No information available
(*) per fiber
(**) Methods: DPU = Deposition-precipitation with urea; PD = Photodeposition; SI = Sol-immobilization; GR = galvanic replacement; DAE = direct anionic exchange; SG = sol-gel; SMAD = solvated metal atom dispersion; IWI = incipient wetness impregnation; GAR = glucose-assisted reduction; C = calcination; D = Drying; VD = vacuum drying.
(***) AQY: apparent quantum yield. AQY = 100 x 2 x H_2 molecules out / photons in. NR = not reported, nor estimable due to the lightened reactor surface is not reported.
([#]) Cocatalyst: Au+Pd ([##]) Cocatalyst: Au+Cu_2O

The catalyst productivity reached in the present work represents a 20% of the highest reported productivity, which used ethanol as sacrificial agent. However, Figure 9 does not show a clear incidence of the type of sacrificial agent on the catalyst productivity. For example, ethanol shows the highest reported productivities, but also appears between the lowest results. Table 3 is more helpful for the analysis, but not enough to identify direct incidence of some factors on catalyst productivity.

Table 3 shows how reduction processes by calcination could help to increase the productivity, compared to the conventional and low-energy demanding sol-gel approach used in this work. However, calcination implies a big energy cost during the surface modification process. Moreover, calcination reduction was used in works with lower productivities too, so, its influence seems to be a result of the combination of several experimental factors. These results show that experimental setup and the mix of operation conditions in the photoreactor can be as relevant as the preparation method. Here, particles modified by conventional sol-gel methods at routine level get high productivity under high intensity of light and low particle concentration, especially due to the high supply of photons with the right energy level to activate the material and the minimum screening effect between particles.

As expected, Table 3 also confirms low sacrificial agent productivity and low AQY due to the extremely low catalyst concentration used during the experiment, one order of magnitude below the lowest concentration of nanoparticles reported in the literature.

Reported information is not enough to analyze the effect of the radiation source or the intensity of light. What is clear is that many factors can affect the productivity and efficiencies of this process, so multifactorial studies are needed to quantify the effect of each factor and manipulate the system in a more effective way to optimize it.

2.4 Conclusions

It was feasible to produce nanoscale aggregates of TiO_2-Au particles using a synthesis method under room conditions. They were appropriate for generating hydrogen gas using a system based on low-consumption UV LED-lights (375 nm; 20 $mW \cdot cm^{-2}$), but not under visible white LED-lights. The simple reactor design and experimental setup based on gauge pressure-temperature measurement, not previously reported, allowed observing the kinetical behavior on hydrogen photo-production without online gas chromatography.

Higher proportion of gold during the synthesis does not generate more gold nanoparticles and it does not affect the proportion of area covered by gold, but makes bigger and more isolated gold particles. An apparent zero order kinetics was corroborated, a sign of saturation of active catalytic centers. The sol-gel approach for surface modification resulted in catalyst productivities of 6,660 $\mu mol \cdot h^{-1} \cdot g^{-1}$. This analysis shows that conditions used in this work were suboptimal for a compact H_2 production system. The influence of different factors is still not clear, such as radiation, type and concentration of electron donor, and nanoparticle concentration. Further research on the influence of more factors and their interactions is necessary.

3 OPERATIONAL CONDITIONS AFFECTING HYDROGEN PRODUCTION VIA PHOTO-REFORMING OF ORGANIC COMPOUNDS USING TiO_2-Au NANOPARTICLES

3.1 Introduction

3.1.1 Hydrogen role in energy scenario

Hydrogen is considered an attractive alternative to improve the human energy system due to its clean emissions. However, one of the barriers to expanding the use of hydrogen is its current non-sustainable production process, mainly based on fossil fuels: steam reforming of methane and gasification of coal share 96% of the world market (C. Grimes, Varghese, & Ranjan, 2008).

Besides the cleaner electrochemical processes (Bhandari, Trudewind, & Zapp, 2013; Fischer, 1986; Kelly, 2014; Koj, Schreiber, Zapp, & Marcuello, 2015; M. Wang, Wang, Gong, & Guo, 2014), numerous production ways have been studied looking for a more sustainable production system such as thermochemical processes using biomass, gasification (G. Chen, Yao, Liu, Yan, & Shan, 2015; Deniz et al., 2015; Haarlemmer, 2015; Hamad, Radwan, Heggo, & Moustafa, 2016; Liao & Guo, 2015; Mikulandrić, Lončar, Böhning, Böhme, & Beckmann, 2015; B. Zhang et al., 2015) and pyrolysis (Alipour Moghadam, Yusup, Azlina, Nehzati, & Tavasoli, 2014; Alvarez et al., 2014; Kim, Lim, & Chun, 2013; Shaomin Liu et al., 2014; X. Xu, Jiang, Wang, & Xu, 2015), and biological processes by dark (Cheng et al., 2015; X. M. Guo, Trably, Latrille, Carrère,

& Steyer, 2010; Han, Ye, Zhu, Zhao, & Li, 2015; Hsu & Lin, 2015; Wong, Wu, & Juan, 2014) and photo fermentations (Cheng et al., 2015; Ghirardi, Dubini, Yu, & Maness, 2009; B.-F. Liu et al., 2015; Zagrodnik & Laniecki, 2015; Z. Zhang, Wang, Hu, Wu, & Zhang, 2015) using bacteria and microalgae. Considering solar energy as a front-running clean, abundant and secure energy source, some researchers have faced the rising energy demand by proposing a photocatalytic hydrogen production process (Bolton, 1996; C. A. Grimes, Varghese, & Ranjan, 2008; Ohta & Veziroglu, 1976) as a way to store solar energy in chemical energy (Teets & Nocera, 2011).

3.1.2 Factors affecting photocatalytic hydrogen generation

Most papers in the field of photocatalysis are focused on the synthesis, characterization of properties and testing of nanomaterials able to catalyze the degradation of pollutants (Ayati et al., 2014; Bansal et al., 2015; Długosz et al., 2015; Fan, Li, Liu, Yang, & Li, 2015; Gar Alalm, Ookawara, Fukushi, Sato, & Tawfik, 2015; H. Gupta & Gupta, 2015; Ling et al., 2015; Majidnia & Idris, 2015; Saud et al., 2015; Sood et al., 2015), the water splitting reaction (Ahmad et al., 2015; Bell, Will, & Bell, 2013; S. Guo et al., 2015; Xiying Li et al., 2014; Ni, Leung, Leung, & Sumathy, 2007; Ortega Méndez et al., 2014; Rosseler et al., 2010; Y. Yan, Cai, Song, & Shi, 2013) or photo-reforming of organic compounds (Daskalaki & Kondarides, 2009; Gunlazuardi & Dewi, 2014; Ni, Leung, & Leung, 2007; Oros-Ruiz et al., 2013).

Some materials used for these applications are: transition metal oxides (Chang et al., 2015; Du & Lu, 2014; Gomathisankar, Hachisuka, et al., 2013; He, Yang, Wang, Zhao, & Duan, 2012; K. Gurunathan, P. Maruthamuthu & Sastri, 1997; M. M. Khan, Adil, & Al-Mayouf, 2015; Xiangqing Li, Zhang, Kang, Li, & Mu, 2014; Pai, Tsai, & Fang, 2013; Sampaio et al., 2015; Sasikala et al., 2009; Shen et al., 2012); oxynitrides (W. Chen et al., 2015; Grigorescu et al., 2014; Hara, Takata, Kondo, & Domen, 2004; Y. Li et al., 2015; X. Liu et al., 2014; Lu et al., 2015; Maeda, Terashima, Kase, & Domen, 2009; Maegli et al., 2012; Matsukawa et al., 2014; Pan et al., 2015; Yokoyama et al., 2011); oxysulfides (Ishikawa et al., 2003, 2004; Jia, Yang, Zhao, Han, & Li, 2014; Pacquette, Hagiwara, Ishihara, & Gewirth, 2014; Tang, Ye, & Hu, 2013; F. Zhang, Maeda, Takata, & Domen, 2011; F. Zhang et al., 2012); metal sulfides (Balcerski et al., 2015; Chang et al., 2015; M. Liu, Du, Ma, Jing, & Guo, 2012; Shan Liu, Wang, Wang, Lv, & Xu, 2013; Majeed et al., 2016; H. Yan et al., 2009; J. Yang et al., 2012; Zhao & Yang, 2016); and perovskite oxides (Grabowska, 2016). However, the most studied material is titanium dioxide (Bowker et al., 2014; Clarizia et al., 2014; B. Gupta et al., 2016; S. Gupta & Tripathi, 2011; Jose et al., 2013; Linsebigler et al., 1995; Ni, Leung, Leung, et al., 2007; Y. Wang et al., 2014). Usually, the catalytic properties of these materials are improved using sacrificial agents or modification techniques. Organic species like alcohols (Al-Azri et al., 2015; Choi & Kang, 2007; D'Elia et al., 2011; Dosado et al., 2015; Gomathisankar, Hachisuka, et al., 2013; Hara et al., 2004; Taboada et al., 2014a) and glycerol (Beltram et al., 2015; Daskalaki & Kondarides, 2009; Fujita et al., 2016; Gunlazuardi & Dewi, 2014;

Jung et al., 2015; R. Liu et al., 2014; Lyubina et al., 2013; Sadanandam et al., 2013) are typical sacrificial agents used as electron donors or hole scavengers. There are three main usual modification techniques to improve the photocatalytic process: the combination with metals (Al-Azri et al., 2015; Ansari et al., 2015; Ayati et al., 2014; Balcerski et al., 2015; Beltram et al., 2015; Bowker et al., 2014; Choi & Kang, 2007; Clarizia et al., 2014; Daskalaki & Kondarides, 2009; Dosado et al., 2015; Gomathisankar, Hachisuka, et al., 2013; B. Gupta et al., 2016; Jose et al., 2013; Jovic, Chen, et al., 2013; Jung et al., 2015; K. Gurunathan, P. Maruthamuthu & Sastri, 1997; W.-S. Lee, Wan, Kuo, Lee, & Cheng, 2007; Xiying Li et al., 2014; Lin, Shi, Yoshida, Li, & Zou, 2013; Shan Liu et al., 2013; Lu et al., 2015; Melián et al., 2014; Murdoch et al., 2011; Oros-Ruiz et al., 2014, 2013; Ortega Méndez et al., 2014; Pai et al., 2013; Rosseler et al., 2010; Sampaio et al., 2015; Sinatra et al., 2015; Sun, Liu, Liang, Hu, & Fan, 2015; Taboada et al., 2014a, 2014b; D. Wang et al., 2015; Y. Xu & Xu, 2015; H. Yan et al., 2009; J. Yang et al., 2012; S. Yang et al., 2016; Y. Yang et al., 2014; YANG, CHANG, & IDRISS, 2006; F. Zhang et al., 2012; Y. Zhang, Ligthart, Quek, Gao, & Hensen, 2014), the combination with other semiconductors (Bai et al., 2015; Bel Hadjltaief et al., 2016; J. Chen et al., 2014; Du & Lu, 2014; Hussein & Shende, 2014; Lam et al., 2015; Lu et al., 2015; Melián et al., 2014; Nsib et al., 2015; Pérez-Larios et al., 2012; Roy et al., 2015; Sinatra et al., 2015; Chao Wang et al., 2015; Q. Wang et al., 2013; Y. Xu & Xu, 2015; Z. Yan et al., 2014), and cation or anion doping (Fujita et al., 2016; R. Liu et al., 2014).

So many options create a very wide net of possible combinations, making it difficult to optimize and quantify the effect of the numerous variables affecting hydrogen productivity. Some of the most studied factors influencing hydrogen production are the presence, type, particle size and loading amount of co-catalysts (Al-Azri et al., 2015; Ayati et al., 2014; Du & Lu, 2014; Lu et al., 2015; Majeed et al., 2016; Murdoch et al., 2011; Subramanian, Wolf, & Kamat, 2004; J. Yang et al., 2012), and the presence, type and concentration of sacrificial agents (Al-Azri et al., 2015; Beltram et al., 2015; W.-T. Chen et al., 2015; Kandiel, Dillert, Robben, & Bahnemann, 2011; Kawai & Sakata, 1980; López et al., 2015; Lyubina et al., 2013; Oros-Ruiz et al., 2013; Sadanandam et al., 2013; Taboada et al., 2014b). Less studied but equally relevant for bigger scale applications are the effects of light intensity (Bell et al., 2013) and photocatalyst concentration (Nsib et al., 2015) because of the possible screening effect on the bulk of the reaction media. Most researches vary one or two factors independently to define the best combinations of factors, so interaction effects are usually not involved in these studies.

The effect of several factors affecting hydrogen productivity simultaneously can be studied by using a factorial design of experiments (DOE), an empirical modelling technique used to evaluate the relationship between experimental variables and corresponding responses (Chowdhury et al., 2011; Krishna Prasad & Srivastava, 2009). Few papers in this field have used this statistical method for analysis with more than three factors such as Chowdhury et al (Chowdhury et al., 2011). They studied the potential for hydrogen generation using Eosin Y-sensitized TiO_2/Pt catalyst under visible solar light in

the presence of triethanolamine as an electron donor, employing a 2^4 full factorial design, where visible light irradiation time and initial Eosin Y concentration showed the highest positive effect, also proposing a regression function that satisfactorily predicts hydrogen generation. Bastos et al (Bastos, Lopes, Santos, & Silva, 2014) used a 2^{5-1} fractional factorial experimental design, followed by a Box–Behnken design, to set the reaction conditions of a photoinduced reforming of a glycerol aqueous solution over Pt/hex-CdS under visible light irradiation for the enhancement of hydrogen production. They assessed irradiation time, mass of photocatalyst, concentration of glycerol, pH and electrolyte concentration (NaCl) as the main factors. They found that all five factors have a significant effect on hydrogen production; pH being the most important parameter.

In this context, this paper will focus on the quantification of the effect of five basic factors and their combinations by using a design of experiments technique to have a better understanding of hydrogen productivity as a tool for further optimization of operational conditions in photocatalytic reactors. Factors under analysis will be: (A) presence of gold as co-catalyst, (B) type of alcohol as electron donor, (C) intensity of UV-light, (D) electron donor concentration, and (E) nanoparticle concentration.

3.1.3 TiO_2 modification by gold and alcohols as a sacrificial agent

The ability of a semiconductor to undergo photoinduced electron transfer to adsorbed species on its surface depends upon the respective positions of the band edges for the conduction and valence bands and the redox potential levels of the adsorbate species

(Linsebigler, Lu, & Yates, 1995). The relevant redox potential level of the acceptor species is thermodynamically required to be below (more positive than) the bottom of the conduction band of the semiconductor. The redox potential level of the donor species needs to be above (more negative than) the top of the valence band of the semiconductor in order to donate an electron to the vacant hole (Al-Azri et al., 2015; W.-T. Chen et al., 2015; Jovic, Al-Azri, et al., 2013; Linsebigler et al., 1995; Rossetti, 2012).

TiO_2 has received great attention because it accomplishes this requirement for water splitting and photo-reforming of several organic compounds. Also, it is stable, noncorrosive, harmless, abundant and inexpensive (Oros-Ruiz et al., 2013). TiO_2 is indeed one of the most widely used semiconductors employed for photocatalytic applications. However, its photocatalytic activity is limited to the ultraviolet region (B. Gupta et al., 2016).

In recent years, catalysis and photocatalysis processes using gold nanoparticles have become popular due to their effectiveness in degrading and mineralizing organic compounds (Ayati et al., 2014) because they are comparatively cheaper to Pt, and because their inherent plasmonic oscillation makes them photoactive in the visible region (B. Gupta et al., 2016), depending upon its particle size, morphology and dielectric constant of the medium (Bashir & Idriss, 2017; M. A. Khan, Sinatra, Oufi, Bakr, & Idriss, 2017). In this state, electrons are transferred from surface-plasmon-stimulated gold nanoparticles to the conduction band of TiO_2 (Aiboushev et al., 2013; Kochuveedu, Kim, & Kim, 2012; Xing et al., 2016).

The flow of electrons is different under UV light. Here, the gold loading on a semiconductor surface under UV light acts as an electron sink, exhibiting movement of the Fermi level towards a more negative direction, sitting it around -0.27 eV, between the bottom of the TiO_2 conduction band and the H^+/H_2 redox couple (W.-T. Chen et al., 2015), which is a key factor for increasing the Schottky barrier effect (B. Gupta et al., 2016; Rajeshwar et al., 2002). Thereby, electrons photoexcited into the conduction band of TiO_2 migrates onto the supported gold nanoparticles, suppressing electron hole pair recombination in TiO_2, whilst the metal nanoparticles themselves function as active surface sites for H_2 evolution (W.-T. Chen et al., 2015). On the other hand, holes migrate to the surface where they oxidize the adsorbed molecules (Rossetti, 2012).

This phenomenon makes the metal particle size a key factor affecting the hydrogen production, but its fundamental understanding still requires considerable work (Al-Azri et al., 2015; López-Tenllado et al., 2017). Several research teams have faced this topic and agree that correlation between Au NP size and photocatalytic activity is still unclear. They have found that both the properties of titania and gold are crucial for resultant photocatalytic activity, but a direct correlation between size and photocatalytic activity has not be obtained since all structural properties changed simultaneously when conditions of photocatalyst preparation are modified (Al-Azri et al., 2015). Murdoch et al. (Murdoch et al., 2011) found that reaction rates under UV light increased with Au particle size up to around 12 nm, and that the normalized reaction rate per Au atom is independent of Au particle size up to 12 nm, with a decrease of the normalized reaction rate at higher Au

sizes, most likely due to a geometric rather than an electronic effect. Wei and his group (Wei et al., 2017) found that under visible light this correlation between photocatalytic activity and the size of gold NPs is clearer than for UV illumination and it indicates that gold properties are decisive for visible light activity rather than titania properties. This factor is not under analysis on this work, but it needs to be mentioned and characterized.

Also, to project real size applications of this process a non-energy intensive synthesis method is necessary. The use of atmospheric pressure and room temperatures to modify the titania nanoparticles is very relevant for increasing the chance of economic feasibility and a positive net energy balance. Several methods are reported to synthesize TiO_2-Au nanoparticles. Some of them are sol–gel, photodeposition, deposition–precipitation, simple reducing and dispersion (B. Gupta et al., 2016). Among this range of options, an adjusted sol-gel method for TiO_2-Au partially covered nanoparticles synthesis is used (Fu et al., 2005; W. Li et al., 2010a) based on the reduction of gold ions over TiO_2 surface due to its low energy requirements and its effective performance. Refer to section 3.2.3 for additional details.

Hydrogen production rates can be increased by several orders of magnitude using renewable sacrificial agents, like alcohols (Dosado et al., 2015), amines or sulphite salts (Osterloh & Parkinson, 2011). Their oxidation potentials, lower than water, further suppresses the electron hole pair recombination in TiO_2. In such systems the process cannot be claimed water splitting, but photo-reforming of organic compounds, even when there could be decomposition of water (Serpone et al., 2016). Some researchers claim

these additives are not viable for any practical system for sustainable energy production (Osterloh & Parkinson, 2011) because they are costly or industrially irrelevant (Tachibana, Vayssieres, & Durrant, 2012). However, the prevailing idea is to use organic compounds currently found in industrial wastewaters (Clarizia et al., 2014), like methanol, ethanol, glycerol, ethylene glycol and formic acid. There is a trend that uses biomass-derived compounds as sacrificial agents for the enhancement of photocatalytic hydrogen production, first investigated by Kawai and Sakata (Kawai & Sakata, 1980; López et al., 2015). In this sense, many studies on the use of methanol as a sacrificial agent consider it a model molecule in the application of photocatalysis in photoreforming (Kandiel et al., 2011; López et al., 2015) because it captures the holes more rapidly than ethanol or 2-propanol(López et al., 2015; Tamaki et al., 2006); it has a high hydrogen/carbon ratio and, like ethanol, can be obtained from biomass (Hamelinck & Faaij, 2002; López et al., 2015). Recent works emphasize the influence of physical properties of the alcohols on the H_2 productivity, like polarity and redox potential. Polarity is critical to the interaction of the alcohol with the TiO_2 surface, where high polarity alcohols will interact strongly with the semiconductor surface, resulting in the injection of more electrons into the TiO_2 valence band, and the larger the potential separation between the alcohol oxidation potential and the TiO_2 valence band, the higher the H_2 production rate (Al-Azri et al., 2015; W.-T. Chen et al., 2015; Puga, 2016).

The lack of comprehensive studies simultaneously examining the effect of changes in low concentrations of nanoparticles on the H_2 production rates in TiO_2-Au systems is a gap in

the current literature. Also, it is unclear whether the relative activities of photocatalysts are altered by the type of alcohol hole scavenger used in the photocatalytic tests (W.-T. Chen et al., 2015). So, in this work, methanol and ethanol are compared as sacrificial agents for the oxidative half-reaction, and gold as a co-catalyst for the hydrogen-reduction part (Diebold, 2011). Although the literature is clear about the relevant effect of gold presence as a co-catalyst, this work will help to compare its relative importance versus other operational conditions and to understand their interaction.

3.2 Experimental Section

3.2.1 Reagents

For the synthesis of TiO_2-Au composites, Aeroxide® P25 Titanium(IV) oxide nanopowder (TiO_2, 80% anatase, 20% rutile, Sigma Aldrich^{TM}), gold(III) chloride hydrate ($HAuCl_4 \bullet 3H_2O$, Sigma AldrichTM), sodium borohydride ($NaBH_4$, Merck^{TM}), and tri-sodium citrate dehydrate ($C_6H_5Na_3O_7 \bullet 2H_2O$, Merck^{TM}) were used as received without further purification. Hydrochloric acid fuming 37% for analysis (Merck^{TM}) was used in solution (0.1 N). Also, for photocatalytic reactions ethanol (C_2H_6O, Merck^{TM}) and methanol (CH_4O, Merck^{TM}) were used without further purification.

3.2.2 Instruments

The photocatalytic reactor system was implemented within a Shin Saeng, model SBOD-201 incubator, as a controlled temperature chamber. The system was based on: four 50 mL

Erlenmeyer flasks (total volume 68 mL) with GL18 screw caps with hole and septum of silicone, as batch reactors, each one over a magnetic stirrer; a USB thermocouple datalogger Pico Technology, model TC-08, with four type K thermocouples; a humidity, temperature, and barometric pressure USB datalogger Extech, RHT50; four 50 W UV-LED light chips of 375 nm, Justar, model JX-50UV10X5G, each one with an aluminum heatsink, fan of 12 V for cooling and a LED driver.

Composites were characterized using an UV-VIS photodiode array spectrophotometer Shimadzu, model MultiSpec-1501, DLS analysis on a Malvern Zetasizer Nano ZS instrument and an ICP-AES Varian Liberty Series II Axial. Microscopic images were obtained using a Philips Tecnai 12 Biotwin TEM.

Radiation measurements were developed using a PCE Instruments, model PCE-UV34 UVA-UVB radiation sensor.

Determination of hydrogen was done using a fast gas chromatograph DANI, model Master GC, equipped with a fused silica capillary column with molecular sieve of 5 A° Supelco, model Mol Sieve 5A PLOT, and a VICI, model TCD-NIFED-220DI micro-volume thermal conductivity detector.

3.2.3 Synthesis of partially covered TiO_2–Au nanoparticles

A method for synthesis of TiO_2@Au core-shell nanoparticles synthesis was used, proposed by Fu, Vary and Lin (Fu et al., 2005), and Li, Guo and Zhang (W. Li et al., 2010a). It was based on the reduction of $[AuCl_4]^-$ over TiO_2 surface using $NaBH_4$ as a

reductive agent. It works at room temperature and pressure. First, a colloidal suspension (100 mL) was prepared with TiO_2 (4 mM) and $HAuCl_4$ (0.2 mM). $HAuCl_4$ worked as a gold precursor giving $[AuCl_4]^-$ ions to the solution. After an ultrasonic bath (5 min) to avoid agglomeration, pH of the reaction media was adjusted (2.2) by dropwise addition of HCl solution (0.1 N) to obtain a negative electric charge on the surface of TiO_2 particles. After a second ultrasonic bath (5 min), sodium citrate solution (5 mL, 25 mM) was added to the colloidal suspension in a round-bottom flask. After stirring (5 min), a solution (5 mL) of citrate (25 mM) and $NaBH_4$ (0.1 M) was added, showing a change of color from white to purple, and thus obtaining the reduced Au^0 over the TiO_2 particles surface. After stirring (10 min), the TiO_2-Au composites were analyzed to obtain the expected UV-vis spectroscopy pattern (Jovic, Chen, et al., 2013; W. Li et al., 2010a). Finally, after a third ultrasonic bath (5 min), the colloidal suspension was stored in darkness at a low temperature (4°C).

3.2.4 Design of experiment

The 2^{5-1} half-fraction factorial completely randomized experimental design used in this work, has a V resolution, where main effects are aliased with four-factor interactions and two-factor interactions are aliased with three-factor interactions. Based on the sparsity-of-effects principle, three-factor or higher interactions are negligible, so the five main effects and the ten two-factor interactions do not confound with other main effects and two-factor interactions (Montgomery, 2012). The design was constructed by selecting I = ABCDE as

the generator, and setting the levels of the fifth factor to E = ABCD (see Table 5 in section 3.3.2). Blocking was not used in this design to avoid confounding two-factor effects with block effects, even when the photocatalytic system allows running just four experimental units at a time. It was verified that batching of experiments was not a significant source of nuisance, keeping temperature and pressure under control, with the same operator, equipment, and reagents for every photocatalytic essay and measurement routine in the whole experiment.

Reduced regression models for mean response were proposed as transfer functions between the factors and the three mentioned responses. They were constructed by analysis of variance (ANOVA) and backward elimination or forward selection of factors with a level of confidence (α) between 95% and 85%, to identify a useful subset of predictors. This process systematically adds the most significant variable or removes the least significant variable during each step (Minitab, 2014). The adjusted coefficient of determination (adj-R^2) was used to compare models with a different number of predictors, and the predicted coefficient of determination (pred-R^2) to determine how well the model predicted new observations and the overfitting of the model (Frost, 2013).

3.2.5 Photocatalytic experiments

Each experimental unit was integrated by a batch reactor covered with aluminum foil with a square window (7 cm^2). The reactor was illuminated with a 375 nm UV-LED light focusing on the window, parallel to the surface of the reactor, during 11 hours under slow

stirring. Intensity of light was regulated by the separation distance between the surface and the LED chip (see Figure 10-a).

Each reactor contained a volume of solution (63 mL), and a headspace (4 mL) filled with argon gas at barometric pressure (950 kPa). It was sealed with PTFE tape and purged with argon (10 min) through the silicon septum using needles under stirring (see Figure 10-b). The solutions of each reactor and the setting of the required light were prepared according to the combinations detailed in Table 5 in the levels described in Table 4, with previous randomization. The experiment was developed within the incubator with temperature control, with space for four experimental units running at the same time. The temperature of the incubator (5°C) was set to increase the radiation delivered by the UV-LED lights. The heat released by the lights raised the temperature of the chamber (20°C) and the temperature of the reactors (25°C average) (see Figure 10-c).

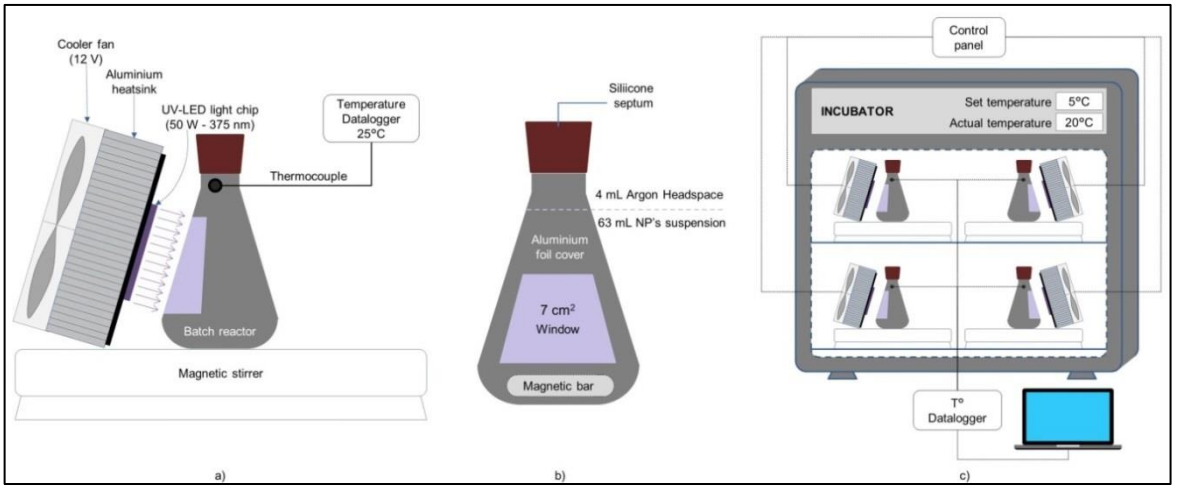

Figure 10. Experimental setup: a) experimental unit configuration; b) batch reactor; c) system configuration with four experimental units running at the same time.

3.3 Results and Discussion

3.3.1 Characterization of the photocatalyst

The photocatalytic experiments used both bare Aeroxide® P25 titanium oxide nanopowder and the same P25 TiO_2 modified with gold nanoparticles on the surface. Gold presence was verified by UV-vis spectroscopy comparing absorption spectra of bare and modified TiO_2 in Figure 11, where the spectrum for TiO_2-Au shows the characteristic peak around 530 nm for gold nanoparticles over TiO_2. This spectra are consistent with reported information (Fu, Vary, & Lin, 2005; W. Li, Guo, & Zhang, 2010b).

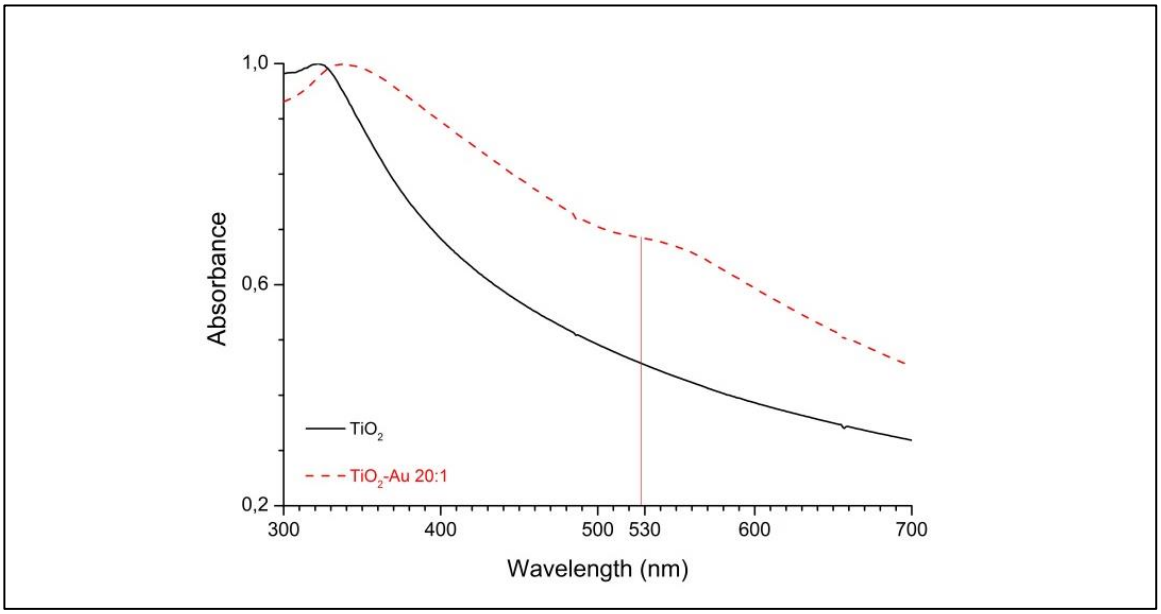

Figure 11. Normalized UV-visible absorption spectra of bare TiO_2 (without peak) and TiO_2-Au synthesized using a molar ratio 20:1 (with localized surface plasmon resonance peak around 530 nm)

Also, inductively coupled plasma atomic emission spectroscopy (ICP-AES) to the gold modified titania, synthesized with a molar ratio [Ti]/[Au] = 20:1, ratified the presence of Ti (6.12 mg L^{-1}) and Au (1.00 mg L^{-1}), which is equivalent to a metal loading of 8.9 wt.%.

Dynamic light scattering (DLS) analysis showed a particle size distribution for modified titania with a peak around 46 nm of radius, which is shown in Figure 12.

The particle size distribution for gold nanoparticles on the surface of titanium dioxide was obtained by analysis with ImageJ (Rasband, n.d.) of images taken by transmission electron microscopy (TEM). One of them is shown in Figure 13. The metal particle size distribution had a peak around 4.5 nm of diameter and it is shown in Figure 14.

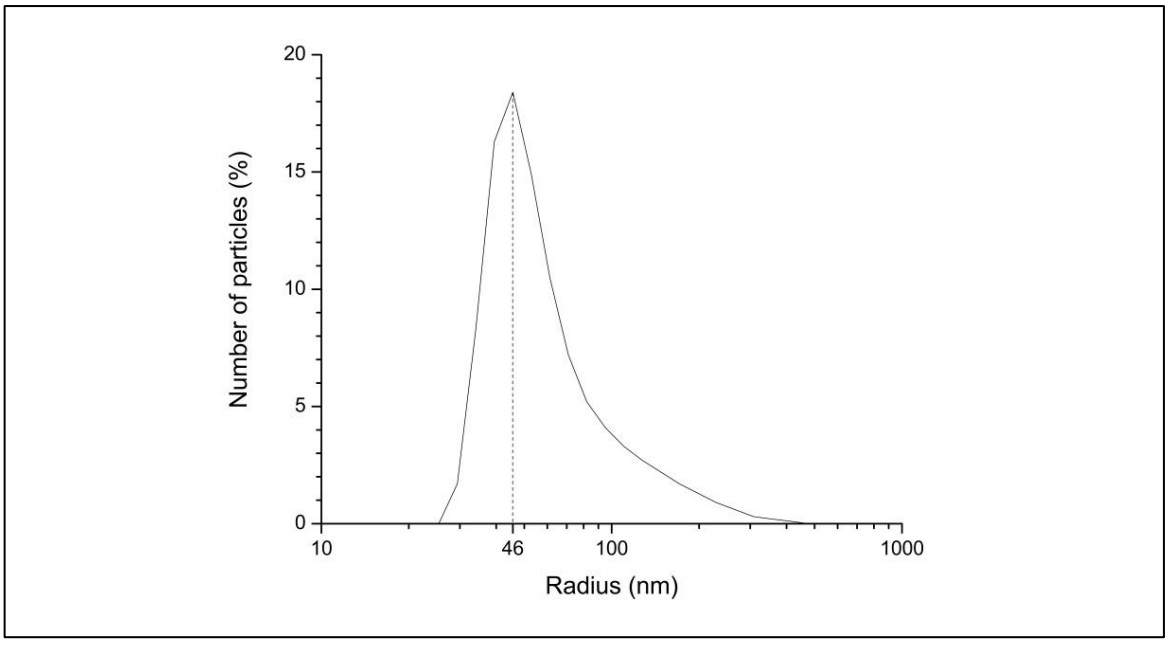

Figure 12. Particle size distribution results from DLS analysis for TiO_2-Au agglomerates, with a peak of particles at 46 nm.

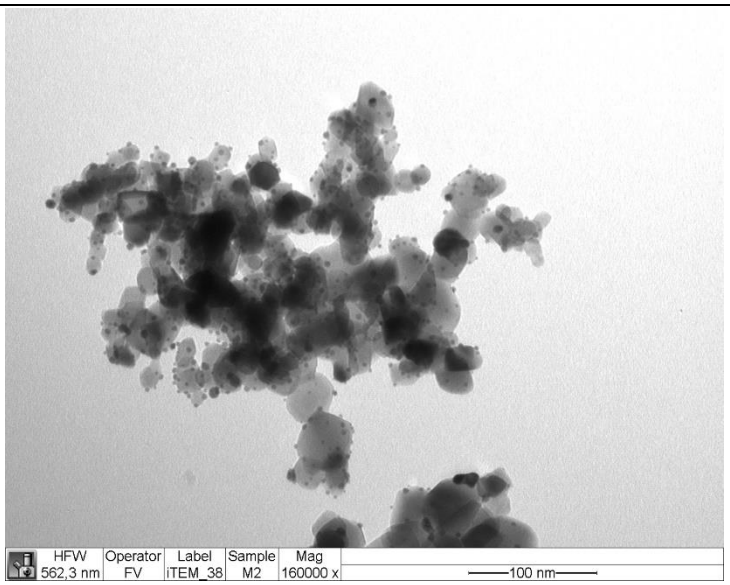

Figure 13. TEM image for an agglomerate TiO_2-Au synthesized using a molar ratio 20:1, where the small rounded spots are the gold nanoparticles over the Titania surface.

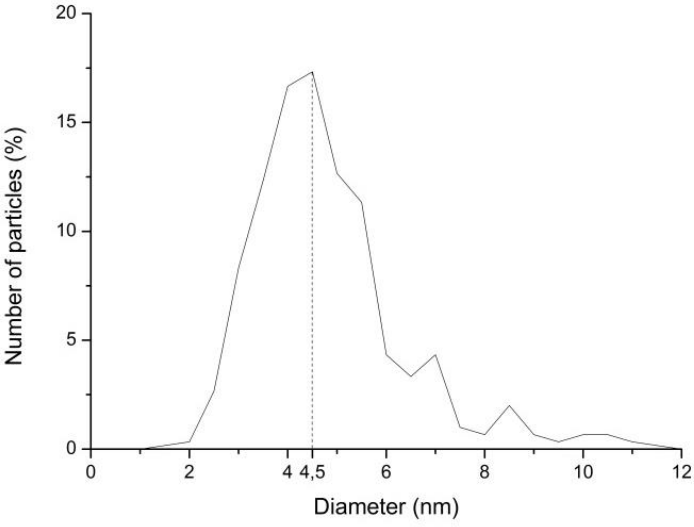

Figure 14. Particle size distribution for gold nanoparticles on the surface of TiO_2-Au with a diameter peak around 4.5 nm.

3.3.2 General results from the factorial experiment

This section contains the results of a 2^{5-1} half-fraction factorial completely randomized experimental design with five factors and three responses. Five operational conditions were investigated as factors which could affect the production of hydrogen: presence of gold as co-catalyst over TiO_2 surface (A: Gold); the type of alcohol used as an electron donor (B: eDonor); the level of intensity of UV-light used as an energy source (C: Intensity); concentration of electron donor (D: eDonor concentration); and concentration of nanoparticles in suspension within the reactor (E: NPs concentration). Two levels were defined for each factor and the original measurement units of each factor were transformed into coded units. The factor levels were coded as -1 (low) and 1 (high). Factors, coded and uncoded values are shown in Table 4, and the design of the experiment is shown in Table 5 with the average results for each response: total hydrogen generation (H), catalyst productivity (H/cat) and electron donor productivity (H/eDon).

Main and interaction effects on the responses are analyzed, and reduced models are proposed for their mean prediction. Potential variability adjustment factors are proposed, and finally, the productivities space is analyzed to show the effect of factors and the best treatments.

Table 4. Coded and uncoded values of the factors used in the experiment for H_2.

	Factors	Coded low level	Uncoded low value	Coded high level	Uncoded high value
A:	Gold	-1	No	1	Yes
B:	Electron donor	-1	Methanol	1	Ethanol
C:	Intensity	-1	10 mW cm^{-2}	1	20 mW cm^{-2}
D:	eDonor concentration	-1	1.2 M	1	2.2 M
E:	NPs concentration	-1	0.05 g L^{-1}	1	0.10 g L^{-1}

Table 5. 2^{5-1}_{V} Design of the experiment and results

	Basic design			*H* μmol		*H/cat* μmol g^{-1} h^{-1}		*H/eDon* μmol mol^{-1} h^{-1}	
Run	ABCD	E = ABCD	Treat-ment	Mean	Std. dev.	Mean	Std. dev.	Mean	Std. dev.
1	– – – –	+	e	10.0	0.2	144	3	12.0	0.3
2	+ – – –	–	a	40.4	0.2	1165	5	48.5	0.2
3	– + – –	–	b	21.7	1.9	628	54	26.1	2.2
4	+ + – –	+	abe	73.4	9.7	1060	140	88.3	11.6
5	– – + –	–	c	13.3	0.8	383	24	16.0	1.0
6	+ – + –	+	**ace**	99.6	6.0	1438	87	**119.8**	7.2
7	– + + –	+	bce	23.5	1.5	339	22	28.3	1.9
8	+ + + –	–	abc	87.7	5.3	2532	152	105.5	6.3
9	– – – +	–	d	16.9	1.1	488	32	11.1	0.7
10	+ – – +	+	ade	66.2	5.0	955	72	43.4	3.3
11	– + – +	+	bde	24.1	2.2	348	32	15.8	1.4
12	+ + – +	–	abd	76.9	8.5	2220	245	50.5	5.6
13	– – + +	+	cde	15.0	1.1	217	16	9.9	0.7
14	+ – + +	–	**acd**	97.6	13.7	**2817**	395	64.0	9.0
15	– + + +	–	bcd	34.7	5.0	1002	145	22.8	3.3
16	+ + + +	+	**abcde**	**113.8**	4.1	1642	59	74.6	2.7
	Global mean			**50.9**		**1086**		**46.0**	

3.3.3 Total hydrogen generation

3.3.3.1 Main and interaction effects on total hydrogen generation and its variability

Figure 15-a presents the main effects plot of total hydrogen generation (H) measured in μmol of H_2 produced in the headspace of the photoreactor (4 cm^3) after 11 hours of reaction. Please be aware that this type of plot is not a linear adjustment with two points. A main effects plot is a commonly used chart type for statistical analysis which shows data means when you have multiple factors. The points in the plot are the raw data means of the response variable at the two levels of each factor, with a reference dashed line drawn at the global mean (51 μmol in this case) of the response data. This plot helps to compare magnitudes of main effects of each factor (Minitab Inc., 2015). To better understanding, the individual value plots with the raw data used in the construction of the main effect plot are shown in the supporting information (Figure - S 10).

The gold presence as a co-catalyst (A) showed the strongest effect obtaining, in average, more than quadruple the amount of gas when gold was present (from 20 to 82 μmol). Gold nanoparticles on titania surface act as electron sinks and have the ability to entrap the excited electrons because of its lower Fermi energy level (Subramanian et al., 2004), promoting charge carrier separation and accumulation, reducing electron/hole recombination and increasing their lifetime, inhibiting the backward reaction in addition to its important role in the creation of active sites for H_2 evolution (X. Chen, Shen, Guo, & Mao, 2010; Linsebigler et al., 1995; Serpone et al., 2016).

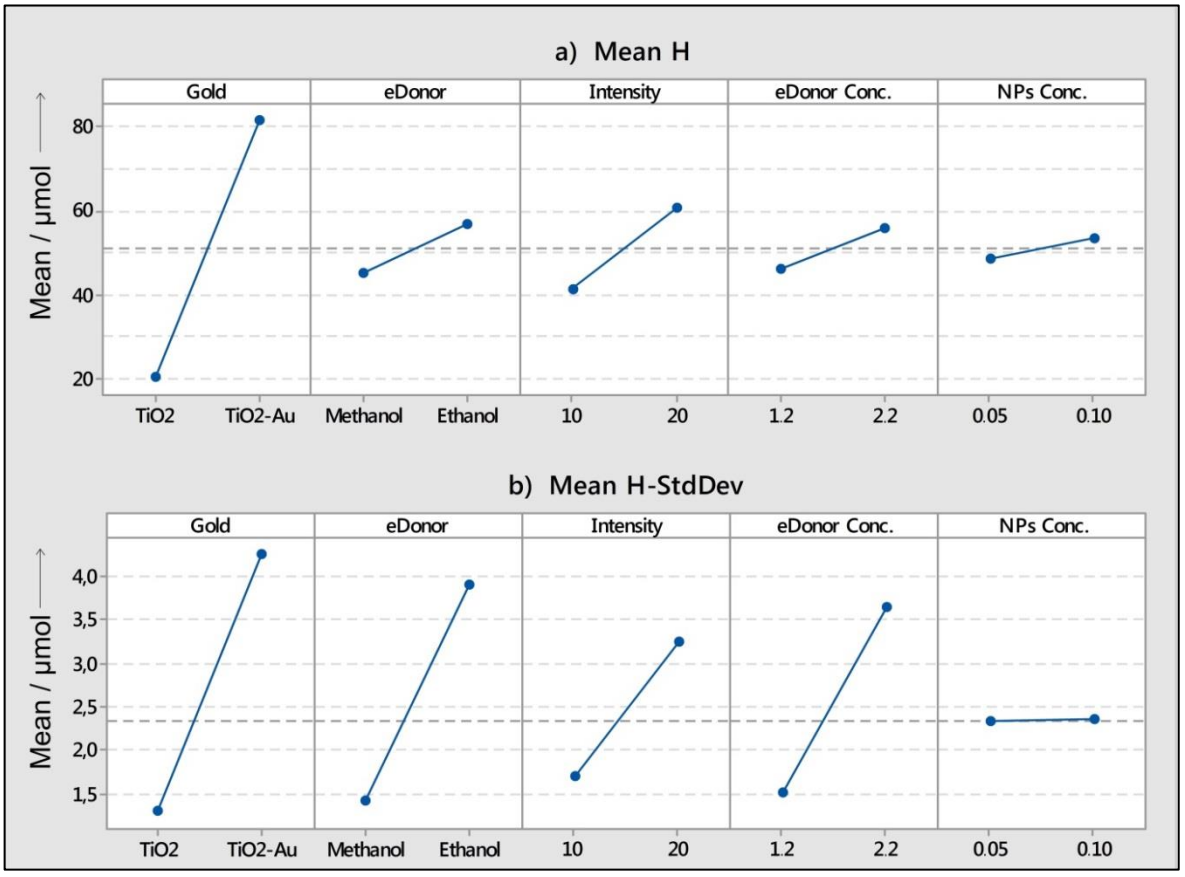

Figure 15. Main effects plot for a) total hydrogen generation (H) and b) for its variability (H-StdDev).

It should be noted that the magnitude of this increment in hydrogen generation could change depending on the metal particle size, shape, metal loading, dispersion over the TiO_2 support and synthesis method of gold nanoparticles (Al-Azri et al., 2015; Bowker et al., 2014; Oros-Ruiz et al., 2013; Ortega Méndez et al., 2014) too – factors which are not under analysis in this study.

Second, the intensity of UV light supplied to the system (C) had a big effect too on hydrogen production when its level changes from 10 to 20 mW cm^{-2}, increasing by 48%

the total H_2 generation (from 41 to 61 μmol). Beside the logical assumption of having more available photons to react, this behavior is explained by Serpone and Emeline groups (Serpone et al., 2016), who analyze how the formation of molecular hydrogen competes with back reactions such as back electron transfer from hydrogen atom to the conduction band of the photocatalyst, and with side reactions like the external electron-hole recombination process. The authors explain that at moderate light intensities, back reactions are more efficient compared to the production of hydrogen. So, higher intensities can help to generate an excess number of electrons to compete with back and side reactions, increasing the hydrogen production.

Moderate and similar average effects were observed with the change of type of electron donor (B) and its concentration (D), rising the average response by 27% (from 45 to 57 μmol) when methanol was replaced with ethanol, and 20% (from 46 to 57 μmol) when its concentration increased from 1.2 M to 2.2 M. This increment with alcohol concentration agrees with results from literature, where hydrogen production showed dependency on alcohol concentration for diluted solutions (Rossetti, 2012) up to 6-7 M (López et al., 2015; Melián et al., 2015) and where direct oxidation of alcohol molecules by photogenerated holes occurs at the TiO_2 surface with concentrations above 0.12 M (0.47 vol.%) (Ahmed, Kandiel, Ivanova, & Bahnemann, 2014; Chuan-yi Wang, Groenzin, & Shultz, 2004). Its influence is related with its sequential process and the lifetimes of the photogenerated electron-hole pairs. First, photodegradation of organic molecules is typically a multielectron loss from a sequential process that involves the formation of

intermediate products, without effective back reactions. On the other hand, recombination of trapped electrons with free holes is about 10 times faster than hole trapping, thus, there is a need for a fast removal of free holes (Rothenberger, Moser, Graetzel, Serpone, & Sharma, 1985; Serpone et al., 2016). As organic compounds that are easily oxidized photocatalytically, they act as hole scavengers and favor the separation of photogenerated electron-hole pairs, increasing charge lifetimes (Melián et al., 2015).

As the least relevant effect, doubling the nanoparticles concentration (E) from 0.05 g L^{-1} to 0.1 g L^{-1} just raised the response by 9% (from 49 to 53 μmol), even when this change of level doubles the available surface. This result agrees with literature where slight increase in hydrogen production can be observed up to a catalyst loading of 1.5 g·L^{-1}. At higher loading, the rate decreased likely due to catalyst particle aggregation, with reduction of active surface area, and to radiation scattering, which impedes transmission of the radiation throughout the photoreactor and therefore impedes the radiation from reaching the active centers of the catalyst particles (Chowdhury, Malekshoar, Ray, Zhu, & Ray, 2013; Kaur & Singh, 2007; Melián et al., 2015; Pulido Melián, González Díaz, Doña Rodríguez, Araña, & Perez Peña, 2013).

It is important to indicate that conclusions about effects of C, D and E are valid just in the space bounded by the values of each level, which were chosen without knowing the saturation levels of each factor. This means that extrapolation of these conclusions must be verified beyond these limits.

Figure 15-b exhibits the main effects on the variability of total hydrogen generation represented by its standard deviation (H-StdDev). This estimator was calculated based on the repetitions of the measurement of gas generation on each experimental run. The plot allows identifying factors A, B and D as the strongest potential variance adjustment factors, factor C as a factor with moderate weight, and factor E with almost null effect on the variability of total hydrogen generation.

Assertions previously exposed are supported by the full matrix of interaction effects in Figure 16. The distance between lines in the first row makes the big effect of factor A visible on the mean response H. Smaller but still visible effects on the mean can be seen on rows of factors B, C and D. Graphically, the relevance of two-factor interactions is defined by the lack of parallelism between the lines, and it is highlighted with cells on a white background. Interactions AC and AE endorse the thesis that factor A has a significant effect on the variability of H, showing certain sensitivity in the response depending on the value of factors C and E. When gold was not present on TiO_2, to double the intensity of light, the mean increased only by 19%, but when there was gold as a co-catalyst, the light increased the response H by 55%. Semiconductors like TiO_2 usually show increments on the charge carriers' recombination rate when intensity increases (Bell et al., 2013). This could explain why a double amount of photons hitting the surface does not double the H_2 generation, but presence of gold on the titania surface seems to successfully make recombination slower than in pristine TiO_2, due to its ability to entrap the excited electrons inside of gold nanoparticles (X. Chen et al., 2010). The metal

presence increases the efficiency of parallel multielectron transfer events, providing efficient charge separation and accumulation of charge owing to the Schottky barrier (Serpone et al., 2016).

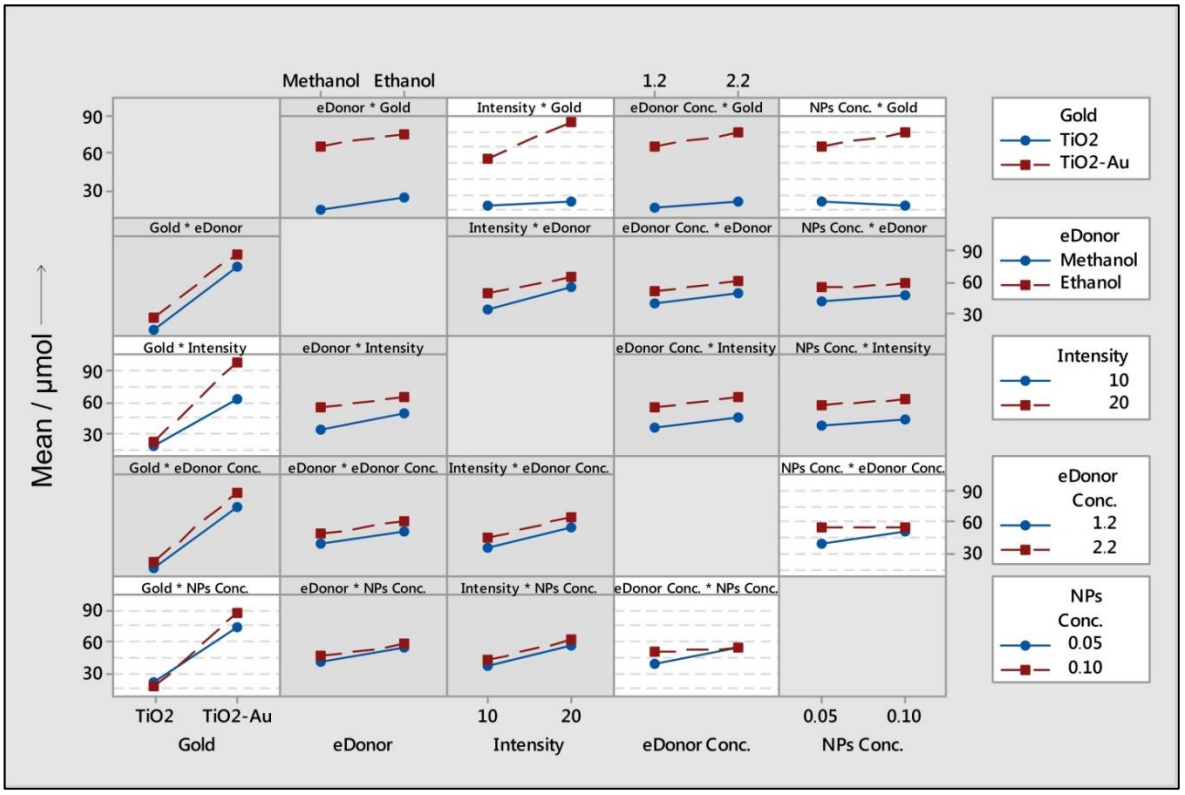

Figure 16. Interaction effects plot for total hydrogen generation (H), where white boxes show significant interactions.

AE and DE interactions seems to contradict the almost null average effect of nanoparticle concentration (E) on H observed on Figure 15-a. Both showed smaller but still significant differences between levels of A and D. When E increased from 0.05 to 0.1 g L^{-1}, TiO_2 and TiO_2-Au showed different responses, hydrogen production increased by 17% when gold

was present and slightly decreased when it was not, which It is also ascribed to the electron sink effect of gold particles.

When the alcohol concentration (D) increased from 1.2 M to 2.2 M, the effect was positive but its magnitude depended on nanoparticle concentration (E) too. So, hydrogen generation is more sensitive to changes in alcohol concentration when the nanoparticle concentration is low. The reason behind this behavior is unclear and requires further research, but one possibility could be related to the collision frequency and diffusional processes between the bulk of solution and the surface of the NPs.

3.3.3.2 Reduced model for total hydrogen generation

The use of all terms of an unreplicated experiment derives in a saturated model, which does not allow distinguishing between unsystematic and systematic variation, and therefore its predictive power is unknown (Lewis-Beck, Bryman, & Liao, 2004). A better fit can be done with a reduced model, releasing degrees of freedom through stepwise regression. Forward selection process adds the most significant factors for each step, stopping the process when all factors that are not in the model have greater p-values than the specified alpha-to-enter value (Minitab, 2014).

A reduced and hierarchical fixed effects model was developed for the total hydrogen generation (H) response with an alpha-to-enter value of 0.05 (Equation 5). The regression analysis shows a good fit to the data (adj-R^2=98.64%) and high power prediction without symptoms of overfitting (pred-R^2=96.68%). The ANOVA shows a sum of squares that

accounts for over 99% of the total variability in total hydrogen generation. Main factors contribute to a 92% of total variability, and two-factor interaction terms just 7%.

Equation 5. Regression equation in uncoded units for a reduced model for total hydrogen generation (H)

$$H = -33.3 - 5.06\,A + 6.06\,B + 1.946\,C + 28.39\,D + 520\,E + 1.601\,AC + 161.0\,AE - 252.6\,DE$$

The Pareto chart of Figure 17 presents the factors considered significant predictors of H, arranged by standardized effect from largest to smallest, allowing to compare the relative weight of main and two-factor interactions between them.

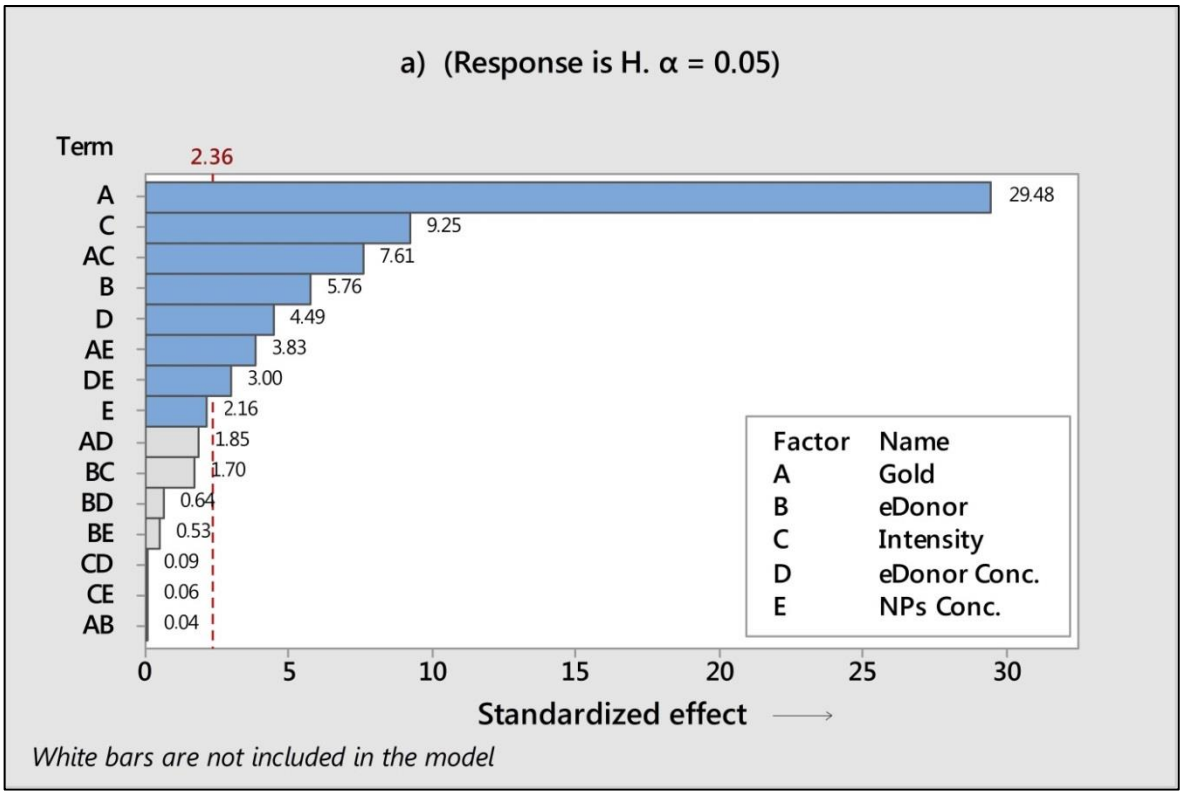

Figure 17. Pareto chart of the standardized effects for the reduced model of H.

As Figure 15-a anticipated, the presence of gold as co-catalyst (A) had the strongest effect on the total hydrogen generation (H). Standardization clarifies that, in the studied range, A had up to three times a bigger effect than C, and almost four times bigger effect than their interaction AC. It also reaffirms the deduction extracted from Figure 15-a, defining the four mentioned single factors as significant, and the inferences from the plot of interaction effects on Figure 16, with AC, AE and DE as significant predictors too. Factor E is also included in the model because it is a hierarchical model. The normal probability plot in Supporting Information (Figure - S 11) shows that just interaction DE had a negative significant effect with a small relative weight, 10 times smaller than the main effect A.

Well behavior of residuals is analyzed with plots for verification of normality, homoscedasticity and independency assumptions behind ANOVA and regression analysis. They show a good fit to normal distribution. Goodness-of-fit tests for normal distribution corroborate it: Anderson-Darling (AD=0.173; p-value=0.912), Ryan-Joiner (RJ=0.992; p-value> 0.1) and Kolmogorov-Smirnov (KS=0.100; p-value>0.15). The plot of standardized residuals versus the predicted values does not show any symptom of heteroscedasticity. Randomness in the plot of residuals versus observation order is observed, without apparent evidence of runs, trends or correlation. The standardized residuals plot shows how the size of residuals changed as a function of a predictor's settings, especially by factor E. This is not a serious symptom to question the statistical validity of the ANOVA output, but a good reason to analyze the variability adjustment factors on H (see section 3.3.6).

3.3.4 Catalyst productivity

3.3.4.1 Main and interaction effects on catalyst productivity and its variability

Since the main cost of any catalytic process is generally given by the cost of the catalyst and the loaded metal (Gololobov et al., 2009), it is very important to analyze its massic productivity. Figure 18-a presents the main effects plot on the mean of the catalyst productivity (H/cat) measured in μmol of H_2 gas per gram of catalyst per hour of reaction. The global average productivity for all treatments was 1086 μmol g^{-1} h^{-1}. Consistent with the total hydrogen production analysis of section 3.3.3.1, the gold presence as a co-catalyst (A) showed the strongest positive effect, quadrupling the average productivity from 444 to 1729 μmol g^{-1} h^{-1} when gold was loaded on titania surface.

In this case, nanoparticle concentration (E) had a strong effect too, as would be expected. The productivity decreased by 45% from 1404 to 768 μmol g^{-1} h^{-1} when E duplicated from 0.05 to 0.1 g L^{-1}. This could be explained by the possible blocking made by the particles, decreasing the available light for each particle in suspension, even when these values were set far below the usual reported experiences (Jose et al., 2013; Oros-Ruiz et al., 2013; Ortega Méndez et al., 2014). Moreover, it is possible to observe that the average productivity increased by 50% (from 876 to 1296 μmol g^{-1} h^{-1}) when the intensity of light (C) duplicated. Doubling the photons availability did not generate a double amount of H_2.

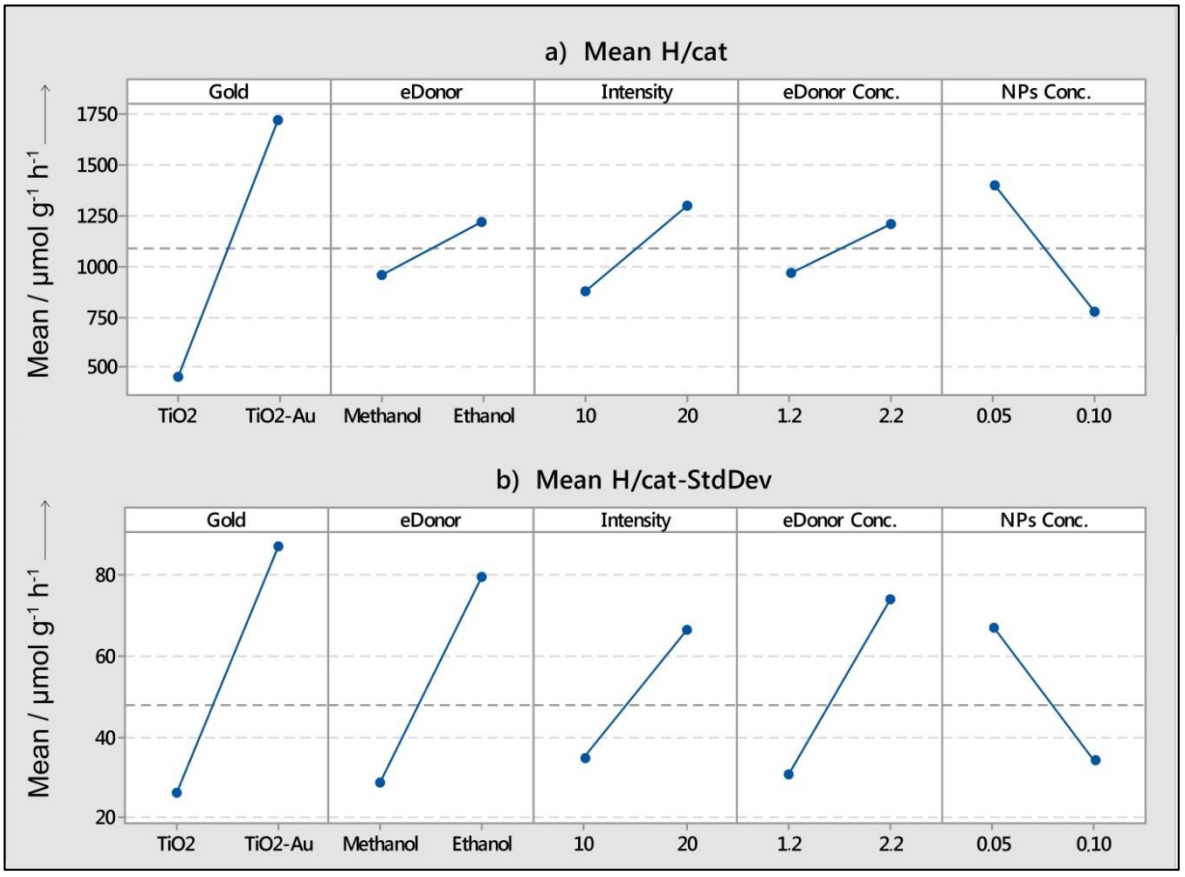

Figure 18. Main effects plot for a) catalyst productivity (H/cat) and b) for its variability (H/cat-StdDev).

This non-proportional increment needs more analysis to be clarified, but possible explanations include the mixed effect of having a faster recombination when more charge carriers are present inside the titania, or some limitation on a diffusional process when more charge porters are available.

This last fact could be coherent with the thesis of hydrogen active sites that are mostly located over the metal nanoparticles or in the metal/support interface (Daskalaki & Kondarides, 2009; Dickinson et al., 1999). So, the adsorption of reagents, the reaction and

desorption of products in such a limited and small zone defined by the gold NPs could be limiting the process. The saturation of the material was discarded as a possible cause when higher intensities were used (above the range of this experiment), and higher catalyst productivities were reached. Factors B and D had lower, but not negligible, positive effects raising the productivity by 27% (from 951 to 1,221 μmol g^{-1} h^{-1}) and 26% (from 961 to 1,211 μmol g^{-1} h^{-1}), respectively.

Figure 18-b exhibits the main effects on the variability of the catalyst productivity represented by its standard deviation (H/cat-StdDev). The plot shows five factors as likely significant variance adjustment factors, with factors A, B and D standing out. Deeper analysis is required to identify which factor is the strongest.

3.3.4.2 Reduced model for catalyst productivity

A reduced and hierarchical model was developed for the catalyst productivity (H/cat) with an alpha-to-remove value of 0.10 (Equation 6). The regression analysis shows a good fit to the data (adj-R^2=94.99%) and high power prediction without symptoms of overfitting (pred-R^2=87.79%). The ANOVA shows a sum of squares that accounts for 98% of the total variability in the H_2 productivity of catalyst. Main factors contribute an 89% of total variability, and two-factor interactions terms just 9%.

Equation 6. Regression equation in uncoded units for a reduced model for catalyst productivity (H/cat)

$$H/cat = -59 + 547\,A + 135.2\,B + 42.04\,C + 865\,D + 1{,}199\,E + 33.68\,AC - 5{,}468\,AE - 8{,}194\,DE$$

The same factors are included in models for H/cat (Equation 6) and H (Equation 5), with significant effects from the five main factors and interactions AC, AE and DE, but their relative weights (Figure 19) and the sign of effects (Supporting information, Figure - S 12) show changes.

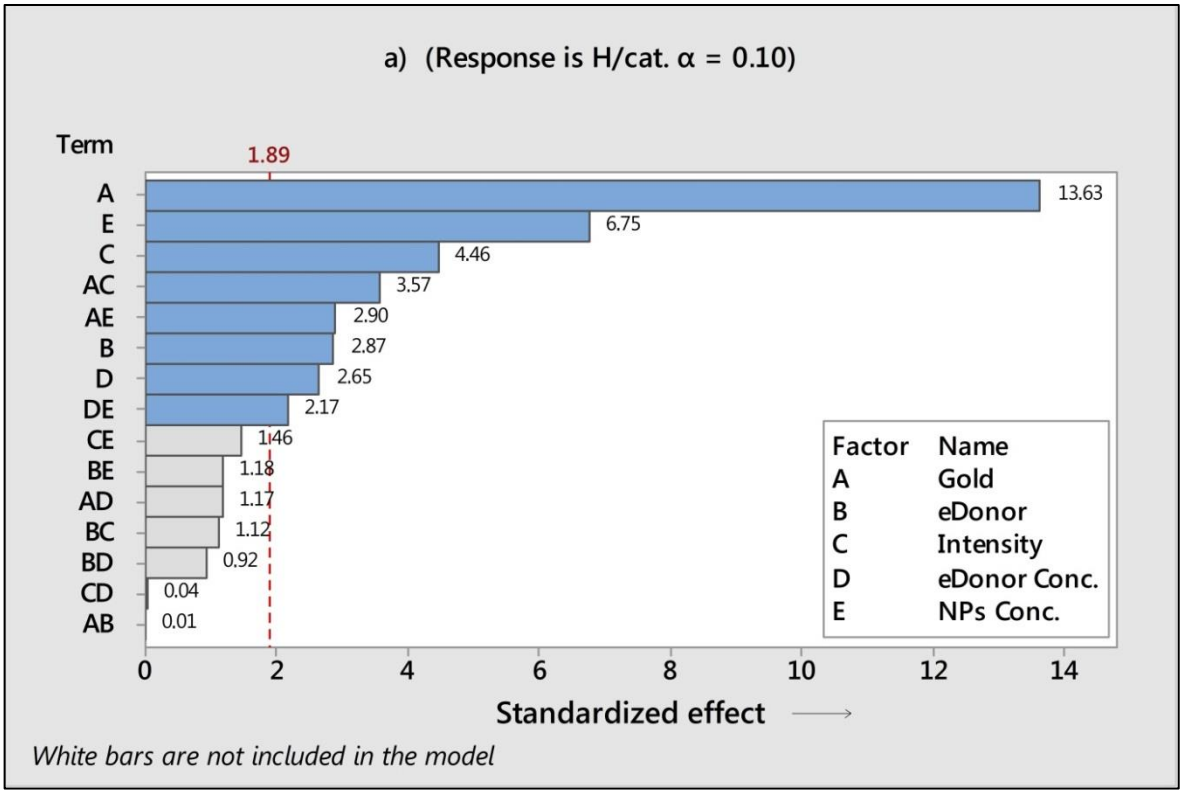

Figure 19. Pareto chart of the standardized effects for the reduced model of H/cat.

The biggest change appears on NPs concentration (E) with a strong negative effect, which is 50% of the effect of factor A, which is the strongest again. So, unlike increasing concentrations of catalyst that led to a higher production of hydrogen, the massic

productivity of catalyst decreased, most likely due to the shielding effect. The negative effect of E could be another reason for the change of sign shown by interaction AE.

The same analysis presented in section 3.3.3.2 shows the well behavior of residuals, validating normality, homoscedasticity, and independency assumptions behind ANOVA and the regression analysis.

3.3.5 Electron donor productivity

3.3.5.1 Main and interaction effects on electron donor productivity and its variability

Another relevant input to this process is the electron donor, since these organic compounds are currently found in industrial wastewaters, they could represent a significant chance to reduce costs in future real scale applications. This fact makes it relevant to analyze the productivity of the electron donor (H/eDon), measured in μmol of H_2 gas per mol of electron donor per hour of reaction. Figure 20-a shows the global average productivity for all treatments, which reaches 46 μmol mol^{-1} h^{-1}. This value is lower than that of other works. This could be linked to the very high ratio between moles of the electron donor and catalyst availability, since a very low nanoparticle concentration was used, there could be an excess of alcohol for this low amount of available NPs. In this experiment, this ratio went from 12 to 44 mol g^{-1} and a maximum of 120 μmol mol^{-1} h^{-1} was reached on treatment *ace* when the ratio was 12 mol g^{-1}. For example, Ortega Méndez (Ortega Méndez et al., 2014) reach productivities of around 590 μmol mol^{-1} h^{-1}, using a ratio of 6 mol g^{-1} on NPs P25 type.

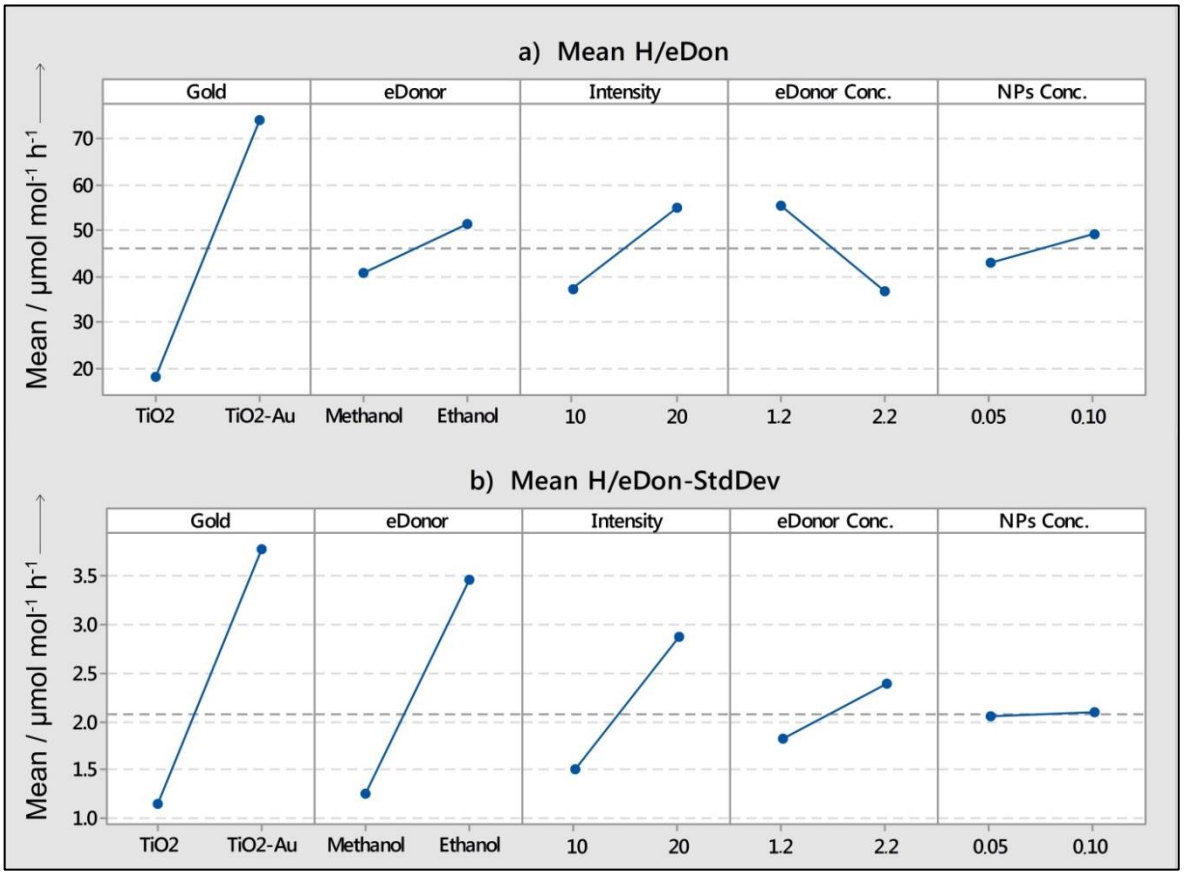

Figure 20. Main effects plot for a) electron donor productivity (H/eDon) and b) for its variability (H/eDon-Std Dev).

Following the same behavior of sections 3.3.3 and 3.3.4, the stronger positive effect corresponded to the gold presence as co-catalyst (A), quadrupling again the average productivity from 17.7 to 74.3 µmol mol^{-1} h^{-1}. As expected, electron donor concentration (D) and intensity of UV light (C) had strong effects too, very similar in magnitude, but with opposite signs. Doubling C generated a raising of 49%, from 37 to 55.1 µmol mol^{-1} h^{-1}, but when D increased from 1.2 to 2.2 M, the alcohol productivity decreased by 34%,

from 54.6 to 36.5 μmol mol^{-1} h^{-1}. We could assume that the increment in available surface of catalyst used in this experiment was not enough to equate the increment in availability of reactant, and the link between the available area of catalyst and amount of alcohol molecules requires deeper analysis. Smaller effects were observed with the change of electron donor (B), which raised productivity by 27% (from 40.6 to 51.5 μmol mol^{-1} h^{-1}) when ethanol replaced methanol, and doubling the concentration of nanoparticles (E) from 0.05 to 0.1 g L^{-1}, increasing productivity just by 14% (from 43.1 to 49.0 μmol mol^{-1} h^{-1}), which differs from recent works where methanol (López et al., 2015) and glycerol (W.-T. Chen et al., 2015) show a bigger influence on hydrogen production rates.

Figure 20-b presents the main effects on the variability of the electron donor productivity represented by its standard deviation (H/eDon-StdDev). The plot shows factors A, B and C as likely significant variance adjustment factors. Factor E has a null effect on the variability of alcohol productivity, and it is not clear the significance of D.

3.3.5.2 Reduced model for electron donor productivity

A reduced and hierarchical model was developed for the electron donor productivity (H/eDon) with an alpha-to-remove value of 0.10 (Equation 7). The regression analysis shows a good fit to the data (adj-R^2=91.02%) and moderately high power prediction with low symptoms of overfitting (pred-R^2=82.97%). The ANOVA shows a sum of squares which explains 95% of the total variability in the H_2 productivity of catalyst. Main factors contribute with an 86% of total variability, and two-factor interaction terms, just 9%.

Equation 7 - Regression equation in uncoded units for a reduced model for the hydrogen yield of the electron donor (H/eDon).

$$H/eDon = 51.2 + 28.2\,A + 5.45\,B + 1.814\,C - 19.06\,D + 1.518\,AC - 13.34\,AD$$

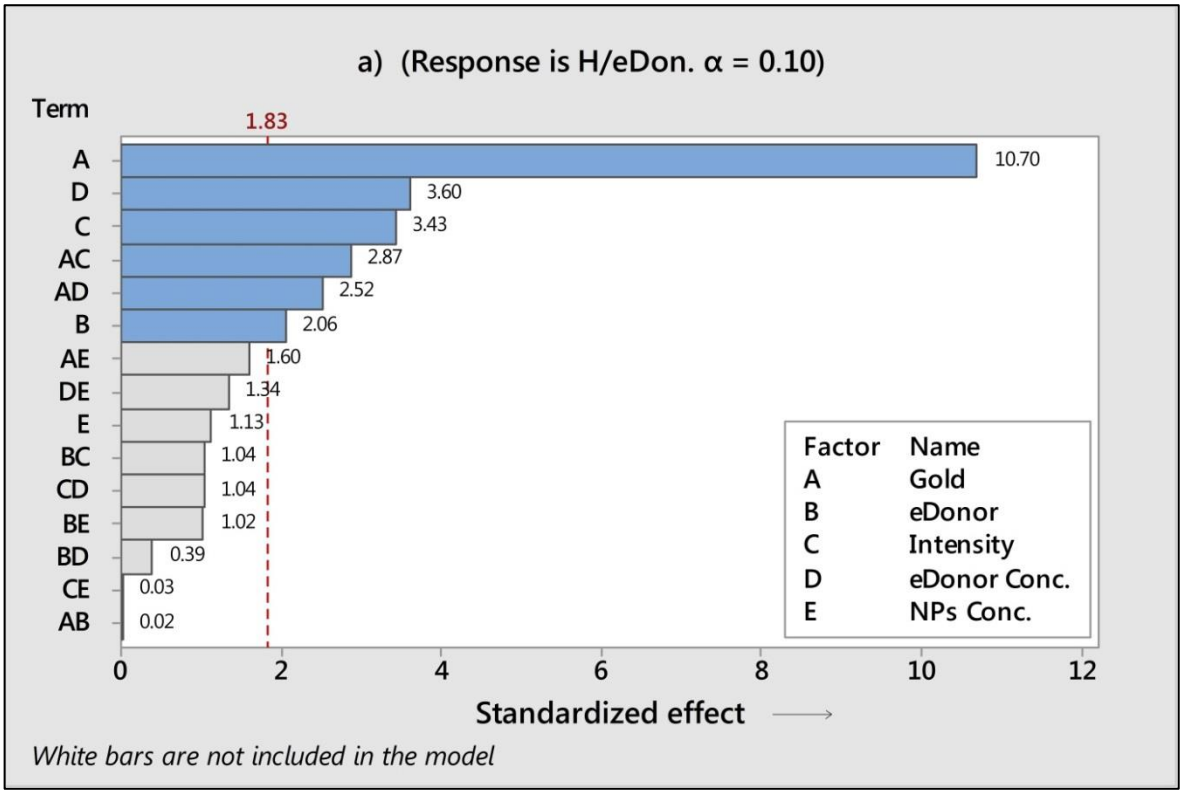

Figure 21. Pareto chart of the standardized effects for the reduced model of H/eDon.

Unlike the previous models for H (Equation 5) and H/cat (Equation 6), in this case nanoparticle concentration (E) is not significant, neither are their interactions. Supremacy of A as the main factor is still observable (Figure 21). Also, the negative effect of electron donor concentration (D) stands out (See supporting information, Figure - S 13). AC and AD are the only significant two factor-interactions with similar relative weights, both

linked to the interaction of A with the next two most important factors. Similar to what happened with nanoparticle concentration in section 3.3.4.2, even when increasing concentrations of electron donor leads to a higher production of hydrogen, the productivity of the electron donor decreases.

The same analysis presented in section 3.3.3.2 shows a well behavior of residuals, validating normality, homoscedasticity, and independency assumptions behind ANOVA and regression analysis.

3.3.6 Variability adjustment factors

The analysis of variability done for these three responses showed a ratio effect indicating that standard deviation increased in a factor of 3.9, 2.7, 1.9, 2.6 and 1.0 when A, B, C, D and E changed from lower to higher levels, respectively. Interaction effects AE, BC, BD and DE also had relevant ratio effects of 1.8, 0.5, 0.6 and 0.6, respectively.

Figure - S 14-S16 in the supporting information shows the Pareto chart visualizing the magnitude of the standardized effects on variability of total hydrogen generation (H-StdDev), variability of catalyst productivity (H/cat-StdDev), and variability of electron donor productivity (H/eDon-StdDev). They clarify how A and B had the strongest effects on variability, which is consistent with observations based in Figure 15-b, Figure 18-b and Figure 20-b. As a conclusion, single factors A, B, C and D are a good set of possible variance adjustment factors for total hydrogen generation. The five factors are significantly related to differences in the variability of catalyst productivity, and only A, B

and C are relevant to adjust the variability of electron donor productivity. Interactions BC and AE need to be considered for the three responses under analysis.

3.3.7 Analysis of productivities space

As a half-fraction factorial experimental design, only half of the total possible treatments were run, so the second half fraction was predicted using the adjusted models in Equation 6 and Equation 7. These values are presented in Figure 22, which shows the space formed by productivities of catalyst (X axis) and the electron donor (Y axis), where best treatments can be easily detected: Treatment abcd can maximize the catalyst productivity; treatment ace maximizes the electron donor productivity; and abc treatment has the best compromise between both types of productivities. Figure 22 also shows two experimental points for validation, with less than 9% of difference in the worst case. Figure 23-A to E show how the change of level in each single factor generates a jump in the responses in the productivities space, where the positive effect of factors A and C are visually relevant. We may also see the negative effect of factor D on electron donor productivity and factor E on catalyst productivity. As mentioned in the previous analysis, the effect of factor B was smaller than other single factors, so it is not visually clear in the productivities space.

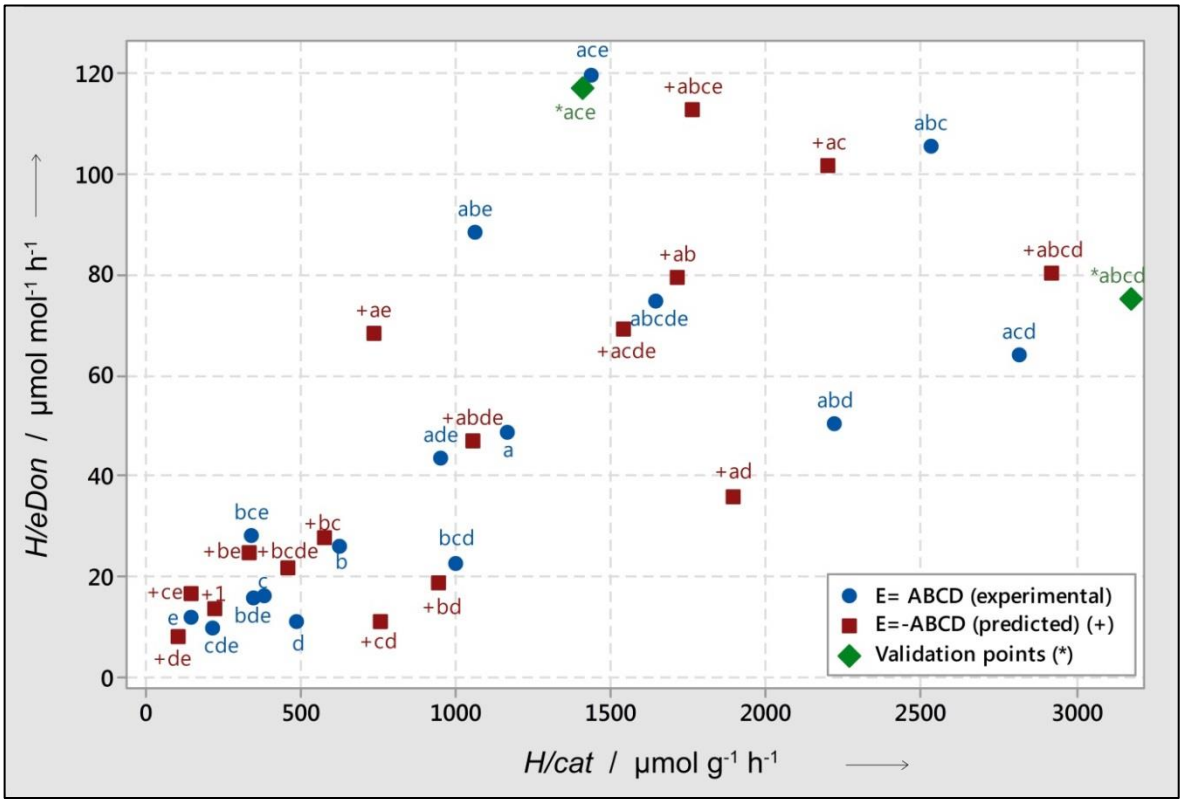

Figure 22. Productivities space formed by experimental and predicted productivities.

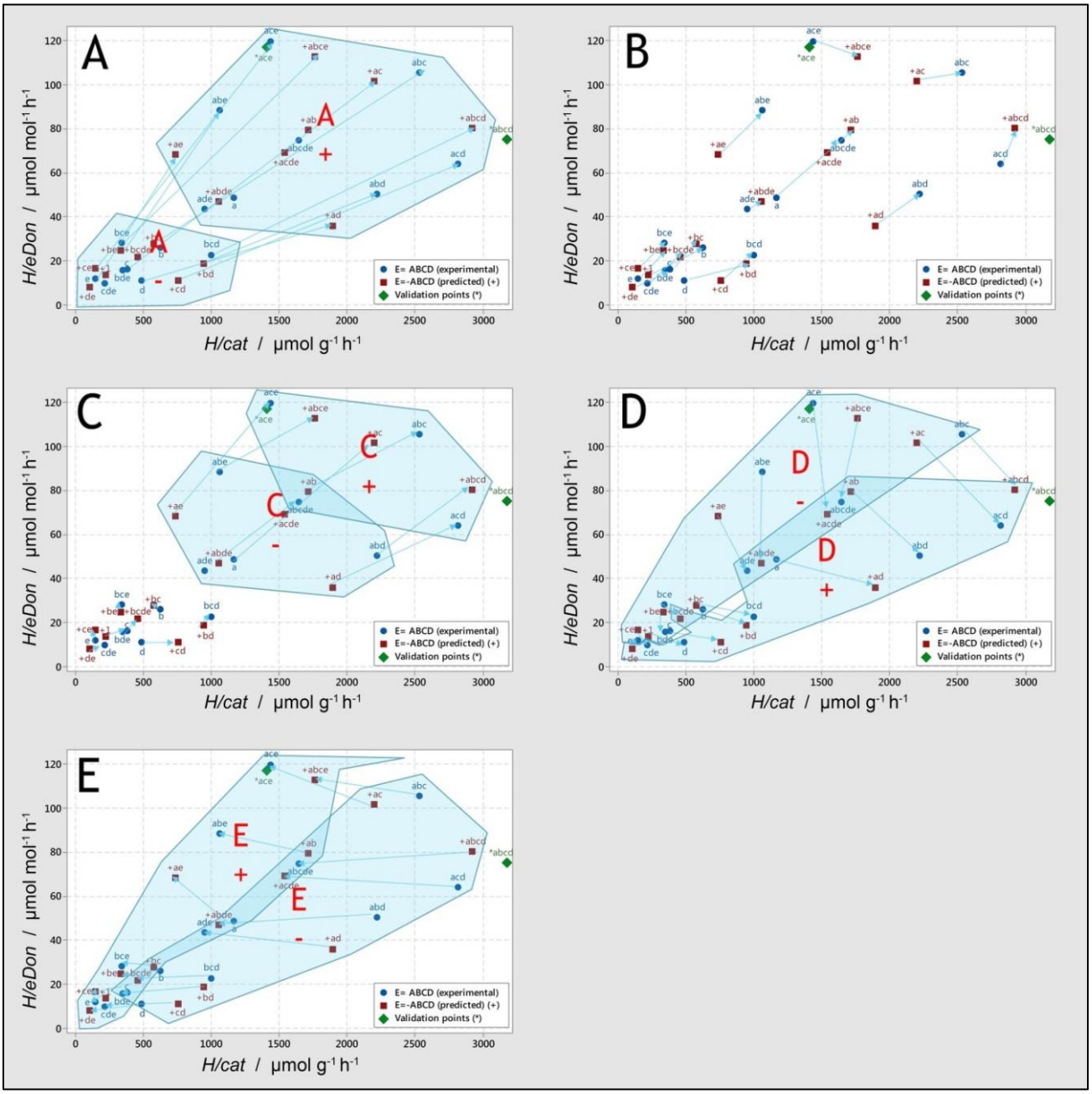

Figure 23. Effect of single factors on productivities space.

3.4 Conclusions

The presence of gold as co-catalyst (A) is definitely the factor with the highest weight on each of the three responses under analysis, followed by the intensity of light (C) and their interaction (AC). In every case, factor A has a weight three times higher than C, and almost four times higher than AC. Concentration of catalyst (E) and concentration of electron donor (D) become relevant for their respective productivities, in similar magnitude to the intensity of light. Relative to the type of alcohol (B), ethanol showed slightly better average productivities than methanol, which disagrees with some sources (W.-T. Chen et al., 2015; López et al., 2015), and its effect is comparatively smaller and less clear than other single factors.

Treatment abcd maximizes the catalyst productivity reaching 2,925 μmol g^{-1} h^{-1}, treatment ace maximizes the electron donor productivity with 120 μmol mol^{-1} h^{-1}, and abc treatment has the best compromise between both type of productivities, resulting in productivities of 2,532 μmol g^{-1} h^{-1} and 106 μmol mol^{-1} h^{-1}. Further work is necessary to realize target productivities of 2–3 mmol g^{-1} min^{-1} under direct sunlight to attract industry interest (Dosado et al., 2015).

4 OPERATIONAL CONDITIONS AFFECTING FORMALDEHYDE AND FORMIC ACID FORMATION AS BY-PRODUCTS OF HYDROGEN PRODUCTION VIA PHOTOREFORMING OF METHANOL

4.1 Introduction

4.1.1 Relevance of formaldehyde and formic acid

Formaldehyde is the simplest aldehyde which is manufactured on an industrial scale due to its widespread applications (Transparency Market Research, 2013). It is used for production of urea formaldehyde (UF) resin, phenol formaldehyde (PF) resin, melamine formaldehyde (MF) resin and rigid polyurethane (PU) foams (ICIS, 2008; Transparency Market Research, 2013). Most of them are widely used in the construction industry and automotive industry. UF and PF account for over half of the world's total formaldehyde consumption (McGregor group, 2014). Commercially, it is sold in liquid form as formalin (Transparency Market Research, 2013), a 37% aqueous solution with 10% methanol (ICIS, 2008).

The global production capacity of formaldehyde surpassed 46.4 million tons in 2012, and in 2017, it is anticipated to exceed 52 million tons (McGregor group, 2014). The Asian-Pacific region held a share of 56% of the world's total formaldehyde capacity and it is also the main consumer (57% of global consumption), and just China accounts for over 51% of the global capacity (McGregor group, 2014).

It is expected that the revenue generated by the global formaldehyde market will reach USD 18,000 million by 2018 (Transparency Market Research, 2013).

Two important routes are used in the industrial production of formaldehyde via a combination of partial oxidation and dehydrogenation of methanol. Both are catalytic methods and are highly energy demanding, working at temperatures between 400°C and 650°C. Nowadays, about 55% of the industrial production is based on silver catalyst (Maldonado, Fierro, Birke, Martínez, & Reyes, 2010).

Likewise, the global formic acid market was valued at USD 517 million in 2016 and is expected to be valued at USD 879 million by the end of 2027. The Asia-Pacific region is the largest market for formic acid too, with more than 35% of the volume share in the global market. Formic acid is mostly produced via carbonylation of methanol and it is mainly used in animal feed, silage preservatives, dyeing and finishing textiles, rubber & leather production and others (Market research Future, 2017).

In this market context, it is worthy to evaluate new production systems for formaldehyde and formic acid, both to reduce energy consumption and to find potential savings in catalyst production. Therefore, the generation of formaldehyde and formic acid as intermediate byproducts in the photocatalytic hydrogen generation via photoreforming of methanol is of great interest as an alternative production system of these compounds for the future.

4.1.2 Formaldehyde and formic acid as by-products of photocatalytic hydrogen

Some researchers have faced the rising energy demand by proposing a photocatalytic hydrogen production process (Bolton, 1996; C. A. Grimes et al., 2008; Ohta & Veziroglu, 1976) as a way to store solar energy in chemical energy (Teets & Nocera, 2011) using nano-sized semiconductors (Varas-Concha, Guzmán, Isaacs, & Sáez-Navarrete, 2017).

Titanium dioxide is the most widely used semiconductor for photocatalytic applications because it is stable, noncorrosive, harmless, abundant, inexpensive (Oros-Ruiz et al., 2013), and able to generate the water splitting reaction and photo-reforming of several organic compounds (Varas-Concha et al., 2017).

Many studies use methanol as a sacrificial agent because it captures the positive charge carriers more rapidly than other alcohols (López et al., 2015; Tamaki et al., 2006); it has a high hydrogen/carbon ratio and it can be obtained from biomass (Hamelinck & Faaij, 2002; López et al., 2015) (Varas-Concha et al., 2017).

The main intermediaries involved in methanol photoreforming are formaldehyde, formic acid and CO_2. The first and second are valuable by-products and increase the chances of economic feasibility in this type of photocatalytic systems.

As reference, formaldehyde solution at 37% purity costs 2-3 times more than pure methanol, and formic acid at 98% purity can cost 200 times more than the pure methanol (Merck Group, 2017). Actually, these prices could lead to change the focus, leaving the hydrogen generation as a secondary by-product. Methane, methyl formate, acetaldehyde,

dimethyl ether and ethane are other by-products, but they appear in insignificant amounts (Melián et al., 2015).

In general, the main accepted mechanism for the methanol reforming reaction takes place in two stages: involving formation of formaldehyde first (1), then formic acid (2), and finally CO_2 (3) (Ortega Méndez et al., 2014):

$$CH_3OH + (h\nu + TiO_2\text{-}Au) \rightarrow CH_2O + H_2 \quad (1)$$

$$CH_2O + (h\nu + TiO_2\text{-}Au) \rightarrow HCOOH + H_2 \quad (2)$$

$$HCOOH + (h\nu + TiO_2\text{-}Au) \rightarrow CO_2 + H_2 \quad (3)$$

4.1.3 Factors affecting formaldehyde and formic acid generation

Reported yields of hydrogen produced via photocatalytic methods have been disappointingly low (Serpone et al., 2016), so it is crucial to focus research on the development of materials science and strategies to achieve significant progress both in water splitting as in photoreforming.

Formaldehyde and formic acid formation are usually correlated with the hydrogen production levels, so the operational conditions impacting the hydrogen yields affect the generation of by-products too.

Among the strategies and operational conditions under study to improve the productivities of hydrogen, depositing noble metal nanoparticles on the photocatalyst surface stands out. The formation of a Schottky barrier at the metal/TiO_2 interface helps the photopromoted

electrons migrate preferentially from the conduction band of the semiconductor to the metal, resulting in a decrease in electron–hole pair recombination. Various metals have been used as co-catalysts on a titanium surface including Pt (Beltram et al., 2015; Jung et al., 2015; Lu et al., 2015), Pd (Gomathisankar, Yamamoto, et al., 2013; X. Liu et al., 2014; H. Yan et al., 2009), Cu (Clarizia et al., 2014; Gomathisankar, Hachisuka, et al., 2013; Jung et al., 2015), Ni (Balcerski et al., 2015; Xiying Li et al., 2014; Melián et al., 2014; Y. Xu & Xu, 2015), Rh (Gomathisankar, Hachisuka, et al., 2013; D. Wang et al., 2015; F. Zhang et al., 2012), Ag (Ansari et al., 2015; S. Yang et al., 2016) and Au (Al-Azri et al., 2015; Jovic, Chen, et al., 2013; Ortega Méndez et al., 2014; Sinatra et al., 2015). Of these, the best yields in terms of photocatalytic production of H_2 have been obtained with Pt/TiO_2 and Au/TiO_2 (Naldoni et al., 2013)(Ortega Méndez et al., 2014).

Another way of increasing efficiency is by varying the concentration of the alcohol submitted to the photoreforming process. These sacrificial agents are easily oxidized photocatalytically and so they act as hole (h+) scavengers in the photocatalysis process. They favor the separation of photogenerated electron-hole pairs, increasing charge lifetimes and enabling the migration of electrons to the photocatalyst surface. An extensive number of organic compounds have been tested, with the best results apparently being obtained with C1- C3 alcohols in water-alcohol mixtures (Dal Santo, Gallo, Naldoni, Guidotti, & Psaro, 2012; Gallo et al., 2012; Melián et al., 2015; Mizukoshi, Sato, Konno, & Masahashi, 2010), where methanol has provided the highest rates of H_2 gas (Melián et al., 2015). Pulido Melián et al. (2015) found that in their photocatalytic system,

the amounts of both formaldehyde and formic acid increased with methanol concentration up to 6.1 and 9.8 M, respectively.

Both the presence of noble metals and the use of alcohols as hole scavengers are widely studied factors influencing hydrogen production as independent factors. Particle size and loading amount of co-catalysts (Al-Azri et al., 2015; Ayati et al., 2014; Du & Lu, 2014; Lu et al., 2015; Majeed et al., 2016; Murdoch et al., 2011; Subramanian et al., 2004; J. Yang et al., 2012), type and concentration of sacrificial agents (Al-Azri et al., 2015; Beltram et al., 2015; W.-T. Chen et al., 2015; Kandiel et al., 2011; Kawai & Sakata, 1980; López et al., 2015; Lyubina et al., 2013; Oros-Ruiz et al., 2013; Sadanandam et al., 2013; Taboada et al., 2014b) have been studied too. Less studied but equally relevant for bigger scale applications are the effects of light intensity (Bell et al., 2013) and photocatalyst concentration (Nsib et al., 2015) because of the possible screening effect on the bulk of the reaction media (Varas-Concha, Guzmán, Isaacs, & Sáez-Navarrete, 2017).

So many options create a very wide net of possible combinations, making it difficult to optimize and quantify the effect of the numerous variables affecting hydrogen productivity and the productivity of their by-products. Most of these factors have been studied as isolated and independent factors, but not as interactive elements with possible synergies or counterproductive effects.

In this context, this work studies the joint effect of four relevant factors: (A) presence of gold as co-catalyst, (B) intensity of light, (C) concentration of methanol and (D)

concentration of nanoparticles. Our last published work (Varas-Concha et al., 2017) deeply analyzed their effect on the hydrogen production using low concentrations of nanoparticles, since a gap exists in the knowledge about photocatalysis using concentrations of nanoparticles below 0.1 $g \cdot L^{-1}$. Along the same lines, this present work explores their combined effect on the formation of formaldehyde and formic acid as potential valuable by-products of the hydrogen production process via photoreforming of methanol, in a low range concentration of nanoparticles.

The factorial design of experiments (DOE) is an empirical modelling technique used to evaluate the relationship between experimental variables and corresponding responses (Chowdhury et al., 2011; Krishna Prasad & Srivastava, 2009; Varas-Concha, Guzmán, Isaacs, & Sáez-Navarrete, 2017). This technique allows quantifying the effect of several factors affecting a response simultaneously. In this case, we evaluate the main and interaction effects of these four mentioned factors on four responses: production of formaldehyde (F), production of formic acid (FA), catalyst productivity for formaldehyde formation (F/cat) and catalyst productivity for formic acid formation (FA/cat).

Finally, we explore the relation between hydrogen and by-product generation.

4.2 Experimental Section

More details about the experimental conditions used in this work can be found in our previous publication (Varas-Concha et al., 2017).

4.2.1 Reagents

For the synthesis of TiO_2-Au composites, Aeroxide® P25 Titanium(IV) oxide nanopowder, gold(III) chloride hydrate, sodium borohydride, and tri-sodium citrate dehydrate were used as received without further purification. Hydrochloric acid fuming 37% for analysis was used in solution (0.1 N).

For photocatalytic reactions, methanol was used without further purification. For formaldehyde and formic acid determination, chromotropic acid ($(HO)_2C_{10}H_4(SO_3Na)_2 \bullet 2H_2O$, Sigma Aldrich^{TM}) was used in a solution 1% w/w, hydrochloric acid was used in a solution 2 M, powder magnesium (Merck^{TM}) and sulfuric acid (Merck^{TM}) were used as received.

4.2.2 Instruments

The photocatalytic reactors were implemented within a Shin Saeng, model SBOD-201 incubator with temperature control. The system used: four 50 mL Erlenmeyer flasks with septum of silicone on their caps, over magnetic stirrers; a USB thermocouple datalogger Pico Technology, model TC-08; a USB datalogger Extech, RHT50 to record humidity, temperature, and barometric pressure; four 50 W UV-LED light chips of 375 nm, Justar, model JX-50UV10X5G.

Characterization of composites used: an UV-VIS photodiode array spectrophotometer Shimadzu, model MultiSpec-1501; a Malvern Zetasizer Nano ZS instrument; an ICP-AES Varian Liberty Series II Axial; a Philips Tecnai 12 Biotwin TEM.

Radiation measurements were taken using a PCE Instruments UVA-UVB radiation sensor, model PCE-UV34.

Determination of hydrogen was done using a fast gas chromatograph DANI, model Master GC, with a VICI thermal conductivity detector, model TCD-NIFED-220DI.

4.2.3 Synthesis of partially covered TiO_2–Au nanoparticles

The synthesis procedure is based on the proposed methods by Fu, Vary and Lin (Fu et al., 2005), and Li, Guo and Zhang (W. Li et al., 2010a), which works at room temperature and pressure. First, a colloidal suspension (100 mL) was prepared with TiO_2 (4 mM) and $HAuCl_4$ (0.2 mM). After an ultrasonic bath (5 min), pH of the reaction media was adjusted (2.2) by dropwise addition of HCl solution (0.1 N). After a second ultrasonic bath (5 min), sodium citrate solution (5 mL, 25 mM) was added to the colloidal suspension. After stirring (5 min), a solution (5 mL) of citrate (25 mM) and $NaBH_4$ (0.1 M) was added.

4.2.4 Design of experiment

The 2^{4-1} half-fraction factorial completely randomized experimental design used in this work has a IV resolution, where no main effects are aliased with any other main effect or 2-factor interactions, but some 2-factor interactions are aliased with other 2-factor

interactions and main effects are aliased with 3-factor interactions. Based on the sparsity-of-effects principle, three-factor or higher interactions are negligible, so the four main effects do not confound with other main effects and two-factor interactions (Montgomery, 2012). The design was constructed by selecting I = ABCD as the generator, and setting the levels of the fourth factor to D = –ABC (Table 7). Blocking was not used in this design to avoid confounding two-factor effects with block effects. It was verified that batching of experiments was not a significant source of nuisance, keeping temperature and pressure under control; with the same operator, equipment, and reagents for every photocatalytic essay and measurement routine in the whole experiment.

Regression models for mean response were proposed as transfer functions between the factors and the four responses mentioned in section 4.1.3. They were constructed by analysis of variance (ANOVA) with a level of confidence α = 95%. The adjusted coefficient of determination (adj-R^2) was used to compare models with a different number of predictors, and the predicted coefficient of determination (pred-R^2) to determine how well the model predicted new observations and the overfitting of the model (Frost, 2013).

4.2.5 Photocatalytic experiments

Each experimental unit was integrated by a batch reactor covered with aluminum foil with a square window (7 cm^2). The reactor was illuminated with a 375 nm UV-LED light focusing on the window, parallel to the surface of the reactor, during 11 hours under slow

stirring. Intensity of light was regulated by the separation distance between the surface and the LED chip (see Figure 24-a).

Each reactor contained a volume of solution (63 mL), and a headspace (4 mL) filled with argon gas at barometric pressure (950 kPa). It was sealed with PTFE tape and purged with argon (10 min) through the silicon septum using needles under stirring (see Figure 24-b). The solutions of each reactor and the setting of the required light were prepared according to the combinations detailed in Table 7 and the levels described in Table 4, with previous randomization. The experiment was developed within the incubator with temperature control, with space for four experimental units running at the same time. The temperature of the incubator (5°C) was set to increase the radiation delivered by the UV-LED lights. The heat released by the lights raised the temperature of the chamber (20°C) and the temperature of the reactors (25°C average) (see Figure 24-c).

4.2.6 Formaldehyde and formic acid measurement

Determination of formaldehyde and formic acid concentrations was done following reported colourimetric methods (García Morgado, 2013; Guzmán, 2016; Paul et al., 1998; Ramos Sende et al., 1995).

For formaldehyde determination, 500 μL of solution after photocatalysis, 500 μL of chromotropic acid solution, and 4000 μL of sulfuric acid reacted during 45 minutes between 80-100°C. Then, 2000 μL of nanopure water was added, and after 20 minutes the

UV-vis spectra was recorded, measuring the absorbance at 575 nm. The concentration of formaldehyde was calculated using a calibration curve represented by the equation 8:

$$[CH_2O]=(\text{Abs}-0.01)\cdot 0.191^{-1}\ \ mg\cdot L^{-1} \qquad \text{Equation 8}$$

For formic acid determination, 500 μL of solution after photocatalysis, 500 μL of hydrochloric acid solution, and a spatula tip of powder magnesium reacted during 10 minutes under constant stirring. Then, the procedure for formaldehyde determination was repeated on the resultant solution, but the concentration of formic acid was calculated using a different calibration curve represented by the equation 9:

$$[CH_2O_2]=(\text{Abs}-0.026)\cdot 0.274^{-1}\ \ mg\cdot L^{-1} \qquad \text{Equation 9}$$

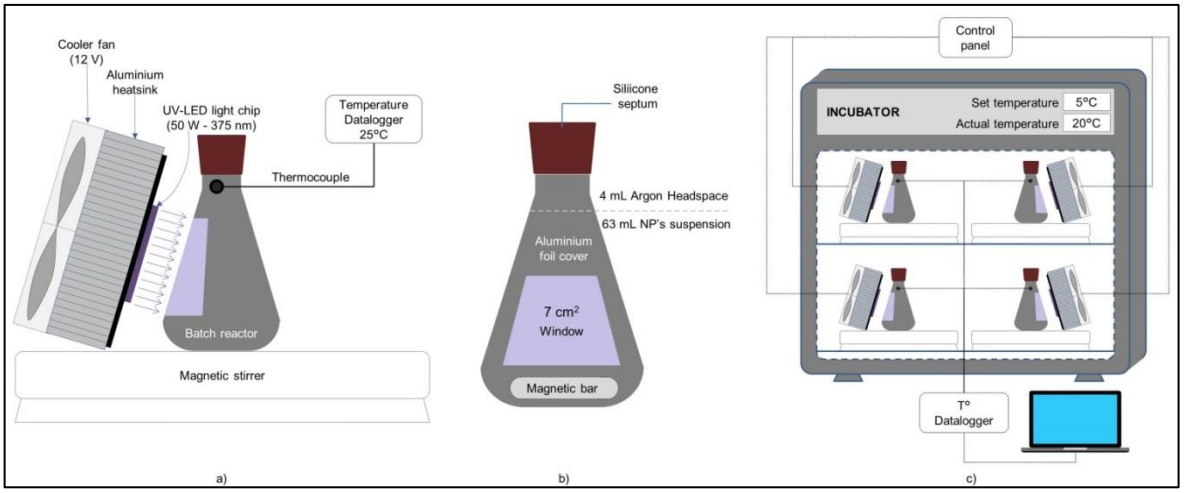

Figure 24. Experimental setup: a) experimental unit configuration; b) batch reactor; c) system configuration with four experimental units running at the same time.

4.3 Results and Discussion

4.3.1 Characterization of the photocatalyst

The photocatalyst used in the experiments was Aeroxide® P25 titanium oxide nanopowder. For some experimental runs the P25 TiO_2 was modified with gold nanoparticles on the surface using a molar ratio Ti:Au=20:1, and gold presence was verified by UV-vis spectroscopy. The absorbance spectrum for TiO_2-Au showed the characteristic peak around 530 nm and was consistent with reported information (Fu, Vary, & Lin, 2005; W. Li, Guo, & Zhang, 2010b). Inductively coupled plasma atomic emission spectroscopy (ICP-AES) ratified the presence of Ti (6.12 mg L^{-1}) and Au (1.00 mg L^{-1}), which is equivalent to a metal loading of 8.9 wt.%.

In terms of particle size, dynamic light scattering (DLS) analysis showed a distribution with a peak around 46 nm of radius for the TiO_2-Au agglomerates. For the gold nanoparticles, the size distribution had a peak around 4.5 nm of diameter. Images were obtained by transmission electron microscopy (TEM) and analyzed using ImageJ (Rasband, n.d.). One of them is shown in Figure 25.

Normalized UV-visible absorption spectra, particle size distribution from DLS analysis for agglomerates, and particle size distribution for gold nanoparticles from ImageJ analysis were reported in full in our last published work (Varas-Concha, Guzmán, Isaacs, & Sáez-Navarrete, 2017).

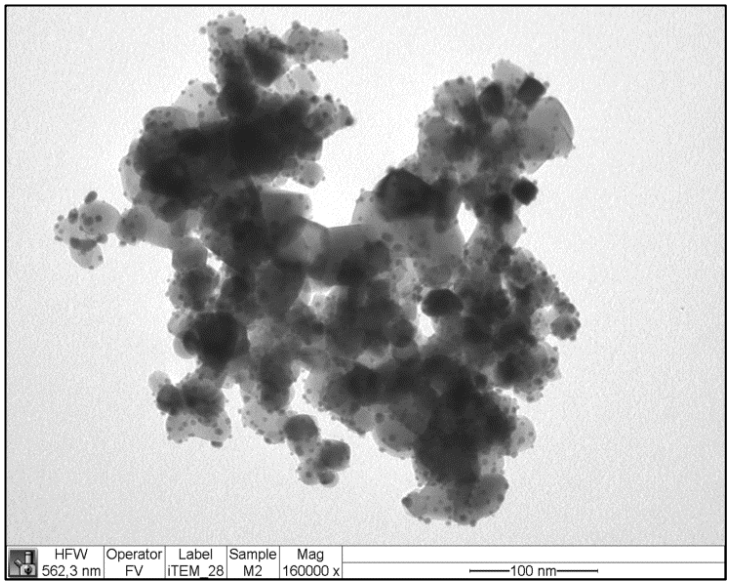

Figure 25. TEM image for an agglomerate TiO_2-Au. The small rounded spots are the gold nanoparticles over the titanium dioxide surface.

4.3.2 General results from the factorial experiment

This section contains the results of a 2^{4-1} half-fraction factorial completely randomized experimental design with four factors and four responses. Four operational conditions were investigated as factors which could affect the production of formaldehyde and formic acid as by-products in the photoproduction of hydrogen: presence of gold as co-catalyst over TiO_2 surface (A: Gold); the level of intensity of UV-light used as an energy source (B: Intensity); concentration of methanol (C: Conc. MetOH); and concentration of nanoparticles in suspension within the reactor (D: Conc. NPs). Two levels were defined for each factor and the original measurement units of each factor were transformed into coded units. The factor levels were coded as -1 (low) and 1 (high). Factors, coded and

uncoded values are shown in Table 6, and the design of the experiment is shown in Table 7 with the average results for each response: total formaldehyde generation (F), total formic acid generation (FA), catalyst productivity for formaldehyde (F/cat) and catalyst productivity for formic acid (FA/cat).

Table 6. Coded and uncoded values of the factors used in the experiment for CH_2O and CH_2O_2.

	Factors	Coded low level	Uncoded low value	Coded high level	Uncoded high value
A:	Gold	-1	No	1	Yes
B:	Intensity	-1	10 mW cm^{-2}	1	20 mW cm^{-2}
C:	MetOH concentration	-1	1.2 M	1	2.2 M
D:	NPs concentration	-1	0.05 g L^{-1}	1	0.10 g L^{-1}

Main and interaction effects on the responses are analyzed, and statistical regression models are proposed for their mean prediction. The production space for formaldehyde and formic acid is analyzed to show the effect of factors and the best treatments. Finally, the relation between catalyst productivity of formic acid and hydrogen is studied.

Table 7. 2^{4-1}_{IV} Design of the experiment and results.

	Basic design			*F* µmol		*FA* µmol		*H* µmol		*F/cat* µmol g^{-1} h^{-1}		*FA/cat* µmol g^{-1} h^{-1}		*H/cat* µmol g^{-1} h^{-1}	
Run	ABC	D = −ABC	Treat-ment	Mean	Std. dev.	Mean	Std. dev.	Mean	Std. dev.	Mean	Std. dev.	Mean	Std. dev.	Mean	Std. dev.
1	− − −	+	d	7.3	0.6	2.8	0.4	10.0	0.2	105	8	41	6	144	3
2	+ − −	−	a	10.1	0.7	5.3	0.0	40.4	0.2	292	19	152	0	1165	5
3	− + −	−	b	8.3	0.3	2.1	2.9	13.3	0.8	239	8	60	85	383	24
4	+ + −	+	abd	27.9	0.7	15.5	0.0	102.9	2.7	402	9	224	0	1485	40
5	− − +	−	c	10.1	1.5	4.3	0.0	16.9	1.1	292	45	123	1	488	32
6	+ − +	+	acd	29.8	2.0	12.0	0.0	66.2	5.0	431	29	174	0	955	72
7	− + +	+	bcd	11.2	0.8	6.1	0.0	15.3	1.3	161	11	88	0	221	19
8	+ + +	−	**abc**	**31.5**	0.4	**16.1**	0.0	**105.1**	6.0	**909**	11	**465**	0	**3034**	172
	Global mean			**17.0**	**10.3**	**8.0**	**5.5**	**46.3**	**38.9**	**354**	**242**	**166**	**132**	**984**	**924**

4.3.3 Formaldehyde generation

4.3.3.1 Main and interaction effects on formaldehyde generation

Figure 26 presents the main effects plot of total formaldehyde generation (F) measured in µmol of CH_2O produced in the liquid phase of the photoreactor after 11 hours of reaction. Please be aware that this type of plot is not a linear adjustment with two points. A main effects plot is a commonly used chart type for statistical analysis that shows data means when you have multiple factors. The points in the plot are the raw data means of the

response variable at the two levels of each factor, with a reference dashed line drawn at the global mean (17.0 μmol in this case) of the response data. This plot helps to compare magnitudes of main effects of each factor (Minitab Inc., 2015). To better understand, the individual value plots with the raw data used in the construction of the main effects plot are shown in the supporting information (Figure - S 17 and Figure - S 18).

The gold presence as a co-catalyst (A) showed the strongest effect obtaining, in average, 2.7 times the amount of formaldehyde when gold was present (from 9.2 to 24.8 μmol). The other factors had effects on the response with similar magnitudes. The concentration of methanol (C) increased the formaldehyde production in 50% (from 13.4 to 20.7 μmol) when it passed from 1.2 M (5%vol) to 2.2 M (10%vol). Intensity of light (B) and concentration of nanoparticles (D) followed it, increasing the formaldehyde production a 38% (from 14.3 to 19.7 μmol) and a 27% (from 15.0 to 19.1 μmol) when they were doubled.

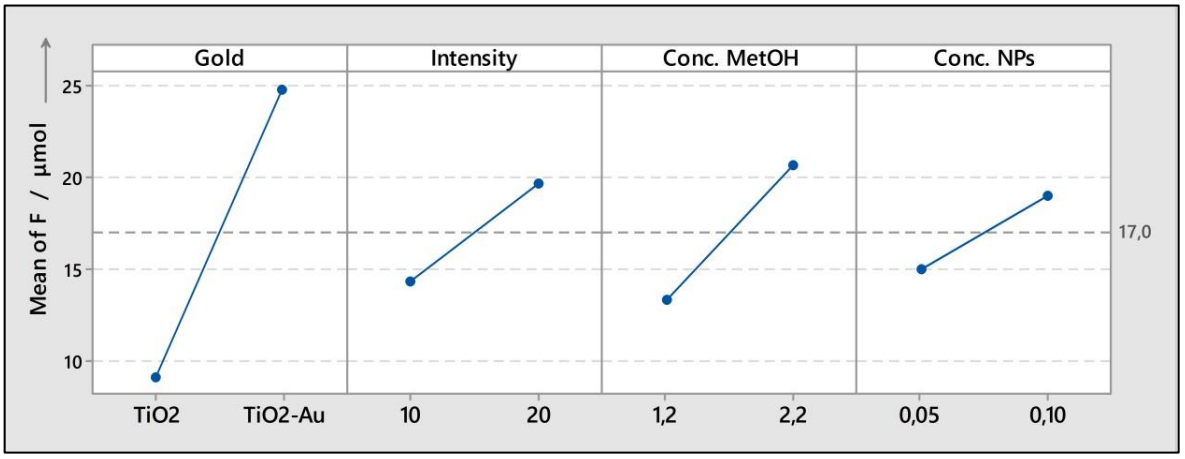

Figure 26. Main effects plot for the total formaldehyde generation (F).

The main effect plot for the catalyst productivity of formaldehyde (F/cat) presented in Figure 27 shows similar magnitude of effects to those in Figure 26 for factors A, B and C. Otherwise, the effect is different for factor D, where doubling the nanoparticles concentration from 0.05 to 0.10 $g \cdot L^{-1}$, reduced the productivity a 36% (from 433 to 275 $\mu mol \cdot g^{-1} \cdot h^{-1}$).

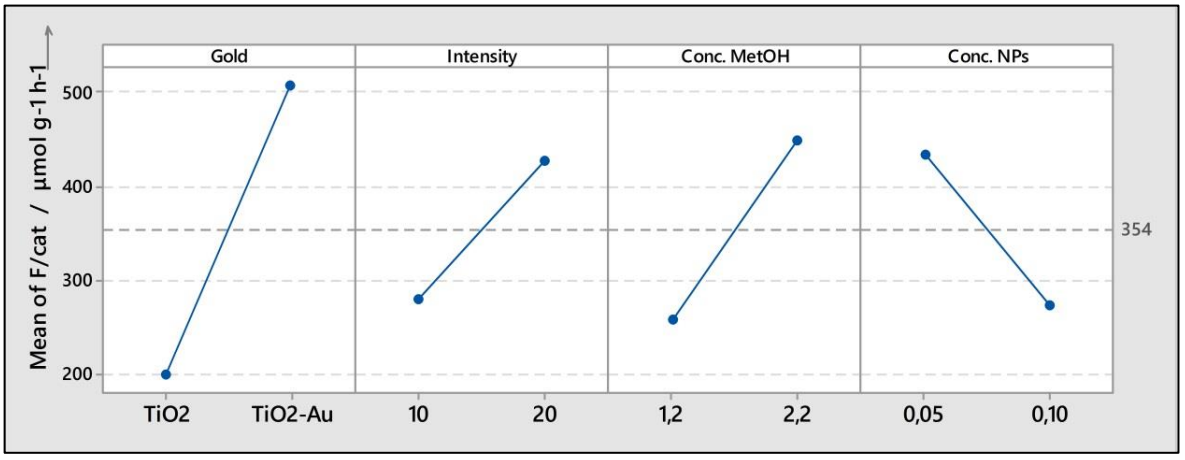

Figure 27. Main effects plot for the catalyst productivity of formaldehyde (F/cat).

Figure 28 shows the half matrix of interaction effects on F. The relevance of factor A is evident in the first column, where it is possible to observe the big change on the mean response of F between the absence and presence of gold as a co-catalyst, independently of their interactions with other factors. Graphically, the relevance of two-factor interactions is defined by the lack of parallelism between the lines. Based on that, interactions AB, AC and AD show a visible sensitivity in the mean response depending on the level of factor A. When gold was not present on TiO_2, a change in the intensity of light or concentration of

nanoparticles did not generate an effect on the mean response, and meanwhile a change in concentration of methanol had a small effect of 35%. On the other hand, when there is gold on the surface of TiO_2, the effect of the same changes on B, C and D levels generate much more observable effects, increasing a 49%, 62% and 40%.

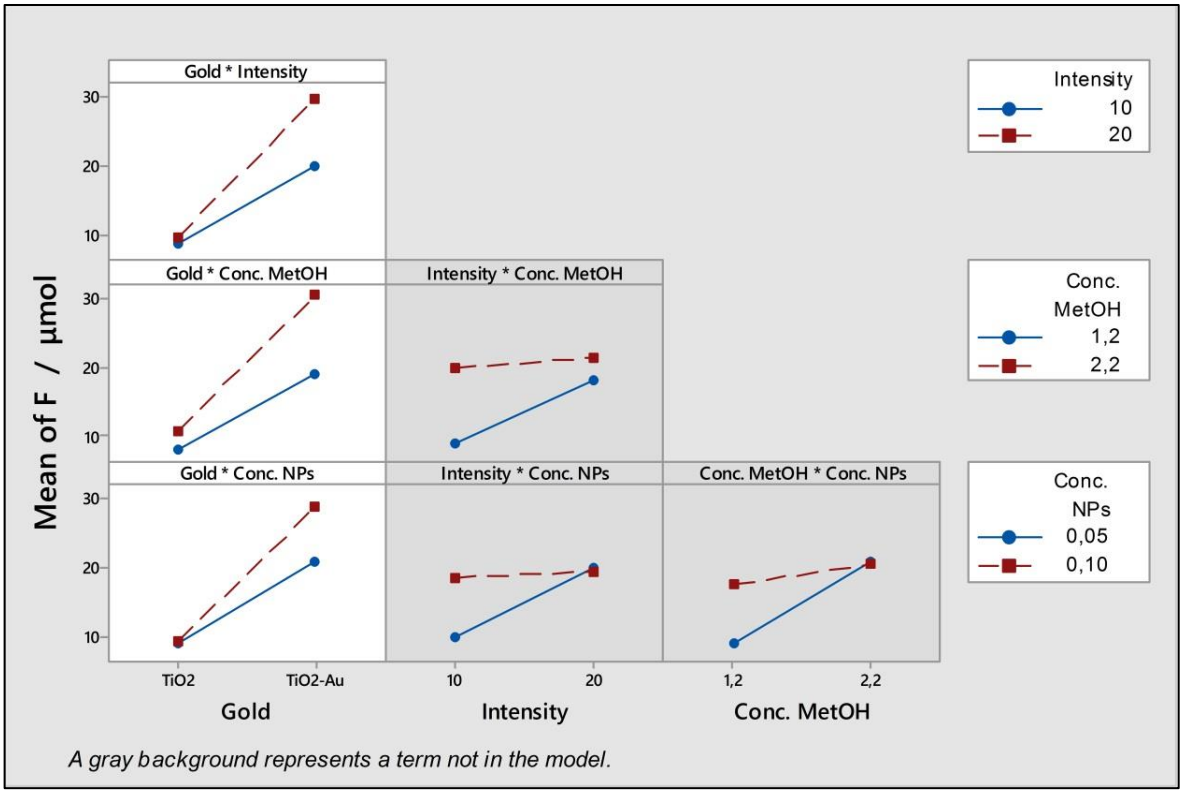

Figure 28. Interaction effects plot for total formaldehyde generation (F)

4.3.3.2 Model for total formaldehyde generation and its catalyst productivity

A fixed effects model was developed for the total formaldehyde generation (F) response with an alpha value of 0.05. The regression analysis showed a good fit to the data (adj-

R^2=99.03%) and high power prediction without symptoms of overfitting (pred-R^2=97.92%). The ANOVA showed a sum of squares that accounted for over 99.4% of the total variability in total formaldehyde generation. Main factors contributed to 86% of total variability, and two-factor interaction terms just 14%. Equation 10 shows the regression equation in uncoded units for response F.

Equation 10.

$$F = -9.46 - 12.23 \cdot A + 0.5379 \cdot B + 7.263 \cdot C + 81.0 \cdot D + 0.4349 \cdot AB + 4.415 \cdot AC + 80.1 \cdot AD$$

The same analysis was run to generate a fixed effects model for the catalyst productivity of formaldehyde (F/cat). Equation 11 shows the regression equation in uncoded units for this response. It showed a good fit to the data (adj-R^2=99.23%) and high power prediction (pred-R^2=98.35%). The sum of squares in the ANOVA accounted for 99.5% of the total variability, main factors explained 81% of total variability, and two-factor interaction terms 18%.

Equation 11.

$$F/cat = 48.1 - 254.8 \cdot A + 14.83 \cdot B + 188.6 \cdot C - 3161 \cdot D + 14.65 \cdot AB + 134.4 \cdot AC - 519 \cdot AD$$

The Pareto chart shown in Figure 29 allows comparing the standardized effects for each main and interaction factor included in the regression model for the formaldehyde production (F). After standardization it is possible to observe the strong effect of including a noble metal such as gold to the TiO_2.

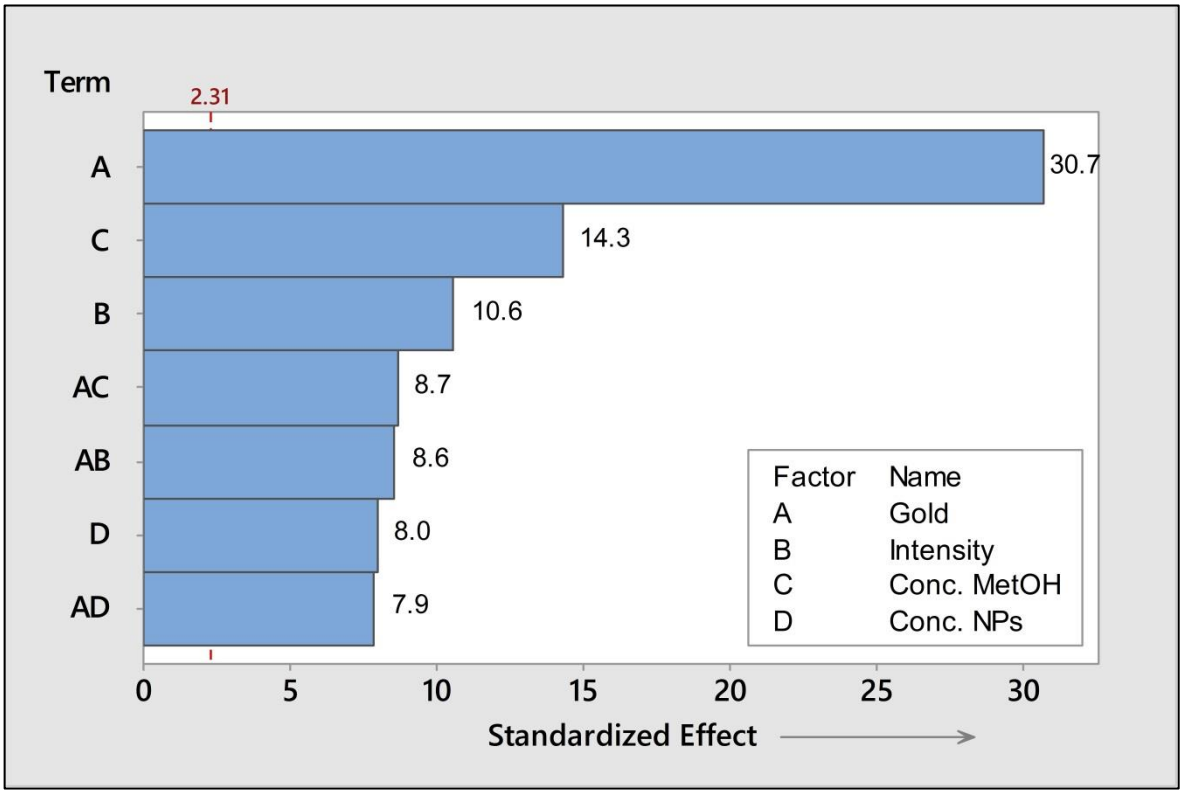

Figure 29. Pareto chart of the standardized effects for the F model.

Incorporating gold has an effect on the formation of CH_2O, it is twice as effective than increasing the concentration of methanol (C) and three times more effective than increasing the intensity of light (B). Its relevance is also reflected in the interaction factors AC and AB, which have a slightly higher effect than increasing the concentration of nanoparticles (D). It is widely agreed that this big effect is due to the metal nanoparticles acting as electron sinks, trapping the excited electrons because of its lower Fermi energy level (Subramanian et al., 2004) and thereby reducing the electron/hole recombination and increasing their lifetime (Bahruji, Bowker, Davies, & Pedrono, 2011). With this, they

inhibit the backward reaction and create active sites for photoreactions (X. Chen et al., 2010; Linsebigler et al., 1995; Serpone et al., 2016; Varas-Concha et al., 2017). The literature reports that hydrogen production, and indirectly intermediates production, are dependent on alcohol concentration for diluted solutions (Rossetti, 2012) up to 6-7 M (López et al., 2015; Melián et al., 2015) and where direct oxidation of alcohol molecules by photogenerated holes occurs at the TiO_2 surface with concentrations above 0.12 M (0.47 vol.%) (Ahmed, Kandiel, Ivanova, & Bahnemann, 2014; Chuan-yi Wang, Groenzin, & Shultz, 2004). Methanol, as an organic compound that is easily oxidized photocatalytically, acts as a hole scavenger and favors the separation of photogenerated electron-hole pairs, increasing charge lifetimes (Melián et al., 2015; Varas-Concha, Guzmán, Isaacs, & Sáez-Navarrete, 2017).

4.3.4 Formic acid generation

4.3.4.1 Main and interaction effects on formic acid generation

Just like Figure 26 does for formaldehyde, Figure 30 shows the main effects plot of total formic acid generation (FA) measured in μmol of CH_2O_2 produced in the liquid phase of the photoreactor after 11 hours of illumination with UV-light, which had a global mean of 8.0 μmol. The individual value plot with the raw data used in the construction of the main effects plot is shown in the supporting information (Figure - S 19 and Figure - S 20).

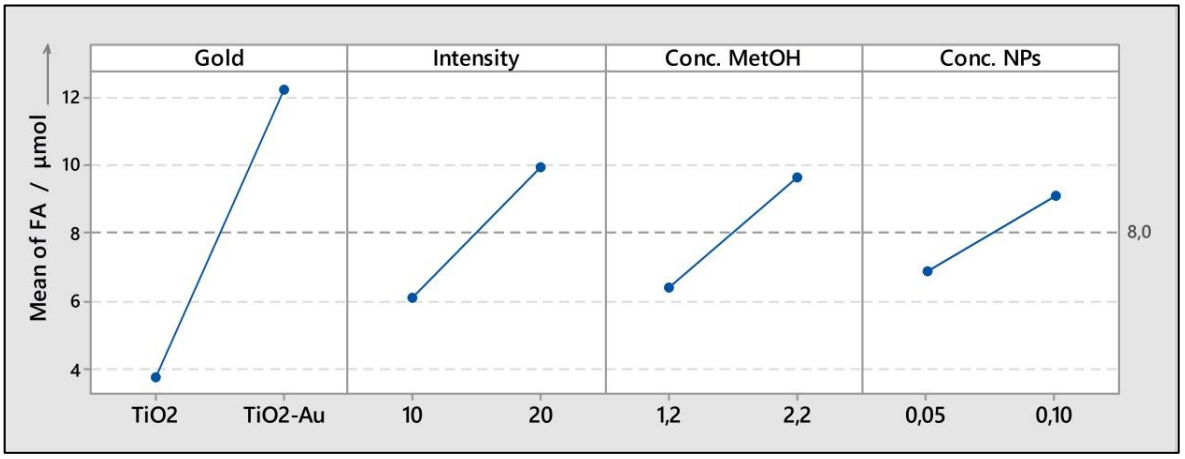

Figure 30. Main effects plot for the total formic acid generation (FA).

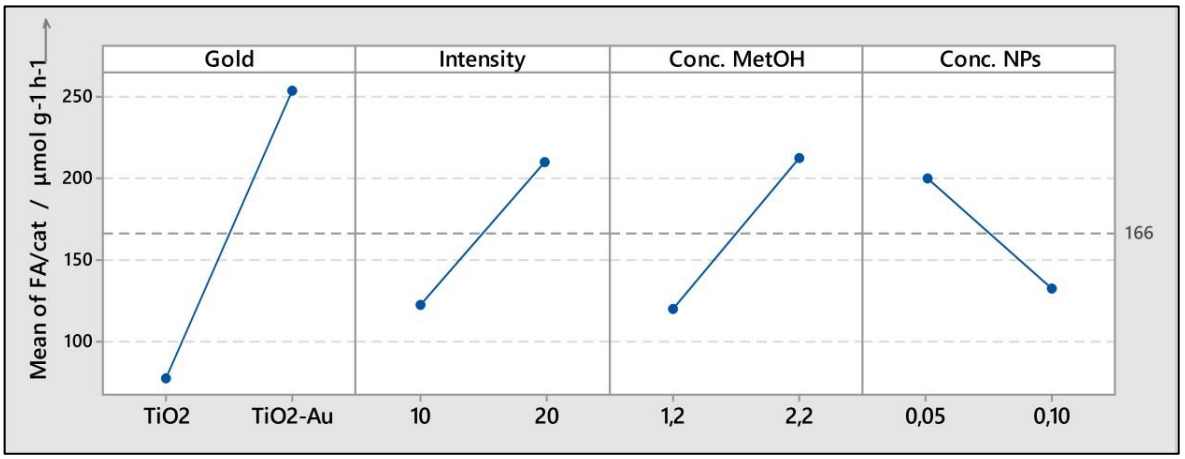

Figure 31. Main effects plot for the catalyst productivity of formic acid (FA/cat).

The effect of the studied factors is similar to the one observed for formaldehyde generation in section 4.3.3.1; in this case, the presence of gold as a co-catalyst (A) showed the strongest effect again. Nanoparticles with gold over the surface showed in average, 3.2 times more formic acid than those with no gold (from 3.8 to 12.2 µmol). The other three factors showed similar effects, smaller than factor A.

The intensity of light (B) supplied to the photoreactor follows factor A in importance, increasing the CH_2O_2 production a 62% (from 6.1 to 9.9 μmol) when it passed from 10 to 20 $mW \cdot cm^{-2}$, showing a higher impact in formic acid formation than in formaldehyde production. The concentration of methanol (C) affected the formic acid production in the same proportion that it impacted the formaldehyde formation, increasing its production a 50% (from 6.4 to 9.6 μmol) when it was doubled.

Finally, concentration of nanoparticles (D) was the minor main effect, increasing FA production a 32% (from 6.9 to 9.1 μmol) when it passed from 0.05 to 0.10 $g \cdot L^{-1}$.

In terms of catalyst productivity for formic acid, the effects are in the next decreasing order: A >> C > B > D. A, B and C increased the productivity in 226%, 78% and 71% respectively, with a change from low to high level. For its part, factor D decreased the productivity a 52% (from 200 to 132 $\mu mol \cdot g^{-1} \cdot h^{-1}$) when the concentration of particles was doubled.

The half matrix of interaction effects on FA is shown in Figure 32. Between the three 2-factor interaction effects considered by the model, only the AB interaction shows an observable significant effect, with a notorious lack of parallelism between the lines. In this case, the response of formic acid production was much more reactive to changes in the intensity of light when there were gold nanoparticles present on the catalyst. So, to double the light intensity raised the formic acid formation 7.2 units (84%) with the presence of gold and only 0.5 units (15%) with bare TiO_2.

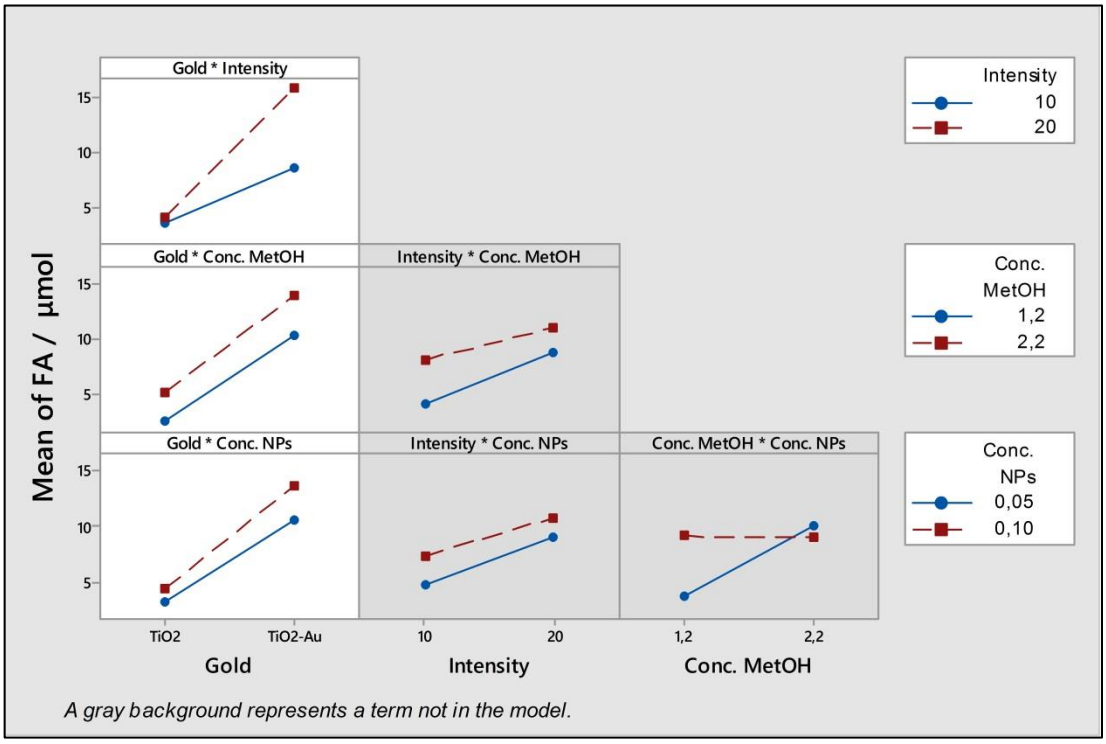

Figure 32. Interaction effects plot for total formic acid generation (FA).

Instead, AC and AD interactions seemed to have similar response, either with presence of gold or not. A change in the concentration of alcohol generated a change of 3.7 units with gold and 2.7 units with no gold, and doubling the concentration of nanoparticles produced a change of 3.1 units with gold and 1.3 units with no gold.

4.3.4.2 Model for total formic acid generation and its catalyst productivity

Likewise in section 4.3.3.2, a fixed effects model was developed for the total formic acid generation (F) using an alpha value of 0.05 (Equation 12). The regression analysis showed a good fit to the data (adj-R^2=96.42%) and good power prediction (pred-R^2=93.37%). The

ANOVA showed a sum of squares that accounted for over 98.1% of the total variability in total formic acid generation: 87.6% due to main factors and 10.5% due to two-factor interaction terms.

Equation 12.

$$FA = -6.49 - 2.95 \cdot A + 0.3854 \cdot B + 3.194 \cdot C + 44.0 \cdot D + 0.3319 \cdot AB + 0.482 \cdot AC + 18.2 \cdot AD$$

The same analysis was run to generate a fixed effects model for the catalyst productivity of formic acid (FA/cat). Equation 13 shows the regression equation in uncoded units for this response. It showed a good fit to the data (adj-R^2=94.85%) and good enough power prediction (pred-R^2=89.00%). The ANOVA showed a sum of squares which explains a 97.3% of the total variability: main factors accounted for 78.8% of total variability, and two-factor interaction terms 18.5%.

Equation 13.

$$FA/cat = -20.6 - 57.9 \cdot A + 8.69 \cdot B + 93.1 \cdot C - 1364 \cdot D + 9.49 \cdot AB + 38.2 \cdot AC - 822 \cdot AD$$

Figure 33 presents a Pareto chart which compares the standardized effects for each factor affecting the formic acid generation (FA). This chart corroborates the observations from Figure 30, showing factor A with the strongest effect. Similar to the case of formaldehyde formation, to include gold in the nanoparticles is twice as effective as the second relevant factor. But in this case, the second one is factor B, so doubling the intensity of light and their AB interaction seem to be more important than increasing the concentration of

methanol (C) or nanoparticles (D). The AD and AC interactions show very small effects on the formic acid production.

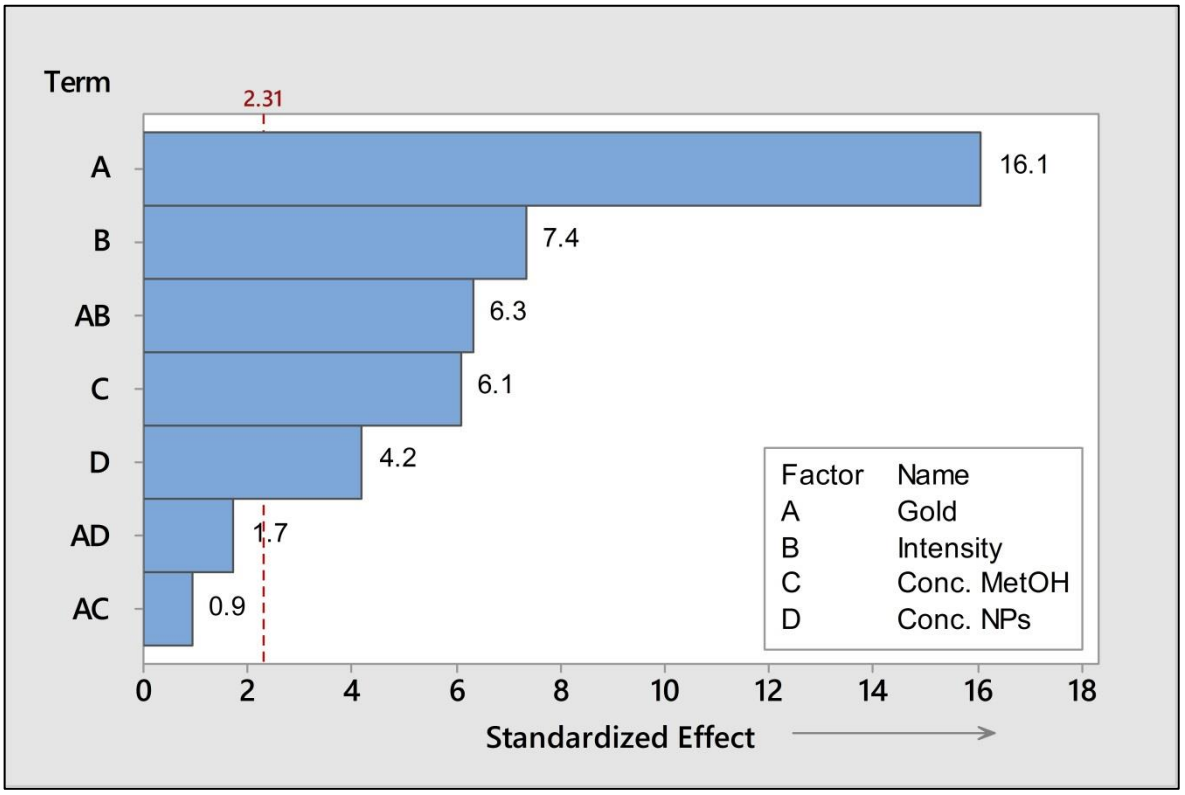

Figure 33. Pareto chart of the standardized effects for the FA model.

The literature reports that the formation of molecular hydrogen and intermediaries, such as formaldehyde and formic acid, compete with back reactions like back electron transfer from hydrogen atoms to the conduction band of the photocatalyst, and with side reactions like the external electron-hole recombination process. At moderate light intensities, back reactions are more efficient compared to the production of hydrogen. So, higher intensities can help generate an excess number of electrons to compete with back and side reactions,

increasing the hydrogen and intermediaries production (Serpone et al., 2016; Varas-Concha et al., 2017).

4.3.5 Analysis of productivities space

The chart in Figure 34 graphically shows the positive effect of the factors on the studied responses as a displacement of each possible treatment in the space formed by the production of formaldehyde (F, X axis) and formic acid (FA, Y axis). As a half-fraction factorial experimental design, only half of the total possible treatments were run (see Table 7), so the second half fraction was predicted using the adjusted models in sections 4.3.3.2 and 4.3.4.2.

The best treatment, abcd, can be easily detected, which can maximize the total production of both compounds. Figure 34 A to D highlight the jump in the responses generated by a change of level in each factor, where the positive effect of factor A is visually relevant. The other three factors show smaller displacement than factor A, but still visually significant. In accordance with the Pareto charts in Figure 29 and Figure 33, the scatterplots B, C and D in Figure 34 also allow observing how a change in factor A affects the response with factors B, C and D. Therefore, the diagonal displacement is much more notorious when the gold is present as a co-catalyst, both to formaldehyde production and formic acid production. A different behavior is observable when there is no gold on the catalyst's surface (points in the lower-left corner), where the movement of treatments is weaker, even in case D the translation is unidirectional.

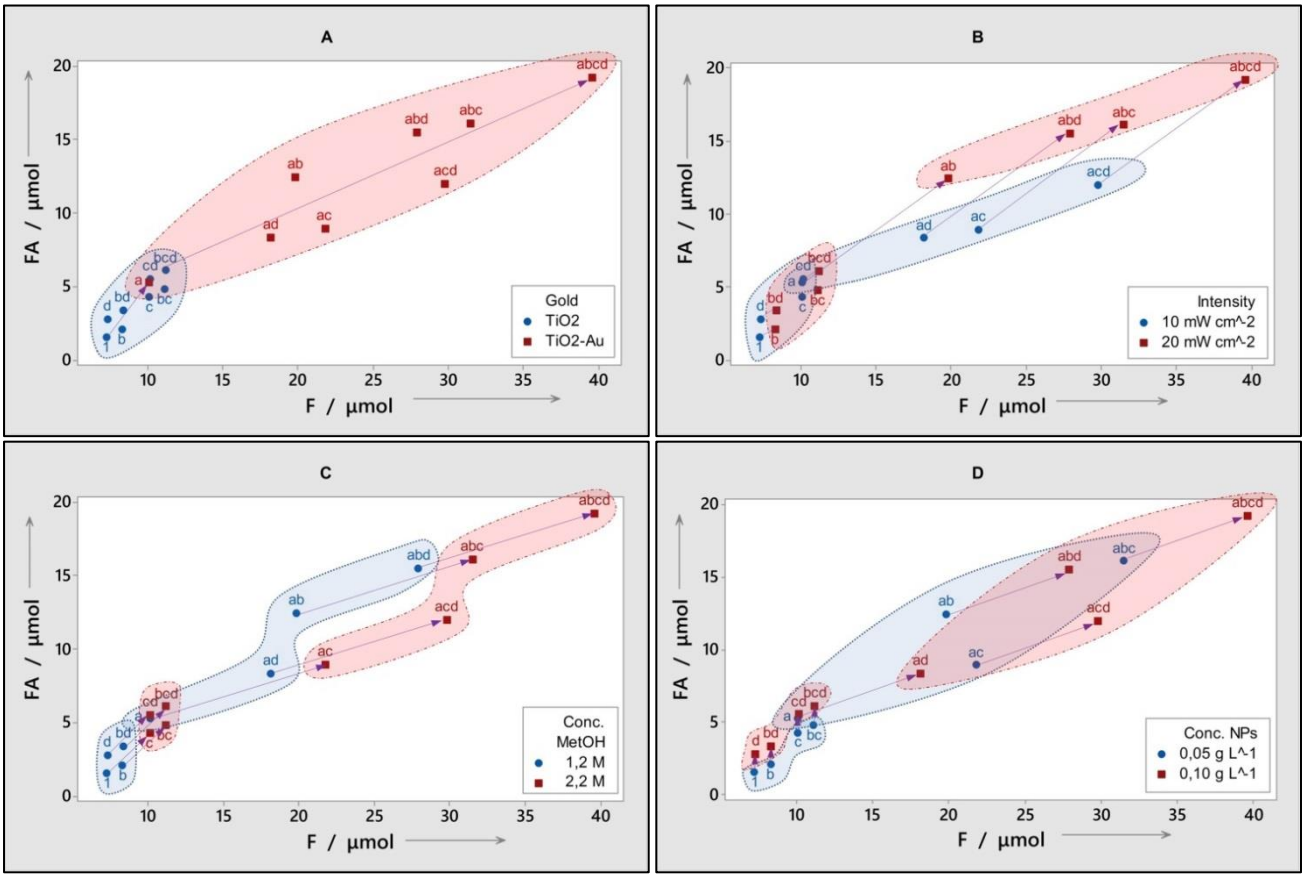

Figure 34. Space of responses for each possible combination of factors of total production of formaldehyde (F) and formic acid (FA), showing the displacement for a level change in factors A, B, C and D.

The four scatterplots in Figure 35 present a similar analysis in the productivity space for formic acid and hydrogen, with similar behavior: Factor A generates the more significant jump for all the treatments and its interaction with other factors is also visible in charts B, C, and D, being more sensitive when the gold is present, producing bigger translations in the productivity space. The main difference is the negative effect of factor D in the responses, decreasing the productivity when the concentration of particles increases.

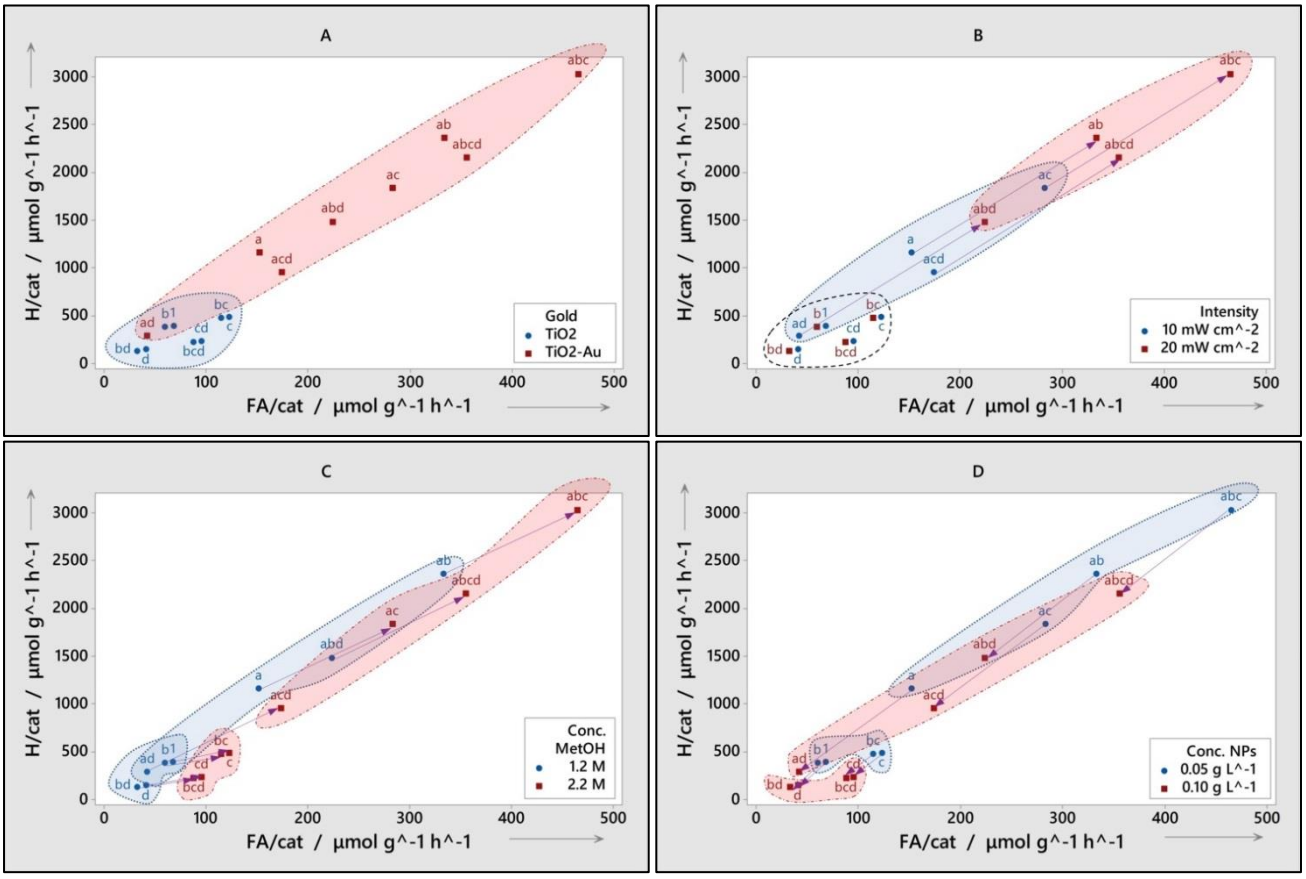

Figure 35. Space of productivities for each possible combination of factors of catalyst productivity of formic acid (FA/cat) and hydrogen (H/cat), showing the displacement for a level change in factors A, B, C and D.

According to this, the treatment which maximizes hydrogen and formic acid productivity is abc.

Figure 36 presents how a level change in each factor generates a displacement in terms of selectivity (F/FA) and catalyst productivity for hydrogen generation (H/cat). A high ratio

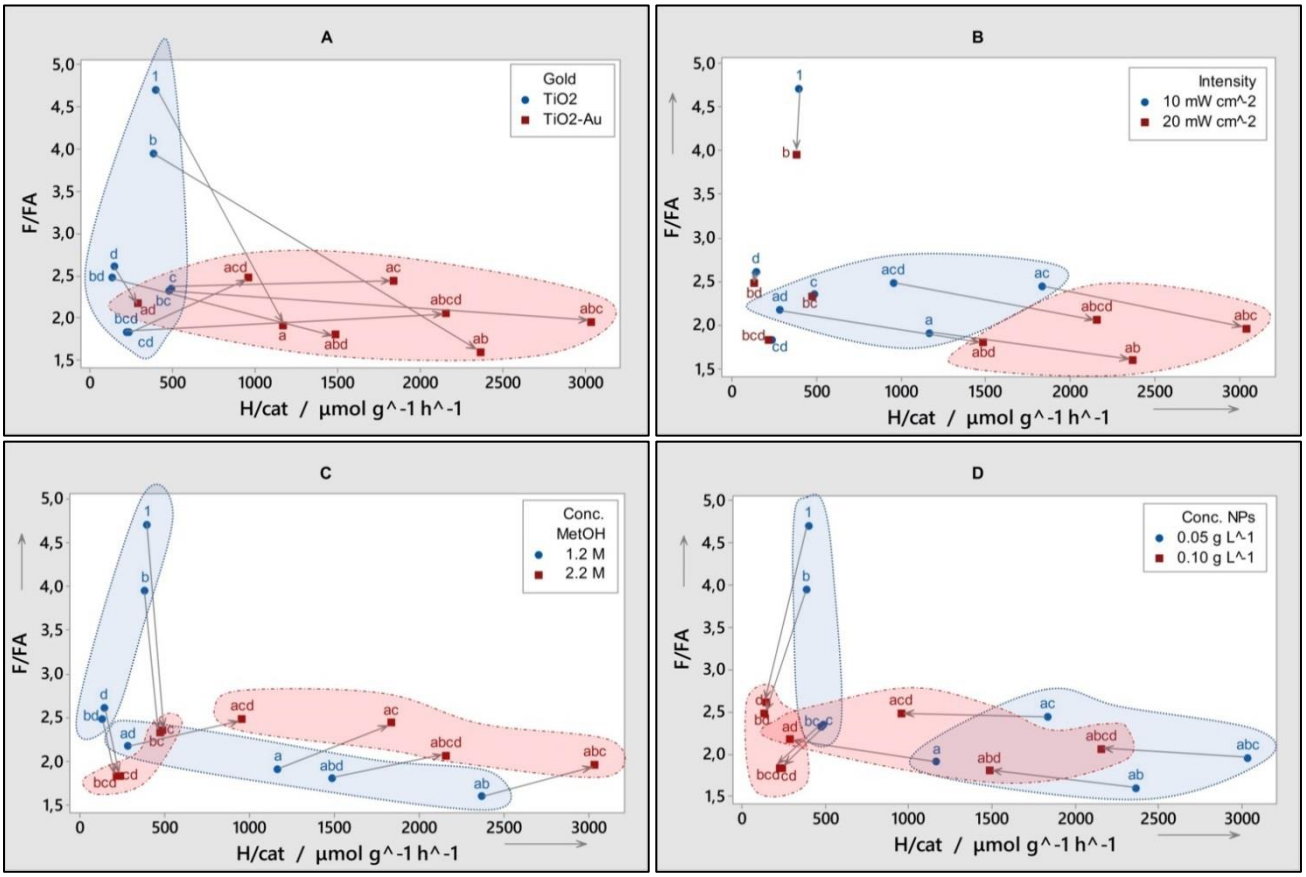

Figure 36. Space of selectivity (F/FA) vs catalyst productivity of hydrogen (H/cat) for each possible combination of factors, showing the displacement due to a level change in factors A, B, C and D.

F/FA shows a tendency to produce more formaldehyde than formic acid. That is the case for treatment 1, which represents bare TiO_2 under low levels of intensity, methanol and nanoparticle concentrations. Due to the economic value, formic acid is more interesting than formaldehyde. This makes treatment ab the most interesting. It shows an inclination to produce more formic acid than the other treatments, with the lowest ratio F/FA producing 1.60 mol of formaldehyde per mol of formic acid, beside a high catalyst

productivity for hydrogen generation of 2365 $\mu mol \cdot g^{-1} \cdot h^{-1}$. Factor abc which maximizes the catalyst productivity of hydrogen and formic acid (see Figure 35) shows an interesting selectivity too, generating 1.96 mol of formaldehyde per mol of formic acid.

Figure 36-A shows how the presence of gold affects more the catalyst productivity of hydrogen than the selectivity, where it is not clear its influence affecting differently each treatment. Figure 36-B shows how an increment in the intensity of light improves catalyst productivity and selectivity, only when gold is present on the TiO_2. When TiO_2 does not have gold on its surface, no significant changes are observed. Figure 36-C shows how an increment of methanol concentration generates an increment in the catalyst productivity, but a different response in selectivity depending upon the gold presence. When there is gold present on the nanoparticles and the methanol concentration increases, the reaction tends to favor the production of formaldehyde, increasing the ratio F/FA. Unlike when there is not gold presence, to increase the amount of methanol favors the formic acid generation. Finally, Figure 36-D shows how an increment on the nanoparticle concentration decreases the hydrogen productivity, but only affects in a significant way the selectivity on bare TiO_2 nanoparticles. When gold is present only marginal changes in selectivity can be observed.

4.4 Conclusions

The presence of gold as a co-catalyst (A) is definitely the factor with the highest weight on each of the four responses under analysis. Nanoparticles with gold produce 2.7 times more formaldehyde and 3.2 times more formic acid than those without gold. In every case, it is twice as effective as the second relevant factor.

Concentration of methanol (C) and intensity of light (B) are relevant factors too. An increment of methanol concentration increases both the formaldehyde and formic acid production by 50%. Doubling the intensity of light is more effective in formic acid production; it increases 38% the formaldehyde production and 62% the formic acid generation.

Interaction effects where factor A is involved are significant, generating more sensitive responses to changes in B, C and D when gold is present. Factors AB and AC affect the selectivity; when gold is present, a high intensity of light and a low concentration of methanol can decrease the ratio F/FA, favoring the formic acid generation. It is important to study this effect more deeply due to their mechanistic repercussions.

Finally, the concentration of nanoparticles (D) is the minor main effect increasing the production of formaldehyde 27% and formic acid 32%. This is the only factor with a negative effect, decreasing the catalyst productivity of formaldehyde and formic acid when the concentration is doubled, 36% and 52% respectively. This makes necessary to explore the shielding effect between particles, especially the dependence of light

penetration in the aquous media varying the concentration of nanoparticles and gold loading.

Treatment abcd maximizes the total production for both compounds, and abc maximizes both catalyst productivities with an interesting selectivity which favors the formic acid generation. It is important to emphasize that these conclusions are valid only in the studied range of factors, and extrapolations need experimental validation. Further work is necessary to explore the combination of factors in more ideal conditions, optimizing the gold loading, the particle size, pH and concentrations of alcohol and nanoparticles.

5 CONCLUSIONS OF DOCTORAL WORK

5.1 Conclusions based on objectives

As a main conclusion, it was corroborated that adding gold over the surface of titanium dioxide nanoparticles is the main factor affecting the production and productivity of hydrogen and by-products in photoreforming of alcohol processes. Its effect can be 2-3 times higher than the effect of the second most relevant factor included in the study (usually, the intensity of light). Also, the magnitude of its effect can be affected by the combined influence of changes in operational conditions, especially by changes in the intensity of light or in concentration of alcohol. Therefore, the proposed hypothesis was validated and the main objective was accomplished.

In terms of specific objectives it is possible to conclude:

- Nanosized particles of TiO_2 modified with gold as a co-catalyst were synthesized and well-characterized with their particle size distribution, their shape parameters, their UV-Vis absorption spectra, and gold loading via elemental analysis.
- Hydrogen gas, formaldehyde and formic acid in solution were produced, via photoreforming of methanol and ethanol using the synthesized TiO_2-Au nanoparticles.
- The main and interaction effects of the selected operational conditions on hydrogen production, catalyst productivity, and alcohol productivity were quantified, detecting that the main factor is the presence of gold, strongly

interacting with the intensity of light. A list of factors organized by magnitude of their effects was presented.

- A reduced fixed effects model was proposed and validated to predict hydrogen production, catalyst productivity, and alcohol productivity, within the range of values considered in the study, defined by the chosen levels for each factor.
- The main and interaction effects on the production of formaldehyde and formic acid, and their catalyst productivities, were quantified.
- A reduced fixed effects model was proposed and validated to estimate the formaldehyde and formic acid production, and their catalyst productivities, within the range of values considered in the study, defined by the chosen levels for each factor.

Next subsections present a summary of the main conclusion of the resultant papers of this work. It is important to emphasize that these conclusions are valid only in the studied range of factors, and extrapolations need experimental validation.

5.2 Conclusions paper 1

It was feasible to produce nanoscale aggregates of TiO_2-Au particles using a synthesis method under room conditions. Hydrogen gas was made using a UV-LED based system. Visible white light did not produce the photocatalytic reaction. The kinetical behavior was monitored without online gas chromatography using an experimental setup based on gauge pressure-temperature measurement.

A higher proportion of gold during the synthesis does not generate more gold nanoparticles.

An apparent zero order kinetics was corroborated and catalyst productivities were around 6,700 $\mu mol \cdot h^{-1} \cdot g^{-1}$.

5.3 Conclusions paper 2

The presence of gold as a co-catalyst (A) was the factor with the highest weight on hydrogen production, followed by the intensity of light (C) and their interaction (AC). Factor A showed a weight three times higher than C, and four times higher than AC. Concentration of catalyst (E) and concentration of electron donor (D) become relevant for their respective productivities. The effect of alcohol type (B) was comparatively smaller and less clear than other single factors, but ethanol showed slightly better average productivities than methanol.

Treatment abcd maximizes the catalyst productivity reaching 2,900 $\mu mol\ g^{-1}\ h^{-1}$, treatment ace maximizes the electron donor productivity with 120 $\mu mol\ mol^{-1}\ h^{-1}$, and abc treatment has the best compromise between both type of productivities.

5.4 Conclusions paper 3

The presence of gold as a co-catalyst (A) is the factor with the highest weight on each of the four responses under analysis, producing 2.7 times more formaldehyde and 3.2 times

more formic acid when gold is present. In every case, it is twice as effective as the second relevant factor.

Concentration of methanol (C) and intensity of light (B) are relevant factors too. An increment of methanol concentration increases both the formaldehyde and formic acid production by 50%. Doubling the intensity of light is more effective in formic acid production; it increases 38% the formaldehyde production and 62% the formic acid generation.

Interaction effects where factor A is involved are significant, generating more sensitive responses to changes in B, C and D when gold is present. Factors AB and AC affect the selectivity; when gold is present, a high intensity of light and a low concentration of methanol can decrease the ratio F/FA, favoring the formic acid generation. It is important to study this effect more deeply due to their mechanistic repercussions.

Finally, the concentration of nanoparticles (D) is the minor main effect increasing the production of formaldehyde 27% and formic acid 32%. This is the only factor with a negative effect, decreasing the catalyst productivity of formaldehyde and formic acid when the concentration is doubled, 36% and 52% respectively. This makes necessary to explore the shielding effect between particles, especially the dependence of light penetration in the aquous media varying the concentration of nanoparticles and gold loading.

Treatment abcd maximizes the total production for both compounds, and abc maximizes both catalyst productivities with an interesting selectivity which favors the formic acid generation. It is important to emphasize that these conclusions are valid only in the studied range of factors, and extrapolations need experimental validation. Further work is necessary to explore the combination of factors in more ideal conditions, optimizing the gold loading, the particle size, pH and concentrations of alcohol and nanoparticles.

5.5 Recommendations and future perspectives

The diminution of catalyst productivities with the increment of light intensity defines the need of further work on the shielding effect in suspensions of nanoparticles. It makes relevant studying the penetration of UV and visible light in aquous media with colloidal suspensions at different depths and concentrations of nanoparticles.

Also, it is recommended to study more deeply the relation between the catalyst selectivity and some operational conditions, like intensity of light and gold presence, to favour the production of more valuable products such as formic acid.

Finally, it is important to extend this analysis to wider parameter ranges than were studied in this thesis.

6 BIBLIOGRAPHY

Ahmad, H., Kamarudin, S. K., Minggu, L. J., & Kassim, M. (2015). Hydrogen from photo-catalytic water splitting process: A review. *Renewable and Sustainable Energy Reviews*, *43*, 599–610. http://doi.org/10.1016/j.rser.2014.10.101

Ahmed, A. Y., Kandiel, T. A., Ivanova, I., & Bahnemann, D. (2014). Photocatalytic and photoelectrochemical oxidation mechanisms ofmethanol on TiO2in aqueous solution. *Applied Surface Science*, *319*(1), 44–49. http://doi.org/10.1016/j.apsusc.2014.07.134

Aiboushev, A., Gostev, F., Shelaev, I., Kostrov, A., Kanaev, A., Museur, L., … Nadtochenko, V. (2013). Spectral properties of the surface plasmon resonance and electron injection from gold nanoparticles to TiO2 mesoporous film: femtosecond study. *Photochemical & Photobiological Sciences : Official Journal of the European Photochemistry Association and the European Society for Photobiology*, *12*(4), 631–637. http://doi.org/10.1039/c2pp25227a

Al-Azri, Z. H. N., Chen, W.-T., Chan, A., Jovic, V., Ina, T., Idriss, H., & Waterhouse, G. I. N. (2015). The roles of metal co-catalysts and reaction media in photocatalytic hydrogen production: Performance evaluation of M/TiO2 photocatalysts (M=Pd, Pt, Au) in different alcohol–water mixtures. *Journal of Catalysis*, *329*, 355–367. http://doi.org/10.1016/j.jcat.2015.06.005

Alipour Moghadam, R., Yusup, S., Azlina, W., Nehzati, S., & Tavasoli, A. (2014). Investigation on syngas production via biomass conversion through the integration of pyrolysis and air–steam gasification processes. *Energy Conversion and Management*, *87*, 670–675. http://doi.org/10.1016/j.enconman.2014.07.065

Alvarez, J., Kumagai, S., Wu, C., Yoshioka, T., Bilbao, J., Olazar, M., & Williams, P. T. (2014). Hydrogen production from biomass and plastic mixtures by pyrolysis-gasification. *International Journal of Hydrogen Energy*, *39*(21), 10883–10891. http://doi.org/10.1016/j.ijhydene.2014.04.189

Ansari, S. A., Khan, M. M., Ansari, M. O., & Cho, M. H. (2015). Silver nanoparticles and defect-induced visible light photocatalytic and photoelectrochemical performance of Ag@m-TiO2 nanocomposite. *Solar Energy Materials and Solar Cells*, *141*, 162–170. http://doi.org/10.1016/j.solmat.2015.05.029

Ayati, A., Ahmadpour, A., Bamoharram, F. F., Tanhaei, B., Mänttäri, M., & Sillanpää, M. (2014). A review on catalytic applications of Au/TiO2 nanoparticles in the removal of water pollutant. *Chemosphere*, *107*, 163–74. http://doi.org/10.1016/j.chemosphere.2014.01.040

Bahruji, H., Bowker, M., Davies, P. R., & Pedrono, F. (2011). New insights into the mechanism of photocatalytic reforming on Pd/TiO2. *Applied Catalysis B: Environmental*, *107*(1–2), 205–209. http://doi.org/10.1016/j.apcatb.2011.07.015

Bai, S., Liu, H., Sun, J., Tian, Y., Chen, S., Song, J., … Liu, C.-C. (2015). Improvement of TiO2 photocatalytic properties under visible light by WO3/TiO2 and MoO3/TiO2 composites. *Applied Surface Science*, *338*, 61–68. http://doi.org/10.1016/j.apsusc.2015.02.103

Balat, M. (2008). Possible Methods for Hydrogen Production. *Energy Sources, Part A: Recovery, Utilization, and Environmental Effects*, *31*(1), 39–50. http://doi.org/10.1080/15567030701468068

Balcerski, W. C., Ryu, S. Y., & Hoffmann, M. R. (2015). Photocatalytic hydrogen production with visible light using nanocomposites of CdS and Ni on niobium oxide. *Separation and Purification Technology*, *156*, 915–921. http://doi.org/10.1016/j.seppur.2015.09.054

Bamwenda, G. R., Tsubota, S., Nakamura, T., & Haruta, M. (1995). Photoassisted hydrogen production from a water-ethanol solution: a comparison of activities of Au□TiO2 and Pt□TiO2. *Journal of Photochemistry and Photobiology A: Chemistry*, *89*(2), 177–189. http://doi.org/10.1016/1010-6030(95)04039-I

Bansal, P., Chaudhary, G. R., & Mehta, S. K. (2015). Comparative study of catalytic activity of ZrO_2 nanoparticles for sonocatalytic and photocatalytic degradation of cationic and anionic dyes. *Chemical Engineering Journal*, *280*, 475–485. http://doi.org/10.1016/j.cej.2015.06.039

Bashir, S., & Idriss, H. (2017). Mechanistic study of the role of Au, Pd and Au-Pd on the surface reactions of ethanol over TiO2 in the dark and under photo-excitation. *Catal. Sci. Technol.* http://doi.org/10.1039/C7CY00961E

Bastos, S. A. L., Lopes, P. A. L., Santos, F. N., & Silva, L. A. (2014). Experimental design as a tool to study the reaction parameters in hydrogen production from photoinduced reforming of glycerol over CdS photocatalyst. *International Journal of Hydrogen Energy*, *39*(27), 14588–14595. http://doi.org/10.1016/j.ijhydene.2014.07.073

Bel Hadjltaief, H., Ben Zina, M., Galvez, M. E., & Da Costa, P. (2016). Photocatalytic degradation of methyl green dye in aqueous solution over natural clay-supported ZnO–TiO2 catalysts. *Journal of Photochemistry and Photobiology A: Chemistry*, *315*, 25–33. http://doi.org/10.1016/j.jphotochem.2015.09.008

Bell, S., Will, G., & Bell, J. (2013). Light intensity effects on photocatalytic water splitting with a titania catalyst. *International Journal of Hydrogen Energy*, *38*(17), 6938–6947. http://doi.org/10.1016/j.ijhydene.2013.02.147

Beltram, A., Romero-Ocaña, I., Josè Delgado Jaen, J., Montini, T., & Fornasiero, P. (2015). Photocatalytic valorization of ethanol and glycerol over TiO2 polymorphs for sustainable hydrogen production. *Applied Catalysis A: General*. http://doi.org/10.1016/j.apcata.2015.09.022

Bhandari, R., Trudewind, C. A., & Zapp, P. (2013). Life cycle assessment of hydrogen production via electrolysis – a review. *Journal of Cleaner Production*, *85*, 151–163. http://doi.org/10.1016/j.jclepro.2013.07.048

Bolton, J. R. (1996). Solar photoproduction of hydrogen: A review. *Solar Energy*, *57*(1),

37–50. http://doi.org/10.1016/0038-092X(96)00032-1

Bowker, M., Morton, C., Kennedy, J., Bahruji, H., Greves, J., Jones, W., … Dimitratos, N. (2014). Hydrogen production by photoreforming of biofuels using Au, Pd and Au–Pd/TiO2 photocatalysts. *Journal of Catalysis*, *310*, 10–15. http://doi.org/10.1016/j.jcat.2013.04.005

Brentner, L. B., Peccia, J., & Zimmerman, J. B. (2010). Challenges in Developing Biohydrogen as a Sustainable Energy Source: Implications for a Research Agenda. *Environmental Science & Technology*, *44*(7), 2243–2254. http://doi.org/10.1021/es9030613

Carp, O., Huisman, C. L., & Reller, A. (2004). Photoinduced reactivity of titanium dioxide. *Progress in Solid State Chemistry*, *32*(1–2), 33–177. http://doi.org/10.1016/j.progsolidstchem.2004.08.001

Carraro, G., MacCato, C., Gasparotto, A., Montini, T., Turner, S., Lebedev, O. I., … Fornasiero, P. (2014). Enhanced hydrogen production by photoreforming of renewable oxygenates through nanostructured Fe2O3 polymorphs. *Advanced Functional Materials*, *24*(3), 372–378. http://doi.org/10.1002/adfm.201302043

Chang, C.-J., Huang, K.-L., Chen, J.-K., Chu, K.-W., & Hsu, M.-H. (2015). Improved photocatalytic hydrogen production of ZnO/ZnS based photocatalysts by Ce doping. *Journal of the Taiwan Institute of Chemical Engineers*, *55*, 82–89. http://doi.org/10.1016/j.jtice.2015.04.024

Chen, G., Yao, J., Liu, J., Yan, B., & Shan, R. (2015). Biomass to hydrogen-rich syngas via catalytic steam gasification of bio-oil/biochar slurry. *Bioresource Technology*. http://doi.org/10.1016/j.biortech.2015.09.009

Chen, J.-J., Wu, J. C. S., Wu, P. C., & Tsai, D. P. (2011). Plasmonic Photocatalyst for H2 Evolution in Photocatalytic Water Splitting. *The Journal of Physical Chemistry C*, *115*(1), 210–216. http://doi.org/10.1021/jp1074048

Chen, J., Shen, S., Guo, P., Wang, M., Wu, P., Wang, X., & Guo, L. (2014). In-situ reduction synthesis of nano-sized Cu2O particles modifying g-C3N4 for enhanced photocatalytic hydrogen production. *Applied Catalysis B: Environmental*, *152–153*, 335–341. http://doi.org/10.1016/j.apcatb.2014.01.047

Chen, W.-T., Chan, A., Al-Azri, Z. H. N., Dosado, A. G., Nadeem, M. A., Sun-Waterhouse, D., … Waterhouse, G. I. N. (2015). Effect of TiO2 polymorph and alcohol sacrificial agent on the activity of Au/TiO2 photocatalysts for H2 production in alcohol–water mixtures. *Journal of Catalysis*, *329*, 499–513. http://doi.org/10.1016/j.jcat.2015.06.014

Chen, W., Chu, M., Gao, L., Mao, L., Yuan, J., & Shangguan, W. (2015). Ni(OH)2 loaded on TaON for enhancing photocatalytic water splitting activity under visible light irradiation. *Applied Surface Science*, *324*, 432–437. http://doi.org/10.1016/j.apsusc.2014.10.114

Chen, X., Shen, S., Guo, L., & Mao, S. S. (2010). Semiconductor-based Photocatalytic Hydrogen Generation. *Chemical Reviews*, *110*(11), 6503–6570. http://doi.org/10.1021/cr1001645

Cheng, J., Ding, L., Xia, A., Lin, R., Li, Y., Zhou, J., & Cen, K. (2015). Hydrogen production using amino acids obtained by protein degradation in waste biomass by combined dark- and photo-fermentation. *Bioresource Technology*, *179*, 13–9. http://doi.org/10.1016/j.biortech.2014.11.109

Choi, H., & Kang, M. (2007). Hydrogen production from methanol/water decomposition in a liquid photosystem using the anatase structure of Cu loaded TiO2TiO2. *International Journal of Hydrogen Energy*, *32*(16), 3841–3848. http://doi.org/10.1016/j.ijhydene.2007.05.011

Chowdhury, P., Gomaa, H., & Ray, A. K. (2011). Factorial design analysis for dye-sensitized hydrogen generation from water. *International Journal of Hydrogen Energy*,

36(21), 13442–13451. http://doi.org/10.1016/j.ijhydene.2011.07.093

Chowdhury, P., Malekshoar, G., Ray, M. B., Zhu, J., & Ray, A. K. (2013). Sacrificial Hydrogen Generation from Formaldehyde with Pt/TiO2 Photocatalyst in Solar Radiation. *Industrial & Engineering Chemistry Research*, *52*(14), 5023–5029. http://doi.org/10.1021/ie3029976

Cihlar, J., & Bartonickova, E. (2013). Low-temperature sol--gel synthesis of anatase nanoparticles modified by Au, Pd and Pt and activity of TiO2/Au, Pd, Pt photocatalysts in water splitting. *Journal of Sol-Gel Science and Technology*, *65*(3), 430–442. http://doi.org/10.1007/s10971-012-2955-8

Clarizia, L., Spasiano, D., Di Somma, I., Marotta, R., Andreozzi, R., & Dionysiou, D. D. (2014). Copper modified-TiO2 catalysts for hydrogen generation through photoreforming of organics. A short review. *International Journal of Hydrogen Energy*, *39*(30), 16812–16831. http://doi.org/10.1016/j.ijhydene.2014.08.037

Cyrankiewicz, M., Wybranowski, T., & Kruszewski, S. (2007). Study of SERS efficiency of metallic colloidal systems. *Journal of Physics: Conference Series*, *79*(1), 12013.

D'Elia, D., Beauger, C., Hochepied, J.-F., Rigacci, A., Berger, M.-H., Keller, N., … Achard, P. (2011). Impact of three different TiO2 morphologies on hydrogen evolution by methanol assisted water splitting: Nanoparticles, nanotubes and aerogels. *International Journal of Hydrogen Energy*, *36*(22), 14360–14373. http://doi.org/10.1016/j.ijhydene.2011.08.007

Dal Santo, V., Gallo, A., Naldoni, A., Guidotti, M., & Psaro, R. (2012). Bimetallic heterogeneous catalysts for hydrogen production. *Catalysis Today*, *197*(1), 190–205. http://doi.org/10.1016/J.CATTOD.2012.07.037

Daskalaki, V. M., & Kondarides, D. I. (2009). Efficient production of hydrogen by photo-induced reforming of glycerol at ambient conditions. *Catalysis Today*, *144*(1–2), 75–80. http://doi.org/10.1016/j.cattod.2008.11.009

Deniz, I., Vardar-Sukan, F., Yüksel, M., Saglam, M., Ballice, L., & Yesil-Celiktas, O. (2015). Hydrogen production from marine biomass by hydrothermal gasification. *Energy Conversion and Management*, *96*, 124–130. http://doi.org/10.1016/j.enconman.2015.02.048

Dickinson, A., James, D., Perkins, N., Cassidy, T., & Bowker, M. (1999). The photocatalytic reforming of methanol. *Journal of Molecular Catalysis A: Chemical*, *146*(1–2), 211–221. http://doi.org/10.1016/S1381-1169(99)00085-0

Diebold, U. (2011). Photocatalysts: Closing the gap. *Nat Chem*, *3*(4), 271–272. Retrieved from http://dx.doi.org/10.1038/nchem.1019

Dincer, I., & Acar, C. (2015). Review and evaluation of hydrogen production methods for better sustainability. *International Journal of Hydrogen Energy*. http://doi.org/10.1016/j.ijhydene.2014.12.035

Długosz, M., Żmudzki, P., Kwiecień, A., Szczubiałka, K., Krzek, J., & Nowakowska, M. (2015). Photocatalytic degradation of sulfamethoxazole in aqueous solution using a floating TiO2-expanded perlite photocatalyst. *Journal of Hazardous Materials*, *298*, 146–53. http://doi.org/10.1016/j.jhazmat.2015.05.016

Dosado, A. G., Chen, W.-T., Chan, A., Sun-Waterhouse, D., & Waterhouse, G. I. N. (2015). Novel Au/TiO2 photocatalysts for hydrogen production in alcohol–water mixtures based on hydrogen titanate nanotube precursors. *Journal of Catalysis*, *330*, 238–254. http://doi.org/10.1016/j.jcat.2015.07.014

Du, Q., & Lu, G. (2014). The roles of various Ni species over SnO2 in enhancing the photocatalytic properties for hydrogen generation under visible light irradiation. *Applied Surface Science*, *305*, 235–241. http://doi.org/10.1016/j.apsusc.2014.03.043

Dunphy Guzman, K. A., Finnegan, M. P., & Banfield, J. F. (2006). Influence of Surface Potential on Aggregation and Transport of Titania Nanoparticles. *Environmental Science & Technology*, *40*(24), 7688–7693. http://doi.org/10.1021/es060847g

Fan, H., Li, H., Liu, Z., Yang, F., & Li, G. (2015). Production of fine chemicals by integrated photocatalytical degradation of alkali lignin solution in corrugated plate reactor and cyclic extraction technology. *Industrial Crops and Products*, *74*, 497–504. http://doi.org/10.1016/j.indcrop.2015.05.027

Ferreira, T., & Rasband, W. (2012). ImageJ User Guide IJ 1.46r. Retrieved from https://imagej.nih.gov/ij/docs/guide/user-guide.pdf

Fischer, M. (1986). Review of hydrogen production with photovoltaic electrolysis systems. *International Journal of Hydrogen Energy*, *11*(8), 495–501. http://doi.org/10.1016/0360-3199(86)90015-7

French, R. A., Jacobson, A. R., Kim, B., Isley, S. L., Penn, R. L., & Baveye, P. C. (2009). Influence of Ionic Strength, pH, and Cation Valence on Aggregation Kinetics of Titanium Dioxide Nanoparticles. *Environmental Science & Technology*, *43*(5), 1354–1359. http://doi.org/10.1021/es802628n

Frost, J. (2013). Multiple Regression Analysis: Use Adjusted R-Squared and Predicted R-Squared to Include the Correct Number of Variables. Retrieved March 17, 2015, from http://blog.minitab.com/blog/adventures-in-statistics/multiple-regession-analysis-use-adjusted-r-squared-and-predicted-r-squared-to-include-the-correct-number-of-variables

Fu, G., Vary, P. S., & Lin, C. (2005). Anatase TiO2 Nanocomposites for Antimicrobial Coatings. *The Journal of Physical Chemistry B*, *109*(18), 8889–8898. http://doi.org/10.1021/jp0502196

Fujishima, A., & Honda, K. (1972). Electrochemical Photolysis of Water at a Semiconductor Electrode. *Nature*, *238*(5358), 37–38. Retrieved from http://dx.doi.org/10.1038/238037a0

Fujishima, A., Zhang, X., & Tryk, D. A. (2008, December 15). TiO2 photocatalysis and related surface phenomena. *Surface Science Reports*. North-Holland. http://doi.org/10.1016/j.surfrep.2008.10.001

Fujita, S., Kawamori, H., Honda, D., Yoshida, H., & Arai, M. (2016). Photocatalytic hydrogen production from aqueous glycerol solution using NiO/TiO2 catalysts: Effects of preparation and reaction conditions. *Applied Catalysis B: Environmental*, *181*, 818–824. http://doi.org/10.1016/j.apcatb.2015.08.048

Gallo , A., Montini, T., Marelli, M., Minguzzi, A., Gombac, V., Psaro, R., … Dal Santo, V. (2012). H2 Production by Renewables Photoreforming on Pt-Au/TiO2 Catalysts Activated by Reduction. *ChemSusChem*, *5*(9), 1800–1811. http://doi.org/10.1002/cssc.201200085

Gallo, A., Marelli, M., Psaro, R., Gombac, V., Montini, T., Fornasiero, P., … Santo, V. D. (2012). Bimetallic Au-Pt/TiO2 photocatalysts active under UV-A and simulated sunlight for H2 production from ethanol. *Green Chem.*, *14*(2), 330–333. http://doi.org/10.1039/C2GC16112E

Gar Alalm, M., Ookawara, S., Fukushi, D., Sato, A., & Tawfik, A. (2015). Improved WO3 photocatalytic efficiency using ZrO2 and Ru for the degradation of carbofuran and ampicillin. *Journal of Hazardous Materials*, *302*, 225–231. http://doi.org/10.1016/j.jhazmat.2015.10.002

García Morgado, M. del P. (2013). *Diseño de electrodos modificados con arreglos del tipo [M(II)TRP]4+/[SiW12O40]4-: estudio de sus propiedades electrocatalíticas y fotoelectrocataliticas en la reducción de CO2 y NO2 para la formación de enlaces C-N*. (M. Isaacs C., M. Campos V., U. de C. F. de Ciencias, & U. de C. F. de C. B. y Farmacéuticas, Eds.). Tesis (doctorado en ciencias con mención química)--Universidad de Chile, 2013., Santiago de Chile .

Ghirardi, M. L., Dubini, A., Yu, J., & Maness, P.-C. (2009). Photobiological hydrogen-producing systems. *Chemical Society Reviews*, *38*(1), 52–61. http://doi.org/10.1039/b718939g

Gololobov, A. M., Bekk, I. E., Bragina, G. O., Zaikovskii, V. I., Ayupov, A. B., Telegina,

N. S., … Stakheev, A. Y. (2009). Platinum nanoparticle size effect on specific catalytic activity in n-alkane deep oxidation: Dependence on the chain length of the paraffin. *Kinetics and Catalysis*, *50*(6), 830–836. http://doi.org/10.1134/S0023158409060068

Gomathisankar, P., Hachisuka, K., Katsumata, H., Suzuki, T., Funasaka, K., & Kaneco, S. (2013). Enhanced photocatalytic hydrogen production from aqueous methanol solution using ZnO with simultaneous photodeposition of Cu. *International Journal of Hydrogen Energy*, *38*(27), 11840–11846. http://doi.org/10.1016/j.ijhydene.2013.06.131

Gomathisankar, P., Yamamoto, D., Katsumata, H., Suzuki, T., & Kaneco, S. (2013). Photocatalytic hydrogen production with aid of simultaneous metal deposition using titanium dioxide from aqueous glucose solution. *International Journal of Hydrogen Energy*, *38*(14), 5517–5524. http://doi.org/10.1016/j.ijhydene.2013.03.014

Gómez-de Pedro, S., Puyol, M., Izquierdo, D., Salinas, Í., & Alonso, J. (n.d.). Synthesis of MUA-protected gold nanoparticles in microfluidic devices with in situ UV-vis characterization. In *Ibersensor 2010*. Lisbon, Portugal.

Grabowska, E. (2016). Selected perovskite oxides: Characterization, preparation and photocatalytic properties—A review. *Applied Catalysis B: Environmental*, *186*, 97–126. http://doi.org/10.1016/j.apcatb.2015.12.035

Grigorescu, S., Bärhausen, B., Wang, L., Mazare, A., Yoo, J. E., Hahn, R., & Schmuki, P. (2014). Tungsten doping of Ta3N5-Nanotubes for Band Gap Narrowing and Enhanced Photoelectrochemical Water Splitting Efficiency. *Electrochemistry Communications*, *51*, 85–88. http://doi.org/10.1016/j.elecom.2014.12.019

Grimes, C. A., Varghese, O. K., & Ranjan, S. (2008). *Light, Water, Hydrogen*. Springer US. http://doi.org/10.1007/978-0-387-68238-9

Grimes, C., Varghese, O., & Ranjan, S. (2008). From Hydrocarbons to Hydrogen: Towards a Sustainable Future. In C. Grimes, O. Varghese, & S. Ranjan (Eds.), *Light, Water, Hydrogen SE - 1* (pp. 1–33). Springer US. http://doi.org/10.1007/978-0-387-

68238-9_1

Gunlazuardi, J., & Dewi, E. L. (2014). Effect of NaBF4 addition on the anodic synthesis of TiO2 nanotube arrays photocatalyst for production of hydrogen from glycerol–water solution. *International Journal of Hydrogen Energy*, *39*(30), 16927–16935. http://doi.org/10.1016/j.ijhydene.2014.07.178

Guo, S., Zhao, T., Jin, Z., Wan, X., Wang, P., Shang, J., & Han, S. (2015). Self-assembly synthesis of precious-metal-free 3D ZnO nano/micro spheres with excellent photocatalytic hydrogen production from solar water splitting. *Journal of Power Sources*, *293*, 17–22. http://doi.org/10.1016/j.jpowsour.2015.05.042

Guo, X. M., Trably, E., Latrille, E., Carrère, H., & Steyer, J.-P. (2010). Hydrogen production from agricultural waste by dark fermentation: A review. *International Journal of Hydrogen Energy*, *35*(19), 10660–10673. http://doi.org/10.1016/j.ijhydene.2010.03.008

Gupta, B., Melvin, A. A., Matthews, T., Dash, S., & Tyagi, A. K. (2016). TiO2 modification by gold (Au) for photocatalytic hydrogen (H2) production. *Renewable and Sustainable Energy Reviews*, *58*, 1366–1375. http://doi.org/10.1016/j.rser.2015.12.236

Gupta, H., & Gupta, B. (2015). Photocatalytic degradation of polycyclic aromatic hydrocarbon benzo[a]pyrene by iron oxides and identification of degradation products. *Chemosphere*, *138*, 924–31. http://doi.org/10.1016/j.chemosphere.2014.12.028

Gupta, S., & Tripathi, M. (2011). A review of TiO2 nanoparticles. *Chinese Science Bulletin*, *56*(16), 1639–1657. http://doi.org/10.1007/s11434-011-4476-1

Guzmán, D. (2016). *Síntesis de nanocristales semiconductores, su incorporación en superficies por layer-by-layer y su uso en la fotoelectroreducción de dióxido de carbono*. Pontificia Universidad Católica de Chile.

Haarlemmer, G. (2015). Simulation study of improved biomass drying efficiency for biomass gasification plants by integration of the water gas shift section in the drying process. *Biomass and Bioenergy*, *81*, 129–136.

http://doi.org/10.1016/j.biombioe.2015.06.002

Hamad, M. A., Radwan, A. M., Heggo, D. A., & Moustafa, T. (2016). Hydrogen rich gas production from catalytic gasification of biomass. *Renewable Energy*, *85*, 1290–1300. http://doi.org/10.1016/j.renene.2015.07.082

Hamelinck, C. N., & Faaij, A. P. . (2002). Future prospects for production of methanol and hydrogen from biomass. *Journal of Power Sources*, *111*(1), 1–22. http://doi.org/10.1016/S0378-7753(02)00220-3

Han, W., Ye, M., Zhu, A. J., Zhao, H. T., & Li, Y. F. (2015). Batch dark fermentation from enzymatic hydrolyzed food waste for hydrogen production. *Bioresource Technology*, *191*, 24–9. http://doi.org/10.1016/j.biortech.2015.04.120

Hara, M., Takata, T., Kondo, J. N., & Domen, K. (2004). Photocatalytic reduction of water by TaON under visible light irradiation. *Catalysis Today*, *90*(3–4), 313–317. http://doi.org/10.1016/j.cattod.2004.04.040

He, Z., Yang, M., Wang, X., Zhao, Z., & Duan, A. (2012). Effect of the transition metal oxide supports on hydrogen production from bio-ethanol reforming. *Catalysis Today*, *194*(1), 2–8. http://doi.org/10.1016/j.cattod.2012.05.004

Hoffmann, M. R., Martin, S. T., Choi, W., & Bahnemann, D. W. (1995). Environmental Applications of Semiconductor Photocatalysis. *Chemical Reviews*, *95*(1). http://doi.org/10.1021/cr00033a004

Hong, S., & Li, X. (2013). Optimal Size of Gold Nanoparticles for Surface-Enhanced Raman Spectroscopy under Different Conditions. *JOURNAL OF NANOMATERIALS*. http://doi.org/10.1155/2013/790323

Hsu, C.-W., & Lin, C.-Y. (2015). Commercialization model of hydrogen production technology in Taiwan: Dark fermentation technology applications. *International Journal of Hydrogen Energy*. http://doi.org/10.1016/j.ijhydene.2015.07.080

Hussein, A. M., & Shende, R. V. (2014). Enhanced hydrogen generation using ZrO2-modified coupled ZnO/TiO2 nanocomposites in the absence of noble metal co-catalyst. *International Journal of Hydrogen Energy*, *39*(11), 5557–5568. http://doi.org/10.1016/j.ijhydene.2014.01.149

ICIS. (2008). Chemical profile: formaldehyde. Retrieved October 25, 2017, from https://www.icis.com/resources/news/2008/03/31/9111425/chemical-profile-formaldehyde/

IEA. (2006). *Hydrogen Production and Storage: R&D Priorities and Gaps*.

IEA. (2007). IEA Energy Technology Essentials: Hydrogen Production & Distribution, 4.

IEA. (2015). *Technology Roadmap: Hydrogen and Fuel Cells*. Paris.

IEA. (2017a). *Key World Energy Statistics 2017*. http://doi.org/http://dx.doi.org/10.1787/key_energ_stat-2017-en

IEA. (2017b). *Market Report Series: Oil 2017*. http://doi.org/http://dx.doi.org/10.1787/9789264272514-en

Iliev, V., Tomova, D., Bilyarska, L., & Tyuliev, G. (2007). Influence of the size of gold nanoparticles deposited on TiO2 upon the photocatalytic destruction of oxalic acid. *Journal of Molecular Catalysis A: Chemical*, *263*(1–2), 32–38. http://doi.org/10.1016/j.molcata.2006.08.019

Ishikawa, A., Takata, T., Matsumura, T., Kondo, J. N., Hara, M., Kobayashi, H., & Domen, K. (2004). Oxysulfides Ln2Ti2S2O5 as Stable Photocatalysts for Water Oxidation and Reduction under Visible-Light Irradiation. *The Journal of Physical Chemistry B*, *108*(8), 2637–2642. http://doi.org/10.1021/jp036890x

Ishikawa, A., Yamada, Y., Takata, T., Kondo, J. N., Hara, M., Kobayashi, H., & Domen, K. (2003). Novel Synthesis and Photocatalytic Activity of Oxysulfide Sm2Ti2S2O5. *Chemistry of Materials*, *15*(23), 4442–4446. http://doi.org/10.1021/cm034540h

Jia, Y., Yang, J., Zhao, D., Han, H., & Li, C. (2014). A Novel Sr2CuInO3S p-type semiconductor photocatalyst for hydrogen production under visible light irradiation. *Journal of Energy Chemistry*, *23*(4), 420–426. http://doi.org/10.1016/S2095-4956(14)60167-4

Jose, D., Sorensen, C. M., Rayalu, S. S., Shrestha, K. M., & Klabunde, K. J. (2013). Au-TiO2 Nanocomposites and Efficient Photocatalytic Hydrogen Production under UV-Visible and Visible Light Illuminations: A Comparison of Different Crystalline Forms of TiO2. *International Journal of Photoenergy*, 1–10. Retrieved from 10.1155/2013/685614

Jovic, V., Al-Azri, Z. H. N., Chen, W.-T., Sun-Waterhouse, D., Idriss, H., & Waterhouse, G. I. N. (2013). Photocatalytic H2 Production from Ethanol--Water Mixtures Over Pt/TiO2 and Au/TiO2 Photocatalysts: A Comparative Study. *Topics in Catalysis*, *56*(12), 1139–1151. http://doi.org/10.1007/s11244-013-0080-8

Jovic, V., Chen, W.-T., Sun-Waterhouse, D., Blackford, M. G., Idriss, H., & Waterhouse, G. I. N. (2013). Effect of gold loading and TiO2 support composition on the activity of Au/TiO2 photocatalysts for H2 production from ethanol–water mixtures. *Journal of Catalysis*, *305*, 307–317. http://doi.org/10.1016/j.jcat.2013.05.031

Jung, M., Hart, J. N., Boensch, D., Scott, J., Ng, Y. H., & Amal, R. (2015). Hydrogen evolution via glycerol photoreforming over Cu–Pt nanoalloys on TiO2. *Applied Catalysis A: General*. http://doi.org/10.1016/j.apcata.2015.10.040

K. Gurunathan, P. Maruthamuthu, M., & Sastri, V. C. (1997). Photocatalytic hydrogen production by dye-sensitized Pt/SnO2 AND Pt/SnO2/RuO2 in aqueous methyl viologen solution. *International Journal of Hydrogen Energy*, *22*(1), 57–62. http://doi.org/10.1016/S0360-3199(96)00075-4

Kandiel, T. A., Dillert, R., Robben, L., & Bahnemann, D. W. (2011). Photonic efficiency and mechanism of photocatalytic molecular hydrogen production over platinized titanium dioxide from aqueous methanol solutions. *Catalysis Today*, *161*(1), 196–201.

http://doi.org/10.1016/j.cattod.2010.08.012

Kaur, S., & Singh, V. (2007). TiO2 mediated photocatalytic degradation studies of Reactive Red 198 by UV irradiation. *Journal of Hazardous Materials*, *141*(1), 230–236. http://doi.org/10.1016/J.JHAZMAT.2006.06.123

Kawai, T., & Sakata, T. (1980). Photocatalytic hydrogen production from liquid methanol and water. *J. Chem. Soc.{,} Chem. Commun.*, (15), 694–695. http://doi.org/10.1039/C39800000694

Kelly, N. A. (2014). *Advances in Hydrogen Production, Storage and Distribution*. *Advances in Hydrogen Production, Storage and Distribution*. Elsevier. http://doi.org/10.1533/9780857097736.2.159

Khan, M. A., Sinatra, L., Oufi, M., Bakr, O. M., & Idriss, H. (2017). Evidence of Plasmonic Induced Photocatalytic Hydrogen Production on Pd/TiO2 Upon Deposition on Thin Films of Gold. *Catalysis Letters*, *147*(4), 811–820. http://doi.org/10.1007/s10562-017-1998-4

Khan, M. M., Adil, S. F., & Al-Mayouf, A. (2015). Metal oxides as photocatalysts. *Journal of Saudi Chemical Society*, *19*(5), 462–464. http://doi.org/10.1016/j.jscs.2015.04.003

Kim, S. C., Lim, M. S., & Chun, Y. N. (2013). Hydrogen-rich gas production from a biomass pyrolysis gas by using a plasmatron. *International Journal of Hydrogen Energy*, *38*(34), 14458–14466. http://doi.org/10.1016/j.ijhydene.2013.09.004

Kochuveedu, S. T., Kim, D.-P., & Kim, D. H. (2012). Surface-Plasmon-Induced Visible Light Photocatalytic Activity of TiO2 Nanospheres Decorated by Au Nanoparticles with Controlled Configuration. *The Journal of Physical Chemistry C*, *116*(3), 2500–2506. http://doi.org/10.1021/jp209520m

Koj, J. C., Schreiber, A., Zapp, P., & Marcuello, P. (2015). Life Cycle Assessment of Improved High Pressure Alkaline Electrolysis. *Energy Procedia*, *75*, 2871–2877.

http://doi.org/10.1016/j.egypro.2015.07.576

Krishna Prasad, R., & Srivastava, S. N. (2009). Sorption of distillery spent wash onto fly ash: kinetics, mechanism, process design and factorial design. *Journal of Hazardous Materials*, *161*(2–3), 1313–22. http://doi.org/10.1016/j.jhazmat.2008.04.092

Kudo, A. (2007). Photocatalysis and solar hydrogen production. *Pure and Applied Chemistry*, *79*(11), 1917–1927. http://doi.org/10.1351/pac200779111917

Lam, S.-M., Sin, J.-C., Abdullah, A. Z., & Mohamed, A. R. (2015). Sunlight responsive WO_3 /ZnO nanorods for photocatalytic degradation and mineralization of chlorinated phenoxyacetic acid herbicides in water. *Journal of Colloid and Interface Science*, *450*, 34–44. http://doi.org/10.1016/j.jcis.2015.02.075

Lee, H.-S., Vermaas, W. F. J., & Rittmann, B. E. (2010). Biological hydrogen production: prospects and challenges. *Trends in Biotechnology*, *28*(5), 262–71. http://doi.org/10.1016/j.tibtech.2010.01.007

Lee, W.-S., Wan, B.-Z., Kuo, C.-N., Lee, W.-C., & Cheng, S. (2007). Maintaining catalytic activity of Au/TiO2 during the storage at room temperature. *Catalysis Communications*, *8*(11), 1604–1608. http://doi.org/10.1016/j.catcom.2007.01.021

Lewis-Beck, M., Bryman, A., & Liao, T. F. (2004). *The SAGE Encyclopedia of Social Science Research Methods*. SAGE Publications. http://doi.org/10.4135/9781412950589

Li, W., Guo, Y., & Zhang, P. (2010a). General Strategy to Prepare TiO2-Core Gold-Shell Nanoparticles as SERS-Tags. *JOURNAL OF PHYSICAL CHEMISTRY C*, *114*(16), 7263–7268. http://doi.org/10.1021/jp908160m

Li, W., Guo, Y., & Zhang, P. (2010b). General Strategy to Prepare TiO2 -Core Gold-Shell Nanoparticles as SERS-Tags, 7263–7268.

Li, X., Wang, H., Chu, T., Li, D., & Mao, L. (2014). Synthesis and peferentially loading of nickel nanoparticle on CdS surface and its photocatalytic performance for hydrogen

evolution under visible light. *Materials Research Bulletin*, *57*, 254–259. http://doi.org/10.1016/j.materresbull.2014.05.016

Li, X., Zhang, J., Kang, S., Li, G., & Mu, J. (2014). Visible light photocatalytic activity of CuO/Cr2O3 co-loaded multiwalled carbon nanotubes sensitized with eosin Y for hydrogen evolution from water. *Ceramics International*, *40*(7), 10171–10176. http://doi.org/10.1016/j.ceramint.2014.02.055

Li, Y., Cheng, X., Ruan, X., Song, H., Lou, Z., Ye, Z., & Zhu, L. (2015). Enhancing photocatalytic activity for visible-light-driven H2 generation with the surface reconstructed LaTiO2N nanostructures. *Nano Energy*, *12*, 775–784. http://doi.org/10.1016/j.nanoen.2015.02.003

Liao, B., & Guo, L. J. (2015). Concentrating Solar Thermochemical Hydrogen Production by Biomass Gasification in Supercritical Water. *Energy Procedia*, *69*, 444–450. http://doi.org/10.1016/j.egypro.2015.03.051

Lin, S., Shi, L., Yoshida, H., Li, M., & Zou, X. (2013). Synthesis of hollow spherical tantalum oxide nanoparticles and their photocatalytic activity for hydrogen production. *Journal of Solid State Chemistry*, *199*, 15–20. http://doi.org/10.1016/j.jssc.2012.11.016

Ling, H., Kim, K., Liu, Z., Shi, J., Zhu, X., & Huang, J. (2015). Photocatalytic degradation of phenol in water on as-prepared and surface modified TiO2 nanoparticles. *Catalysis Today*, *258*, 96–102. http://doi.org/10.1016/j.cattod.2015.03.048

Linsebigler, A. L., Lu, G., & Yates, J. T. (1995). Photocatalysis on TiO2 Surfaces: Principles, Mechanisms, and Selected Results. *Chemical Reviews*, *95*(3), 735–758. http://doi.org/10.1021/cr00035a013

Liu, B.-F., Jin, Y.-R., Cui, Q.-F., Xie, G.-J., Wu, Y.-N., & Ren, N.-Q. (2015). Photo-fermentation hydrogen production by Rhodopseudomonas sp. nov. strain A7 isolated from the sludge in a bioreactor. *International Journal of Hydrogen Energy*, *40*(28), 8661–8668. http://doi.org/10.1016/j.ijhydene.2015.05.001

Liu, H. H., Surawanvijit, S., Rallo, R., Orkoulas, G., & Cohen, Y. (2011). Analysis of Nanoparticle Agglomeration in Aqueous Suspensions via Constant-Number Monte Carlo Simulation. *Environmental Science & Technology*, *45*(21), 9284–9292. http://doi.org/10.1021/es202134p

Liu, M., Du, Y., Ma, L., Jing, D., & Guo, L. (2012). Manganese doped cadmium sulfide nanocrystal for hydrogen production from water under visible light. *International Journal of Hydrogen Energy*, *37*(1), 730–736. http://doi.org/10.1016/j.ijhydene.2011.04.111

Liu, R., Yoshida, H., Fujita, S., & Arai, M. (2014). Photocatalytic hydrogen production from glycerol and water with NiOx/TiO2 catalysts. *Applied Catalysis B: Environmental*, *144*, 41–45. http://doi.org/10.1016/j.apcatb.2013.06.024

Liu, S., Wang, X., Wang, K., Lv, R., & Xu, Y. (2013). ZnO/ZnS–PdS core/shell nanorods: Synthesis, characterization and application for photocatalytic hydrogen production from a glycerol/water solution. *Applied Surface Science*, *283*, 732–739. http://doi.org/10.1016/j.apsusc.2013.07.009

Liu, S., Zhu, J., Chen, M., Xin, W., Yang, Z., & Kong, L. (2014). Hydrogen production via catalytic pyrolysis of biomass in a two-stage fixed bed reactor system. *International Journal of Hydrogen Energy*, *39*(25), 13128–13135. http://doi.org/10.1016/j.ijhydene.2014.06.158

Liu, X., Zhao, L., Domen, K., & Takanabe, K. (2014). Photocatalytic hydrogen production using visible-light-responsive Ta3N5 photocatalyst supported on monodisperse spherical SiO2 particulates. *Materials Research Bulletin*, *49*, 58–65. http://doi.org/10.1016/j.materresbull.2013.08.069

Lkhagvadulam, B., Kim, J. H., Yoon, I., & Shim, Y. K. (2013). Size-Dependent Photodynamic Activity of Gold Nanoparticles Conjugate of Water Soluble Purpurin-18-N-Methyl-D-Glucamine. *BioMed Research International*, *2013*(Article ID 720579), 10. Retrieved from doi:10.1155/2013/720579

López-Tenllado, F. J., Hidalgo-Carrillo, J., Montes, V., Marinas, A., Urbano, F. J., Marinas, J. M., … Reid, F. (2017). A comparative study of hydrogen photocatalytic production from glycerol and propan-2-ol on M/TiO 2 systems (M=Au, Pt, Pd). *Catalysis Today*, *280*, 58–64. http://doi.org/10.1016/j.cattod.2016.05.009

López, C. R., Melián, E. P., Ortega Méndez, J. A., Santiago, D. E., Doña Rodríguez, J. M., & González Díaz, O. (2015). Comparative study of alcohols as sacrificial agents in H2 production by heterogeneous photocatalysis using Pt/TiO2 catalysts. *Journal of Photochemistry and Photobiology A: Chemistry*, *312*, 45–54. http://doi.org/10.1016/j.jphotochem.2015.07.005

Lu, C., Chen, Y., Li, Y., Ma, C., Guo, Y., Li, Y., & Wang, J. (2015). The effect of different co-catalysts (CuO, MoS2 and Pt) on hydrogen production of Er3+:YAlO3/NaTaO3 by visible-light-induced methanol splitting. *Energy*, *93*, 749–757. http://doi.org/10.1016/j.energy.2015.09.074

Lyubina, T. P., Markovskaya, D. V., Kozlova, E. A., & Parmon, V. N. (2013). Photocatalytic hydrogen evolution from aqueous solutions of glycerol under visible light irradiation. *International Journal of Hydrogen Energy*, *38*(33), 14172–14179. http://doi.org/10.1016/j.ijhydene.2013.08.031

Maeda, K., Terashima, H., Kase, K., & Domen, K. (2009). Nanoparticulate precursor route to fine particles of TaON and ZrO2–TaON solid solution and their photocatalytic activity for hydrogen evolution under visible light. *Applied Catalysis A: General*, *357*(2), 206–212. http://doi.org/10.1016/j.apcata.2009.01.024

Maegli, A. E., Otal, E. H., Hisatomi, T., Yoon, S., Leroy, C. M., Schäuble, N., … Weidenkaff, A. (2012). Perovskite-Type LaTiO2N Oxynitrides for Solar Water Splitting: Influence of the Synthesis Conditions. *Energy Procedia*, *22*, 61–66. http://doi.org/10.1016/j.egypro.2012.05.218

Majeed, I., Nadeem, M. A., Al-Oufi, M., Nadeem, M. A., Waterhouse, G. I. N., Badshah,

A., … Idriss, H. (2016). On the role of metal particle size and surface coverage for photo-catalytic hydrogen production: A case study of the Au/CdS system. *Applied Catalysis B: Environmental*, *182*, 266–276. http://doi.org/10.1016/j.apcatb.2015.09.039

Majidnia, Z., & Idris, A. (2015). Photocatalytic reduction of iodine in radioactive waste water using maghemite and titania nanoparticles in PVA-alginate beads. *Journal of the Taiwan Institute of Chemical Engineers*, *54*, 137–144. http://doi.org/10.1016/j.jtice.2015.03.005

Maldonado, C., Fierro, J. L. G., Birke, G., Martínez, E., & Reyes, P. (2010). Conversion of methanol to formaldehyde on TiO2 supported Ag nanoparticles. *Journal of the Chilean Chemical Society*, *55*, 506–510. Retrieved from http://www.scielo.cl/scielo.php?script=sci_arttext&pid=S0717-97072010000400021&nrm=iso

Market research Future. (2017). Formic Acid Market Research Report- Forecast to 2027. Retrieved October 26, 2017, from https://www.marketresearchfuture.com/reports/formic-acid-market-1132

Maschmeyer, T., & Che, M. (2010). Catalytic Aspects of Light-Induced Hydrogen Generation in Water with TiO2 and Other Photocatalysts: A Simple and Practical Way Towards a Normalization? *Angewandte Chemie International Edition*, *49*(9), 1536–1539. http://doi.org/10.1002/anie.200903921

Matsukawa, M., Ishikawa, R., Hisatomi, T., Moriya, Y., Shibata, N., Kubota, J., … Domen, K. (2014). Enhancing Photocatalytic Activity of LaTiO2N by Removal of Surface Reconstruction Layer. *Nano Letters*, *14*(2), 1038–1041. http://doi.org/10.1021/nl404688h

McGregor group. (2014). World Formaldehyde Production to Exceed 52 Mln Tonnes in 2017. Retrieved October 25, 2017, from https://mcgroup.co.uk/news/20140627/formaldehyde-production-exceed-52-mln-tonnes.html

Melián, E. P., López, C. R., Santiago, D. E., Quesada-Cabrera, R., Méndez, J. A. O., Rodríguez, J. M. D., & Díaz, O. G. (2015). Study of the photocatalytic activity of Pt-modified commercial TiO2 for hydrogen production in the presence of common organic sacrificial agents. *Applied Catalysis A: General*. http://doi.org/10.1016/j.apcata.2015.09.033

Melián, E. P., Suárez, M. N., Jardiel, T., Rodríguez, J. M. D., Caballero, A. C., Araña, J., … Díaz, O. G. (2014). Influence of nickel in the hydrogen production activity of TiO2. *Applied Catalysis B: Environmental*, *152–153*, 192–201. http://doi.org/10.1016/j.apcatb.2014.01.039

Melo, M. de O., & Silva, L. A. (2011). Photocatalytic production of hydrogen: an innovative use for biomass derivatives. *Journal of the Brazilian Chemical Society*, *22*(8), 1399–1406. http://doi.org/10.1590/S0103-50532011000800002

Melvin, A. A., Illath, K., Das, T., Raja, T., Bhattacharyya, S., & Gopinath, C. S. (2015). M-Au/TiO2 (M = Ag{,} Pd{,} and Pt) nanophotocatalyst for overall solar water splitting: role of interfaces. *Nanoscale*, *7*(32), 13477–13488. http://doi.org/10.1039/C5NR03735B

Merck Group. (2017). Merck Millipore. Retrieved October 26, 2017, from http://www.merckmillipore.com

Mikulandrić, R., Lončar, D., Böhning, D., Böhme, R., & Beckmann, M. (2015). Process performance improvement in a co-current, fixed bed biomass gasification facility by control system modifications. *Energy Conversion and Management*, *104*, 135–146. http://doi.org/10.1016/j.enconman.2015.05.048

Minitab. (2014). Basics of stepwise regression. Retrieved March 11, 2015, from http://support.minitab.com/en-us/minitab/17/topic-library/modeling-statistics/regression-and-correlation/basics/basics-of-stepwise-regression/

Minitab Inc. (2015). Minitab 17 User's guide. Pensilvania: Minitab Inc. Retrieved from http://www.minitab.com

Mizukoshi, Y., Makise, Y., Shuto, T., Hu, J., Tominaga, A., Shironita, S., & Tanabe, S. (2007). Immobilization of noble metal nanoparticles on the surface of TiO2 by the sonochemical method: Photocatalytic production of hydrogen from an aqueous solution of ethanol. *Ultrasonics Sonochemistry*, *14*(3), 387–392. http://doi.org/10.1016/j.ultsonch.2006.08.001

Mizukoshi, Y., Sato, K., Konno, T. J., & Masahashi, N. (2010). Dependence of photocatalytic activities upon the structures of Au/Pd bimetallic nanoparticles immobilized on TiO2 surface. *Applied Catalysis B: Environmental*, *94*(3–4), 248–253. http://doi.org/10.1016/J.APCATB.2009.11.015

Montgomery, D. C. (2012). *Design and Analysis of Experiments* (Eighth Edi). John Wiley & Sons, Incorporated.

Murdoch, M., Waterhouse, G. I. N., Nadeem, M. A., Metson, J. B., Keane, A. M., Howe, R. F., … Idriss, H. (2011). The effect of gold loading and particle size on photocatalytic hydrogen production from ethanol over Au/TiO2 nanoparticles. *Nature Chemistry*, *3*(6), 489–492. http://doi.org/10.1038/nchem.1048

Naldoni, A., D'Arienzo, M., Altomarec, M., Marelli, M., Scotti, R., Morazzoni, F., … Santo, V. D. (2013). Pt and Au/TiO2 photocatalysts for methanol reforming: Role of metal nanoparticles in tuning charge trapping properties and photoefficiency. *Applied Catalysis B: Environmental*, *130–131*, 239–248. http://doi.org/10.1016/J.APCATB.2012.11.006

Ni, M., Leung, D. Y. C., & Leung, M. K. H. (2007). A review on reforming bio-ethanol for hydrogen production. *International Journal of Hydrogen Energy*, *32*(15), 3238–3247. http://doi.org/10.1016/j.ijhydene.2007.04.038

Ni, M., Leung, M. K. H., Leung, D. Y. C., & Sumathy, K. (2007). A review and recent developments in photocatalytic water-splitting using TiO2 for hydrogen production. *Renewable and Sustainable Energy Reviews*, *11*(3), 401–425. http://doi.org/10.1016/j.rser.2005.01.009

Nowotny, J., Bak, T., Nowotny, M. K., & Sheppard, L. R. (2007). Titanium dioxide for solar-hydrogen I. Functional properties. *International Journal of Hydrogen Energy*, *32*(14), 2609–2629. http://doi.org/10.1016/j.ijhydene.2006.09.004

Nowotny, J., & Veziroglu, T. N. (2011). Impact of hydrogen on the environment. *International Journal of Hydrogen Energy*, *36*(20), 13218–13224. http://doi.org/10.1016/j.ijhydene.2011.07.071

Nsib, M. F., Naffati, N., Rayes, A., Moussa, N., & Houas, A. (2015). Effect of some operational parameters on the hydrogen generation efficiency of Ni-ZnO/PANI composite under visible-light irradiation. *Materials Research Bulletin*, *70*, 530–538. http://doi.org/10.1016/j.materresbull.2015.04.067

Ohta, T., & Veziroglu, T. N. (1976). Hydrogen production using solar radiation. *International Journal of Hydrogen Energy*, *1*(3), 255–263. http://doi.org/10.1016/0360-3199(76)90021-5

Oros-Ruiz, S., Zanella, R., Collins, S. E., Hernández-Gordillo, A., & Gómez, R. (2014). Photocatalytic hydrogen production by Au–MxOy (MAg, Cu, Ni) catalysts supported on TiO2. *Catalysis Communications*, *47*, 1–6. http://doi.org/10.1016/j.catcom.2013.12.033

Oros-Ruiz, S., Zanella, R., López, R., Hernández-Gordillo, A., & Gómez, R. (2013). Photocatalytic hydrogen production by water/methanol decomposition using Au/TiO2 prepared by deposition-precipitation with urea. *Journal of Hazardous Materials*, *263 Pt 1*, 2–10. http://doi.org/10.1016/j.jhazmat.2013.03.057

Ortega Méndez, J. A., López, C. R., Pulido Melián, E., González Díaz, O., Doña Rodríguez, J. M., Fernández Hevia, D., & Macías, M. (2014). Production of hydrogen by water photo-splitting over commercial and synthesised Au/TiO2 catalysts. *Applied Catalysis B: Environmental*, *147*, 439–452. http://doi.org/10.1016/j.apcatb.2013.09.029

Osterloh, F. E., & Parkinson, B. A. (2011). Recent developments in solar water-splitting photocatalysis. *MRS Bulletin*, *36*(1), 17–22.

Pacquette, A. L., Hagiwara, H., Ishihara, T., & Gewirth, A. A. (2014). Fabrication of an oxysulfide of bismuth Bi2O2S and its photocatalytic activity in a Bi2O2S/In2O3 composite. *Journal of Photochemistry and Photobiology A: Chemistry*, *277*, 27–36. http://doi.org/10.1016/j.jphotochem.2013.12.007

Pai, Y.-H., Tsai, C.-T., & Fang, S.-Y. (2013). Enhanced photocatalytic hydrogen generation with Pt Nanoparticles on multi-phase polycrystalline microporous MnO2 photocatalyst. *Journal of Power Sources*, *223*, 107–113. http://doi.org/10.1016/j.jpowsour.2012.09.024

Pan, Z., Hisatomi, T., Wang, Q., Nakabayashi, M., Shibata, N., Pan, C., … Domen, K. (2015). Application of LaMg1/3Ta2/3O2N as a hydrogen evolution photocatalyst of a photocatalyst sheet for Z-scheme water splitting. *Applied Catalysis A: General*. http://doi.org/10.1016/j.apcata.2015.10.034

Paul, P., Tyagi, B., Bilakhiya, A. K., Bhadbhade, M. M., Suresh, E., & Ramachandraiah, G. (1998). Synthesis and Characterization of Rhodium Complexes Containing 2,4,6-Tris(2-pyridyl)-1,3,5-triazine and Its Metal-Promoted Hydrolytic Products: Potential Uses of the New Complexes in Electrocatalytic Reduction of Carbon Dioxide. *Inorganic Chemistry*, *37*(22), 5733–5742. http://doi.org/10.1021/ic9709739

Pérez-Larios, A., Lopez, R., Hernández-Gordillo, A., Tzompantzi, F., Gómez, R., & Torres-Guerra, L. M. (2012). Improved hydrogen production from water splitting using TiO2–ZnO mixed oxides photocatalysts. *Fuel*, *100*, 139–143. http://doi.org/10.1016/j.fuel.2012.02.026

Puga, A. V. (2016). Photocatalytic production of hydrogen from biomass-derived feedstocks. *Coordination Chemistry Reviews*, *315*, 1–66. http://doi.org/10.1016/J.CCR.2015.12.009

Pulido Melián, E., González Díaz, O., Doña Rodríguez, J. M., Araña, J., & Perez Peña, J. (2013). Adsorption and photocatalytic degradation of 2,4-dichlorophenol in TiO2

suspensions. Effect of hydrogen peroxide, sodium peroxodisulphate and ozone. *Applied Catalysis A: General*, *455*, 227–233. http://doi.org/10.1016/J.APCATA.2013.02.007

Rajeshwar, K., Chenthamarakshan, C. ., Ming, Y., & Sun, W. (2002). Cathodic photoprocesses on titania films and in aqueous suspensions. *Journal of Electroanalytical Chemistry*, *538–539*, 173–182. http://doi.org/10.1016/S0022-0728(02)00902-6

Ramos Sende, J. A., Arana, C. R., Hernandez, L., Potts, K. T., Keshevarz-K, M., & Abruna, H. D. (1995). Electrocatalysis of CO2 Reduction in Aqueous Media at Electrodes Modified with Electropolymerized Films of Vinylterpyridine Complexes of Transition Metals. *Inorganic Chemistry*, *34*(12), 3339–3348. http://doi.org/10.1021/ic00116a028

Rasband, W. S. (n.d.). ImageJ. Bethesda, Maryland, USA: U.S. National Institutes of Health. Retrieved from http://imagej.nih.gov/ij/

Rosseler, O., Shankar, M. V., Du, M. K.-L., Schmidlin, L., Keller, N., & Keller, V. (2010). Solar light photocatalytic hydrogen production from water over Pt and Au/TiO2(anatase/rutile) photocatalysts: Influence of noble metal and porogen promotion. *Journal of Catalysis*, *269*(1), 179–190. http://doi.org/10.1016/j.jcat.2009.11.006

Rossetti, I. (2012). Hydrogen Production by Photoreforming of Renewable Substrates. *ISRN Chemical Engineering*, *2012*, 1–21. http://doi.org/10.5402/2012/964936

Rothenberger, G., Moser, J., Graetzel, M., Serpone, N., & Sharma, D. K. (1985). Charge carrier trapping and recombination dynamics in small semiconductor particles. *Journal of the American Chemical Society*, *107*(26), 8054–8059. http://doi.org/10.1021/ja00312a043

Roy, A., Lingampalli, S. R., Saha, S., & Rao, C. N. R. (2015). Effects of morphology and surface area of the oxide nanostructures on the visible–light induced generation of hydrogen in ZnO(TiO2)/Cd1−xZnxS and ZnO(TiO2)/Pt/Cd1−xZnxS heterostructures (x=0.0, 0.2). *Chemical Physics Letters*, *637*, 137–142. http://doi.org/10.1016/j.cplett.2015.08.005

Sadanandam, G., Lalitha, K., Kumari, V. D., Shankar, M. V., & Subrahmanyam, M.

(2013). Cobalt doped TiO2: A stable and efficient photocatalyst for continuous hydrogen production from glycerol: Water mixtures under solar light irradiation. *International Journal of Hydrogen Energy*, *38*(23), 9655–9664. http://doi.org/10.1016/j.ijhydene.2013.05.116

Sampaio, M. J., Oliveira, J. W. L., Sombrio, C. I. L., Baptista, D. L., Teixeira, S. R., Carabineiro, S. A. C., … Faria, J. L. (2015). Photocatalytic performance of Au/ZnO nanocatalysts for hydrogen production from ethanol. *Applied Catalysis A: General*. http://doi.org/10.1016/j.apcata.2015.10.013

Sasikala, R., Shirole, A., Sudarsan, V., Sakuntala, T., Sudakar, C., Naik, R., & Bharadwaj, S. R. (2009). Highly dispersed phase of SnO2 on TiO2 nanoparticles synthesized by polyol-mediated route: Photocatalytic activity for hydrogen generation. *International Journal of Hydrogen Energy*, *34*(9), 3621–3630. http://doi.org/10.1016/j.ijhydene.2009.02.085

Saud, P. S., Pant, B., Alam, A.-M., Ghouri, Z. K., Park, M., & Kim, H.-Y. (2015). Carbon quantum dots anchored TiO2 nanofibers: Effective photocatalyst for waste water treatment. *Ceramics International*, *41*(9), 11953–11959. http://doi.org/10.1016/j.ceramint.2015.06.007

Serpone, N., Emeline, A. V, Ryabchuk, V. K., Kuznetsov, V. N., Artem'ev, Y. M., & Horikoshi, S. (2016). Why do Hydrogen and Oxygen Yields from Semiconductor-Based Photocatalyzed Water Splitting Remain Disappointingly Low? Intrinsic and Extrinsic Factors Impacting Surface Redox Reactions. *ACS Energy Letters*, *1*(5), 931–948. http://doi.org/10.1021/acsenergylett.6b00391

Shen, T. F.-R., Lai, M.-H., Yang, T. C.-K., Fu, I.-P., Liang, N.-Y., & Chen, W.-T. (2012). Photocatalytic production of hydrogen by vanadium oxides under visible light irradiation. *Journal of the Taiwan Institute of Chemical Engineers*, *43*(1), 95–101. http://doi.org/10.1016/j.jtice.2011.06.004

Sinatra, L., LaGrow, A. P., Peng, W., Kirmani, A. R., Amassian, A., Idriss, H., & Bakr, O. M. (2015). A Au/Cu2O–TiO2 system for photo-catalytic hydrogen production. A pn-junction effect or a simple case of in situ reduction? *Journal of Catalysis*, *322*, 109–117. http://doi.org/10.1016/j.jcat.2014.11.012

Sood, S., Kumar, S., Umar, A., Kaur, A., Mehta, S. K., & Kansal, S. K. (2015). TiO2 quantum dots for the photocatalytic degradation of indigo carmine dye. *Journal of Alloys and Compounds*, *650*, 193–198. http://doi.org/10.1016/j.jallcom.2015.07.164

Stern, N. (2006). The Stern Review on the Economic Effects of Climate Change. *Population and Development Review*, *32*(4), 793–798. http://doi.org/10.1111/j.1728-4457.2006.00153.x

Su, R., Tiruvalam, R., Logsdail, A. J., He, Q., Downing, C. A., Jensen, M. T., … Besenbacher, F. (2014). Designer Titania-Supported Au–Pd Nanoparticles for Efficient Photocatalytic Hydrogen Production. *ACS Nano*, *8*(4), 3490–3497. http://doi.org/10.1021/nn500963m

Subramanian, V., Wolf, E. E., & Kamat, P. V. (2004). Catalysis with TiO2/Gold Nanocomposites. Effect of Metal Particle Size on the Fermi Level Equilibration. *Journal of the American Chemical Society*, *126*(15), 4943–4950. http://doi.org/10.1021/ja0315199

Sun, T., Liu, E., Liang, X., Hu, X., & Fan, J. (2015). Enhanced hydrogen evolution from water splitting using Fe-Ni codoped and Ag deposited anatase TiO2 synthesized by solvothermal method. *Applied Surface Science*, *347*, 696–705. http://doi.org/10.1016/j.apsusc.2015.04.162

Taboada, E., Angurell, I., & Llorca, J. (2014a). Dynamic photocatalytic hydrogen production from ethanol–water mixtures in an optical fiber honeycomb reactor loaded with Au/TiO2. *Journal of Catalysis*, *309*, 460–467. http://doi.org/10.1016/j.jcat.2013.10.025

Taboada, E., Angurell, I., & Llorca, J. (2014b). Hydrogen photoproduction from bio-

derived alcohols in an optical fiber honeycomb reactor loaded with Au/TiO2. *Journal of Photochemistry and Photobiology A: Chemistry*, *281*, 35–39. http://doi.org/10.1016/j.jphotochem.2014.03.004

Tachibana, Y., Vayssieres, L., & Durrant, J. R. (2012). Artificial photosynthesis for solar water-splitting. *Nat Photon*, *6*(8), 511–518. Retrieved from http://dx.doi.org/10.1038/nphoton.2012.175

Takei, T., Akita, T., Nakamura, I., Fujitani, T., Okumura, M., Okazaki, K., … Haruta, M. (2012). Chapter One – Heterogeneous Catalysis by Gold. In *Advances in Catalysis* (Vol. 55, pp. 1–126). http://doi.org/10.1016/B978-0-12-385516-9.00001-6

Tamaki, Y., Furube, A., Murai, M., Hara, K., Katoh, R., & Tachiya, M. (2006). Direct Observation of Reactive Trapped Holes in TiO2 Undergoing Photocatalytic Oxidation of Adsorbed Alcohols: Evaluation of the Reaction Rates and Yields. *Journal of the American Chemical Society*, *128*(2), 416–417. http://doi.org/10.1021/ja055866p

Tang, X., Ye, H., & Hu, H. (2013). Sulfurization synthesis and photocatalytic activity of oxysulfide La3NbS2O5. *Transactions of Nonferrous Metals Society of China*, *23*(9), 2644–2649. http://doi.org/10.1016/S1003-6326(13)62780-6

Teets, T. S., & Nocera, D. G. (2011). Photocatalytic hydrogen production. *Chemical Communications*, *47*(33), 9268–9274. http://doi.org/10.1039/C1CC12390D

Transparency Market Research. (2013). Formaldehyde Market for UF Resins, PF Resins, MF Resins, Polyacetal Resins, Pentaerythritol, MDI, 1, 4-Butanediol, and Other Applications - Global Industry Analysis, Size, Share, Growth, Trends and Forecast, 2012 - 2018. Retrieved October 25, 2017, from https://www.transparencymarketresearch.com/formaldehyde-market.html

Turner, J., Sverdrup, G., Mann, M. K., Maness, P.-C., Kroposki, B., Ghirardi, M., … Blake, D. (2008). Renewable hydrogen production. *International Journal of Energy Research*, *32*(5), 379–407. http://doi.org/10.1002/er.1372

US DOE. (2002). *National Vision of America's Transition to a Hydrogen Economy - To 2030 and beyond*.

Varas-Concha, F., Guzmán, D., Isaacs, M., & Sáez-Navarrete, C. (2017). Operational conditions affecting hydrogen production via photo-reforming of organic compounds using TiO_2 -Au nanoparticles. *Energy Technology*, n/a-n/a. http://doi.org/10.1002/ente.201700546

Wang, C., Cai, X., Chen, Y., Cheng, Z., Luo, X., Mo, S., … Yang, Z. (2017). Improved hydrogen production from glycerol photoreforming over sol-gel derived TiO2 coupled with metal oxides. *Chemical Engineering Journal*, *317*, 522–532. http://doi.org/10.1016/j.cej.2017.02.033

Wang, C., Groenzin, H., & Shultz, M. J. (2004). Direct Observation of Competitive Adsorption between Methanol and Water on TiO2: An in Situ Sum-Frequency Generation Study. *Journal of the American Chemical Society*, *126*(26), 8094–8095. http://doi.org/10.1021/ja048165l

Wang, C., Wu, M., Yan, M., Shen, H., Cai, F., Hu, B., & Shi, W. (2015). Enhanced visible-light photocatalytic activity and the mechanism study of WO3 nanosheets coupled with Ag3PO4 nanocrystals. *Ceramics International*, *41*(5), 6784–6792. http://doi.org/10.1016/j.ceramint.2015.01.125

Wang, D., Li, Y., Li Puma, G., Wang, C., Wang, P., Zhang, W., & Wang, Q. (2015). Dye-sensitized photoelectrochemical cell on plasmonic Ag/AgCl @ chiral TiO2 nanofibers for treatment of urban wastewater effluents, with simultaneous production of hydrogen and electricity. *Applied Catalysis B: Environmental*, *168–169*, 25–32. http://doi.org/10.1016/j.apcatb.2014.11.012

Wang, M., Wang, Z., Gong, X., & Guo, Z. (2014). The intensification technologies to water electrolysis for hydrogen production – A review. *Renewable and Sustainable Energy Reviews*, *29*, 573–588. http://doi.org/10.1016/j.rser.2013.08.090

Wang, Q., An, N., Bai, Y., Hang, H., Li, J., Lu, X., … Lei, Z. (2013). High photocatalytic hydrogen production from methanol aqueous solution using the photocatalysts CuS/TiO2. *International Journal of Hydrogen Energy*, *38*(25), 10739–10745. http://doi.org/10.1016/j.ijhydene.2013.02.131

Wang, Y., He, Y., Lai, Q., & Fan, M. (2014). Review of the progress in preparing nano TiO2: an important environmental engineering material. *Journal of Environmental Sciences (China)*, *26*(11), 2139–77. http://doi.org/10.1016/j.jes.2014.09.023

Waterhouse, G. I. N., Wahab, A. K., Al-Oufi, M., Jovic, V., Anjum, D. H., Sun-Waterhouse, D., … Idriss, H. (2013). Hydrogen production by Tuning the Photonic Band Gap with the Electronic Band Gap of TiO2. *Scientific Reports*, *3*, 2849. Retrieved from http://dx.doi.org/10.1038/srep02849

Wei, Z., Rosa, L., Wang, K., Endo, M., Juodkazis, S., Ohtani, B., & Kowalska, E. (2017). Size-controlled gold nanoparticles on octahedral anatase particles as efficient plasmonic photocatalyst. *APPLIED CATALYSIS B-ENVIRONMENTAL*, *206*, 393–405. http://doi.org/10.1016/j.apcatb.2017.01.043

Wong, Y. M., Wu, T. Y., & Juan, J. C. (2014). A review of sustainable hydrogen production using seed sludge via dark fermentation. *Renewable and Sustainable Energy Reviews*, *34*, 471–482. http://doi.org/10.1016/j.rser.2014.03.008

Xing, Z., Zong, X., Butburee, T., Pan, J., Bai, Y., & Wang, L. (2016). Nanohybrid materials of titania nanosheets and plasmonic gold nanoparticles for effective hydrogen evolution. *Applied Catalysis A: General*, *521*(Supplement C), 96–103. http://doi.org/https://doi.org/10.1016/j.apcata.2016.01.014

Xu, X., Jiang, E., Wang, M., & Xu, Y. (2015). Dry and steam reforming of biomass pyrolysis gas for rich hydrogen gas. *Biomass and Bioenergy*, *78*, 6–16. http://doi.org/10.1016/j.biombioe.2015.03.015

Xu, Y., & Xu, R. (2015). Nickel-based cocatalysts for photocatalytic hydrogen

production. *Applied Surface Science*, *351*, 779–793. http://doi.org/10.1016/j.apsusc.2015.05.171

Yan, H., Yang, J., Ma, G., Wu, G., Zong, X., Lei, Z., … Li, C. (2009). Visible-light-driven hydrogen production with extremely high quantum efficiency on Pt–PdS/CdS photocatalyst. *Journal of Catalysis*, *266*(2), 165–168. http://doi.org/10.1016/j.jcat.2009.06.024

Yan, Y., Cai, F., Song, Y., & Shi, W. (2013). InVO4 nanocrystal photocatalysts: Microwave-assisted synthesis and size-dependent activities of hydrogen production from water splitting under visible light. *Chemical Engineering Journal*, *233*, 1–7. http://doi.org/10.1016/j.cej.2013.06.121

Yan, Z., Yu, X., Zhang, Y., Jia, H., Sun, Z., & Du, P. (2014). Enhanced visible light-driven hydrogen production from water by a noble-metal-free system containing organic dye-sensitized titanium dioxide loaded with nickel hydroxide as the cocatalyst. *Applied Catalysis B: Environmental*, *160–161*, 173–178. http://doi.org/10.1016/j.apcatb.2014.05.017

Yang, J., Yan, H., Wang, X., Wen, F., Wang, Z., Fan, D., … Li, C. (2012). Roles of cocatalysts in Pt–PdS/CdS with exceptionally high quantum efficiency for photocatalytic hydrogen production. *Journal of Catalysis*, *290*, 151–157. http://doi.org/10.1016/j.jcat.2012.03.008

Yang, S., Wang, H., Yu, H., Zhang, S., Fang, Y., Zhang, S., & Peng, F. (2016). A facile fabrication of hierarchical Ag nanoparticles-decorated N-TiO2 with enhanced photocatalytic hydrogen production under solar light. *International Journal of Hydrogen Energy*. http://doi.org/10.1016/j.ijhydene.2015.12.190

YANG, Y., CHANG, C., & IDRISS, H. (2006). Photo-catalytic production of hydrogen form ethanol over M/TiO2 catalysts (M=Pd, Pt or Rh). *Applied Catalysis B: Environmental*, *67*(3–4), 217–222. http://doi.org/10.1016/j.apcatb.2006.05.007

Yang, Y., Liu, E., Dai, H., Kang, L., Wu, H., Fan, J., … Liu, H. (2014). Photocatalytic activity of Ag–TiO2-graphene ternary nanocomposites and application in hydrogen evolution by water splitting. *International Journal of Hydrogen Energy*, *39*(15), 7664–7671. http://doi.org/10.1016/j.ijhydene.2013.09.109

Yokoyama, D., Hashiguchi, H., Maeda, K., Minegishi, T., Takata, T., Abe, R., … Domen, K. (2011). Ta3N5 photoanodes for water splitting prepared by sputtering. *Thin Solid Films*, *519*(7), 2087–2092. http://doi.org/10.1016/j.tsf.2010.10.055

Zagrodnik, R., & Laniecki, M. (2015). The role of pH control on biohydrogen production by single stage hybrid dark- and photo-fermentation. *Bioresource Technology*, *194*, 187–95. http://doi.org/10.1016/j.biortech.2015.07.028

Zanella, R., Giorgio, S., Henry, C. R., Louis, C., Curie, M., Cedex, P., … Luminy, C. De. (2002). Alternative Methods for the Preparation of Gold Nanoparticles Supported on TiO2. *The Journal of Physical Chemistry B*, *106*(31), 7634–7642.

Zeng, K., & Zhang, D. (2010, June 1). Recent progress in alkaline water electrolysis for hydrogen production and applications. *Progress in Energy and Combustion Science*. Pergamon. http://doi.org/10.1016/j.pecs.2009.11.002

Zhang, B., Zhang, L., Yang, Z., Yan, Y., Pu, G., & Guo, M. (2015). Hydrogen-rich gas production from wet biomass steam gasification with CaO/MgO. *International Journal of Hydrogen Energy*, *40*(29), 8816–8823. http://doi.org/10.1016/j.ijhydene.2015.05.075

Zhang, F., Maeda, K., Takata, T., & Domen, K. (2011). Improvement of the photocatalytic hydrogen evolution activity of Sm2Ti2S2O5 under visible light by metal ion additives. *Journal of Catalysis*, *280*(1), 1–7. http://doi.org/10.1016/j.jcat.2011.01.027

Zhang, F., Maeda, K., Takata, T., Hisatomi, T., & Domen, K. (2012). Investigation of cocatalysts on silver-modified Sm2Ti2S2O5 photocatalyst for water reduction and oxidation under visible light irradiation. *Catalysis Today*, *185*(1), 253–258. http://doi.org/10.1016/j.cattod.2011.09.025

Zhang, Y., Ligthart, D. A. J. M., Quek, X.-Y., Gao, L., & Hensen, E. J. M. (2014). Influence of Rh nanoparticle size and composition on the photocatalytic water splitting performance of Rh/graphitic carbon nitride. *International Journal of Hydrogen Energy*, *39*(22), 11537–11546. http://doi.org/10.1016/j.ijhydene.2014.05.126

Zhang, Z., Wang, Y., Hu, J., Wu, Q., & Zhang, Q. (2015). Influence of mixing method and hydraulic retention time on hydrogen production through photo-fermentation with mixed strains. *International Journal of Hydrogen Energy*, *40*(20), 6521–6529. http://doi.org/10.1016/j.ijhydene.2015.03.118

Zhao, D., & Yang, C.-F. (2016). Recent advances in the TiO2/CdS nanocomposite used for photocatalytic hydrogen production and quantum-dot-sensitized solar cells. *Renewable and Sustainable Energy Reviews*, *54*, 1048–1059. http://doi.org/10.1016/j.rser.2015.10.100

Zhou, D., Ji, Z., Jiang, X., Dunphy, D. R., Brinker, J., & Keller, A. A. (2013). Influence of Material Properties on TiO2 Nanoparticle Agglomeration. *PLoS ONE*, *8*(11), e81239. Retrieved from http://www.plosone.org/article/info:doi/10.1371/journal.pone.0081239

ANNEX I. SUPPORTING INFORMATION FOR PAPER 1

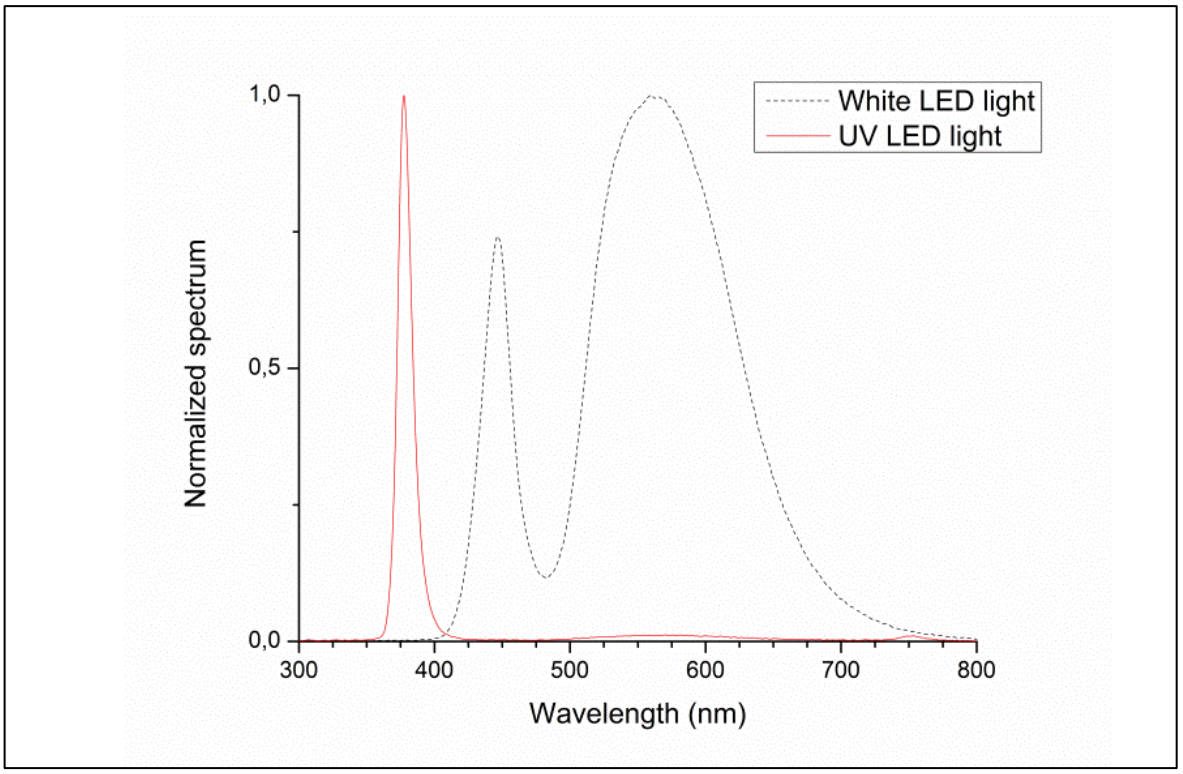

Figure - S 1: Measured emission spectrum for the light sources used in the photocatalytic reactor: UV-LED light with a peak on wavelength 378 nm (red and solid line) and cold-white visible LED light with its typical spectrum with peaks at 447 and 560 nm.

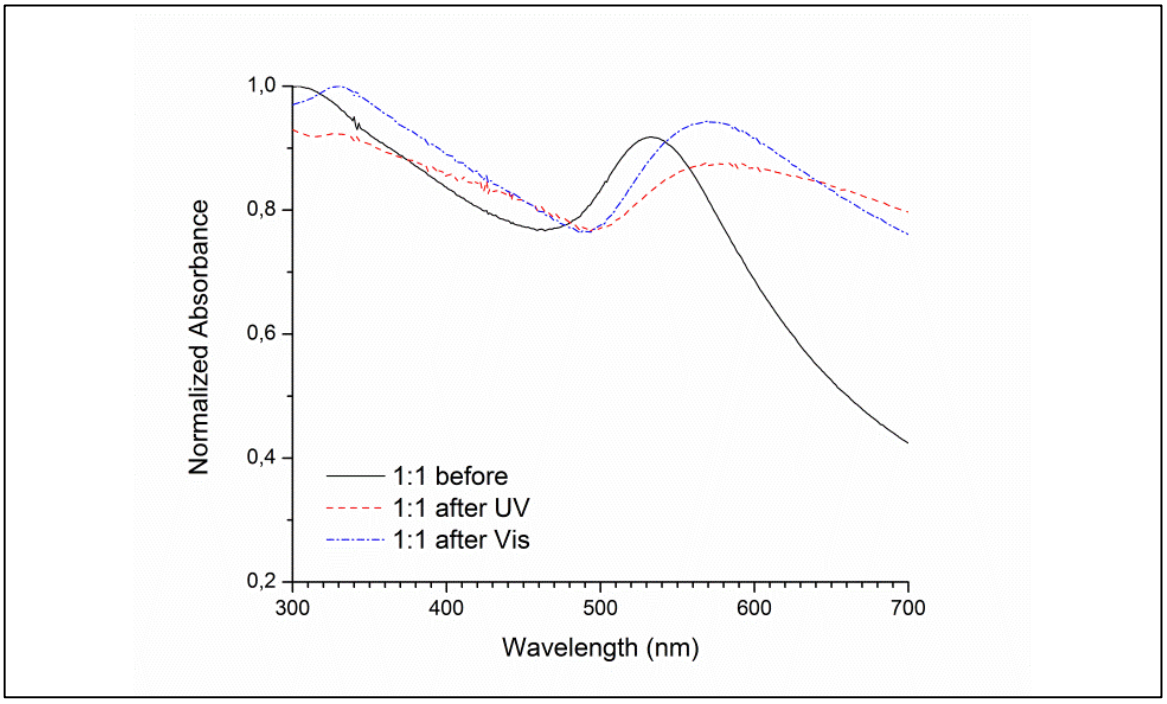

Figure - S 2: Normalized UV-visible absorption spectra of TiO_2-Au synthesized using molar ratio 1:1 ($[TiO_2]$=0,2 mM), before catalysis experiments, after catalysis using UV light, and after catalysis using white visible light. The spectrums after experiments show a small red-shift, moving the surface plasmon resonance peak from 530 to 580 nm. Catalysis with UV light shows a higher decrement in intensity, which could indicate signs of aggregation and degradation of gold nanoparticles.

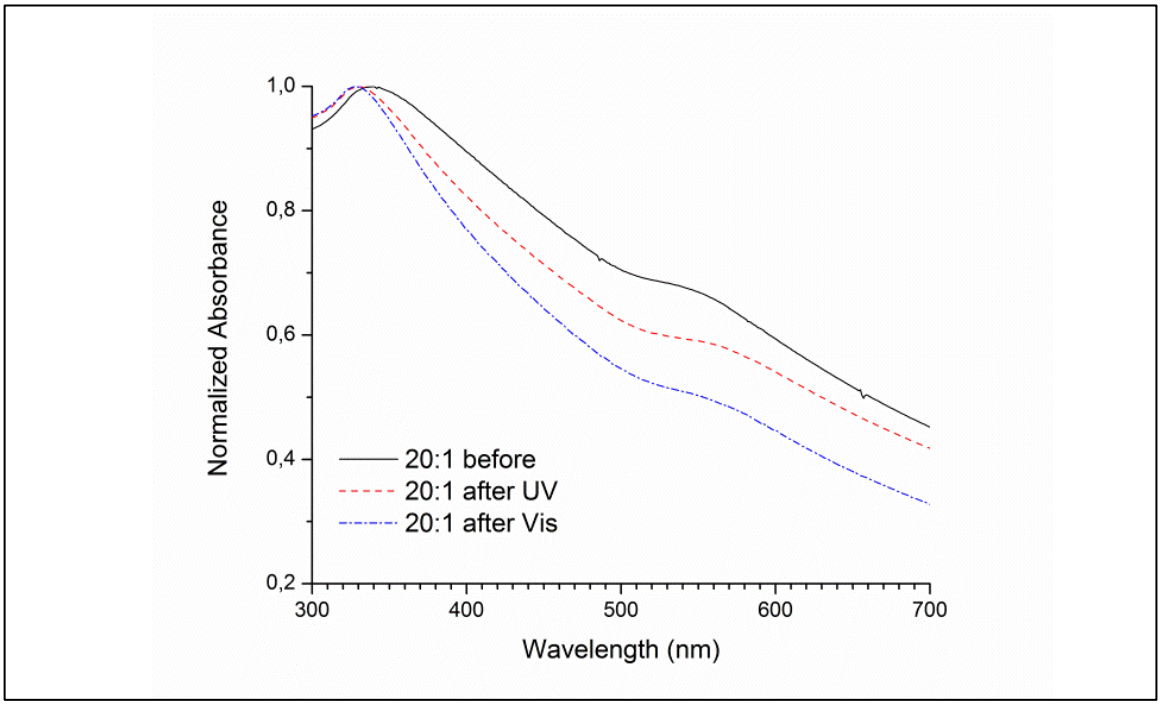

Figure - S 3: Normalized UV-visible absorption spectra of TiO_2-Au synthesized using molar ratio 20:1 ($[TiO_2]$=4 mM), before catalysis experiments, after catalysis using UV light, and after catalysis using white visible light. As in Figure-S2, for both types of light, the spectre after experiments shows a red-shift, moving the surface plasmon resonance peak from 530 to 550 nm. Catalysis with UV light and visible light show signs of aggregation and degradation.

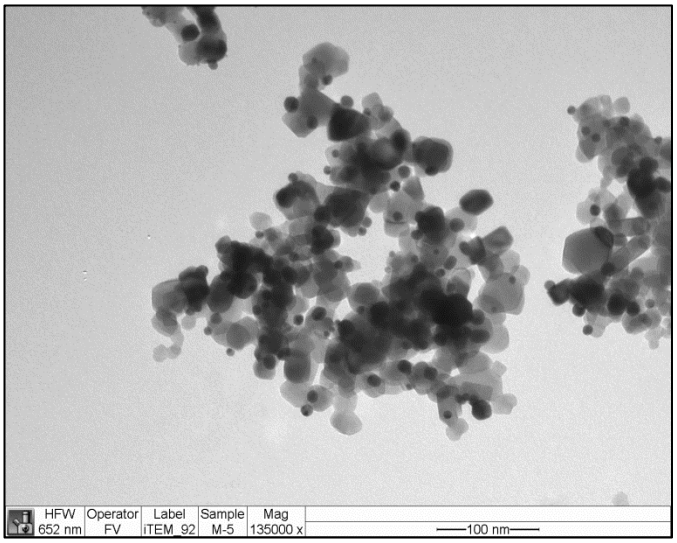

Figure - S 4: TEM image for TiO_2-Au synthetized using a molar ratio [TiO_2]:[Au] 1:1 in low volumes (100 mL) of colloid, before the catalysis

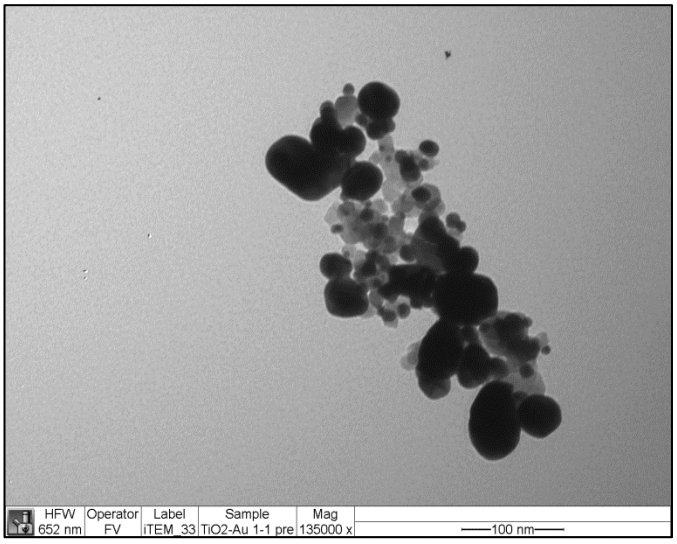

Figure - S 5: TEM image for TiO_2-Au synthetized using a molar ratio [TiO_2]:[Au] 1:1 in high volume (500 mL) of colloid, before the catalysis

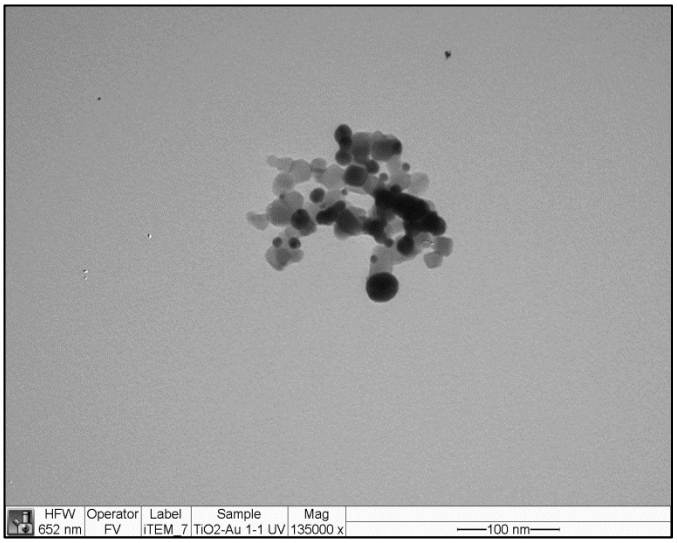

Figure - S 6: TEM image for TiO_2-Au synthetized using a molar ratio [TiO_2]:[Au] 1:1 in high volume (500 mL) of colloid, after 6 hours of catalysis under UV light

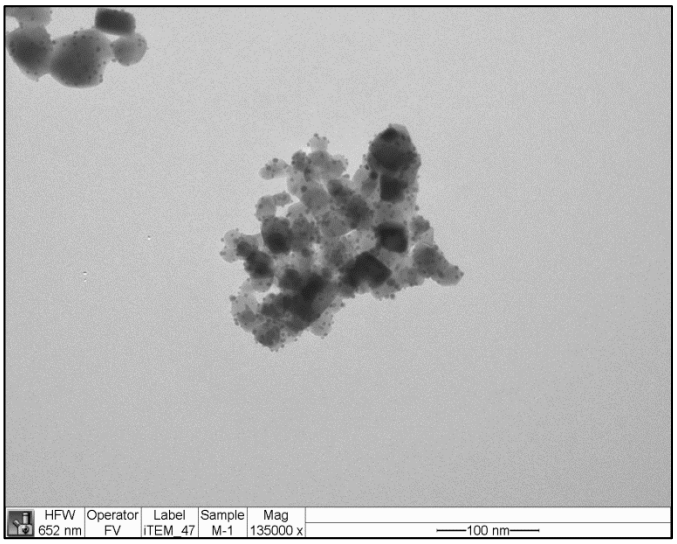

Figure - S 7: TEM image for TiO_2-Au synthetized using a molar ratio [TiO_2]:[Au] 20:1 in low volumes (100 mL) of colloid, before the catalysis

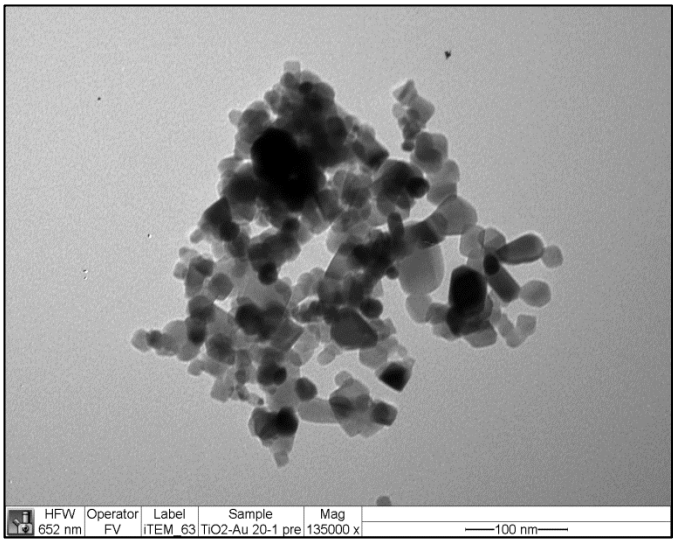

Figure - S 8: TEM image for TiO_2-Au synthetized using a molar ratio [TiO_2]:[Au] 20:1 in high volume (500 mL) of colloid, before the catalysis

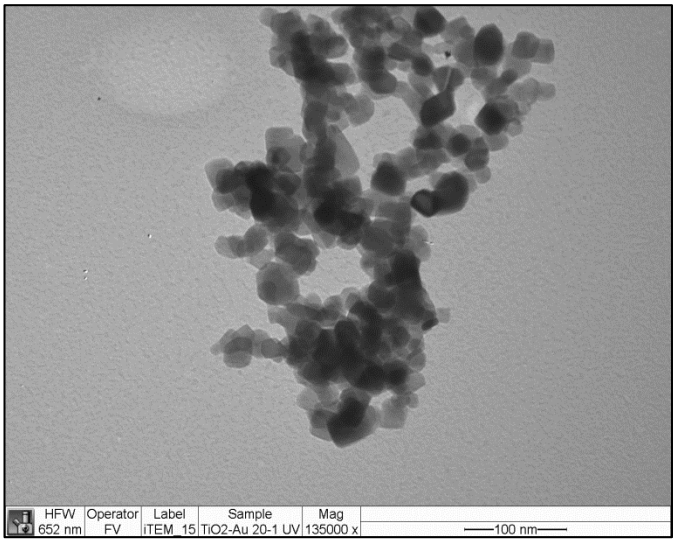

Figure - S 9: TEM image for TiO_2-Au synthetized using a molar ratio [TiO_2]:[Au] 20:1 in high volume (500 mL) of colloid, after 6 hours of catalysis under UV light

Photocatalytic hydrogen production: Formulas and calculations

- **Rate of hydrogen generation (v_{H_2})**

$$v_{H_2} = \frac{N_{H_2}}{\Delta t} = \frac{140.91\ \mu mol}{6\ h} = 23.5\ \mu mol \cdot h^{-1}$$

Where:

N_{H_2}: Total amount of hydrogen produced in time Δt (μmol)

Δt: Reaction time (h)

- **Estimated reaction rate (r_{H_2})**

$$r_{H_2} = \frac{v_{H_2}}{vol} = \frac{23.5\ \mu mol \cdot h^{-1}}{63\ mL} = 372.9\ \mu mol \cdot L^{-1} \cdot h^{-1}$$

Where:

vol: Liquid volume of reaction (mL)

- **Mass productivity of the catalyst or turnover rate ($p_{cat,m}$)**

$$p_{cat,m} = \frac{v_{H_2}}{C_{cat} \cdot vol} = \frac{23.5\ \mu mol \cdot h^{-1}}{0.056\ g \cdot L^{-1} \cdot 63\ mL} = 6661\ \mu mol \cdot h^{-1} \cdot g^{-1}$$

Where:

C_{cat}: Concentration of catalyst in reactor volume ($g \cdot L^{-1}$)

- **Molar productivity of methanol ($p_{OH,M}$)**

$$p_{OH,M} = \frac{v_{H_2}}{M_{OH} \cdot vol} = \frac{23.5\ \mu mol \cdot h^{-1}}{1.2\ M \cdot 63\ mL} = 311\ \mu mol \cdot h^{-1} \cdot mol^{-1}$$

Where:

M_{OH}: Concentration of methanol (M)

- **Overall energy conversion efficiency (e)**

$$e = \frac{energy_{H_2,out}}{energy_{light,in}} = \frac{v_{H_2} \cdot HHV_{H_2}}{I \cdot A \cdot (1-\alpha)} = \frac{23.5\ \mu mol \cdot h^{-1} \cdot 285.8\ kJ \cdot mol^{-1}}{20\ mW \cdot cm^{-2} \cdot 22\ cm^2 \cdot (1-0.09)} \cdot 100\% = 0.46\%$$

Where:

HHV_{H_2}: Higher heating value of hydrogen ($kJ \cdot mol^{-1}$)

$\boldsymbol{I}$: Intensity of light supplied to the reactor ($\boldsymbol{mW \cdot cm^{-2}}$)

$\boldsymbol{A}$: Illuminated surface ($\boldsymbol{cm^2}$)

$\boldsymbol{\alpha}$: Reflective fraction for borosilicate (0.09)

- **Apparent quantum yield ($\boldsymbol{AQY}$)**

$$\boldsymbol{AQY = \frac{2 \cdot N_{H_2,out}}{N_{photons,in}} = \frac{2 \cdot v_{H_2}}{\frac{I \cdot A \cdot (1-\alpha)}{e_{375nm} \cdot N_A}} = \frac{2 \cdot 23.5\ \mu mol \cdot h^{-1}}{\frac{20\ mW \cdot cm^{-2} \cdot 22\ cm^2 \cdot (1-0,09)}{5.29719 \cdot 10^{-19} J \cdot 6.022141 \cdot 10^{23} mol^{-1}}} \cdot 100\% = 1.03\%}$$

Where:

$\boldsymbol{N_{H_2,out}}$: mole dihydrogen produced

$\boldsymbol{N_{photons,in}}$: mole of incident photons

$\boldsymbol{e_{375nm}}$: Energy in a photon with wavelength 375 nm ($\boldsymbol{J}$)

$\boldsymbol{N_A}$: Avogadro constant ($\boldsymbol{mol^{-1}}$)

ANNEX II. SUPPORTING INFORMATION FOR PAPER 2

Figure - S 10. Individual value plots with the raw data behind the main effects plots of total hydrogen generation (H) for each factor under analysis.

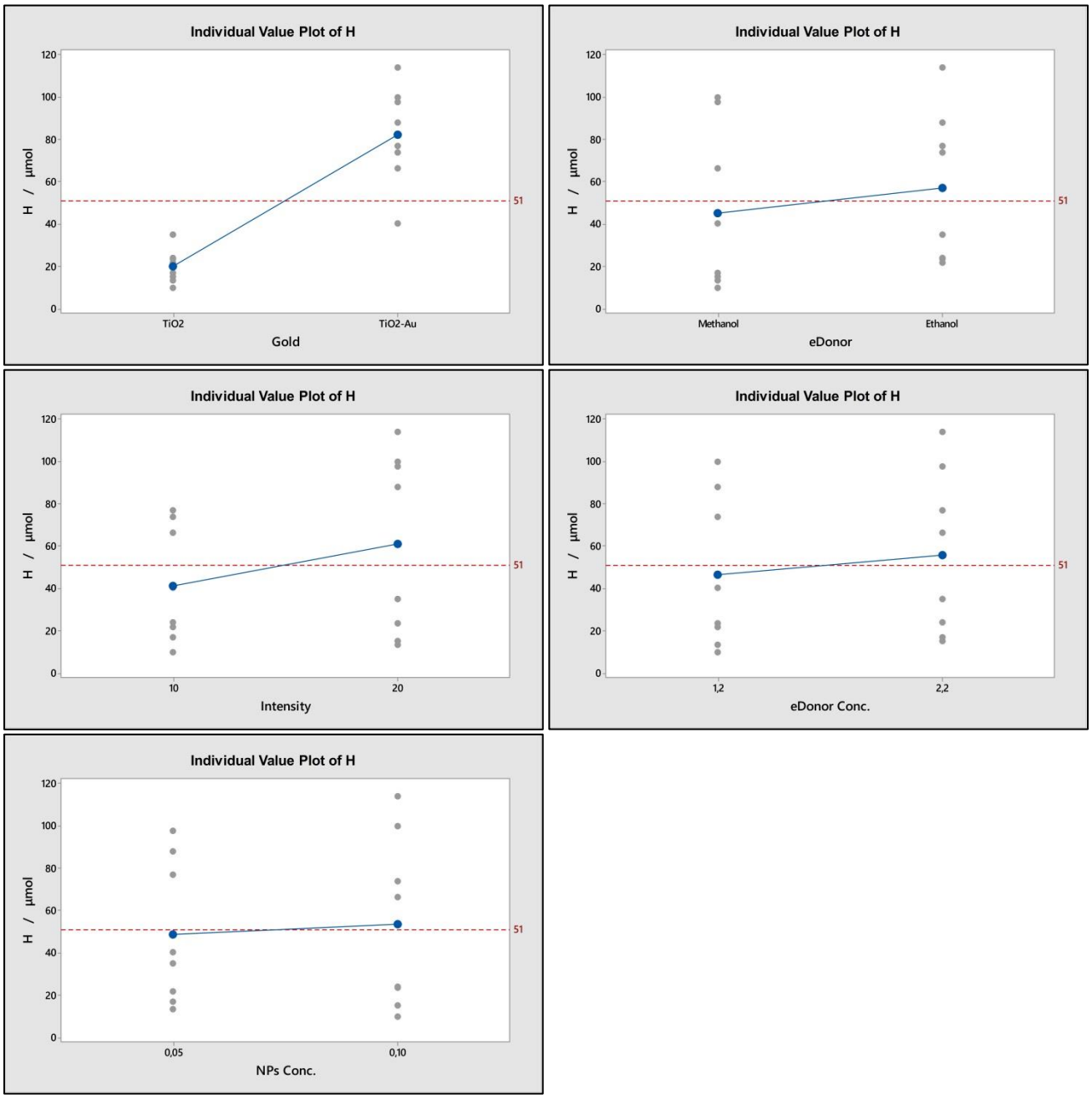

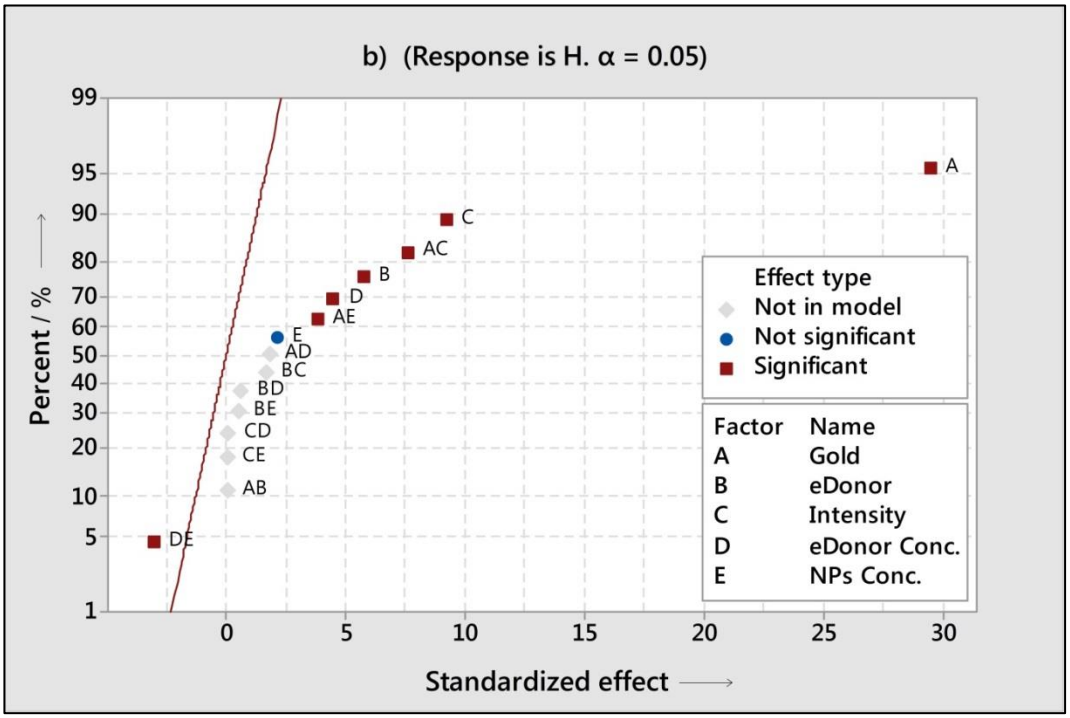

Figure - S 11. Normal plot of the standardized effects for the reduced model of H.

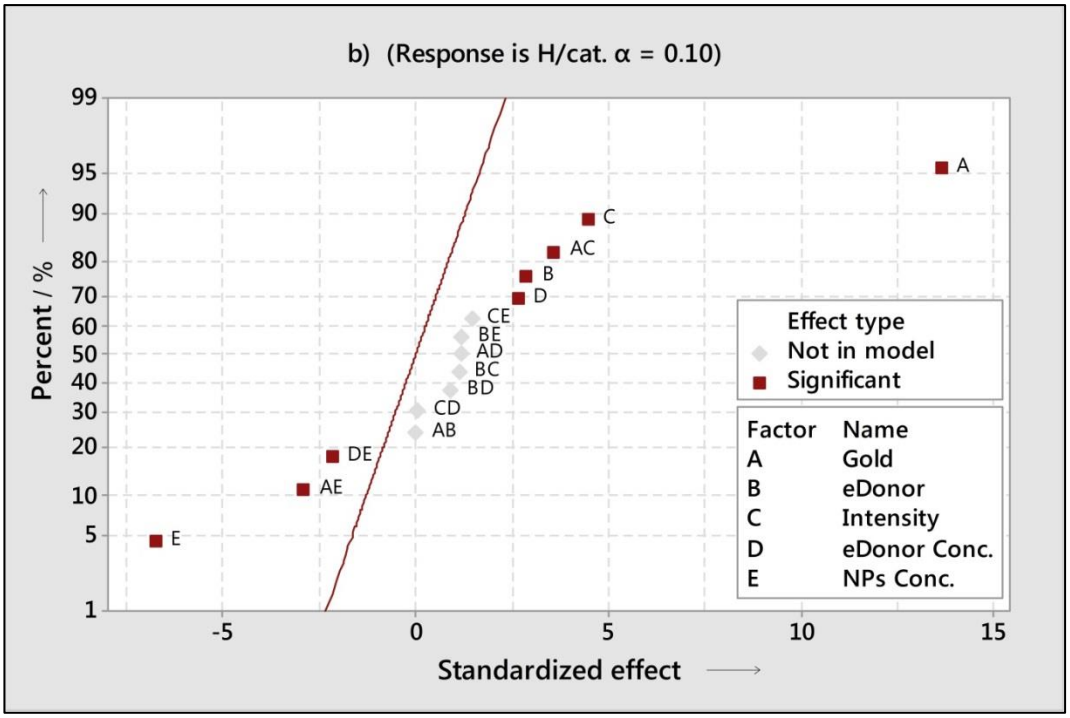

Figure - S 12.Normal plot of the standardized effects for the reduced model of H/cat.

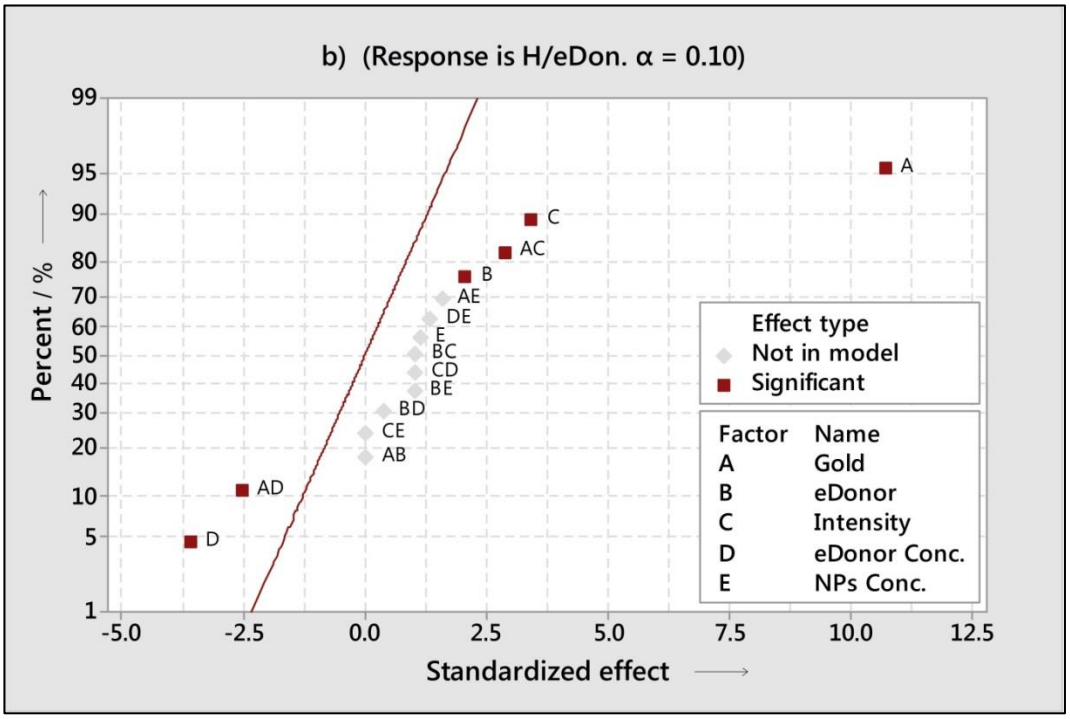

Figure - S 13. Normal plot of the standardized effects for the reduced model of H/eDon.

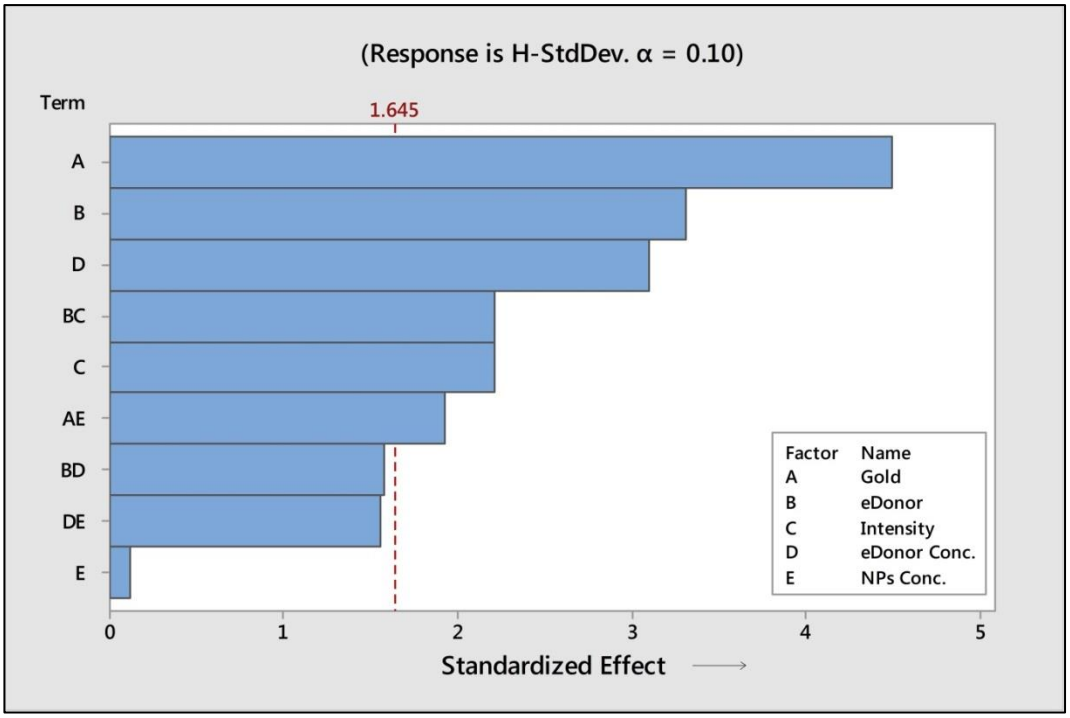

Figure - S 14. Pareto chart of the standardized effects for the variability of H.

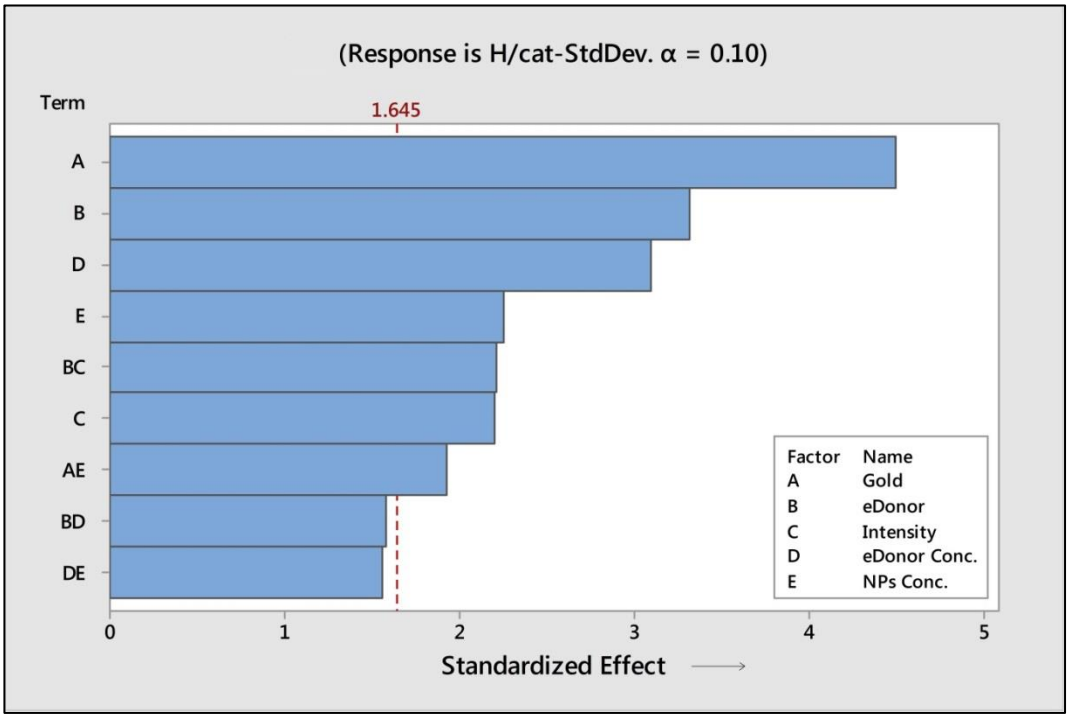

Figure - S 15. Pareto chart of the standardized effects for the variability of H/cat.

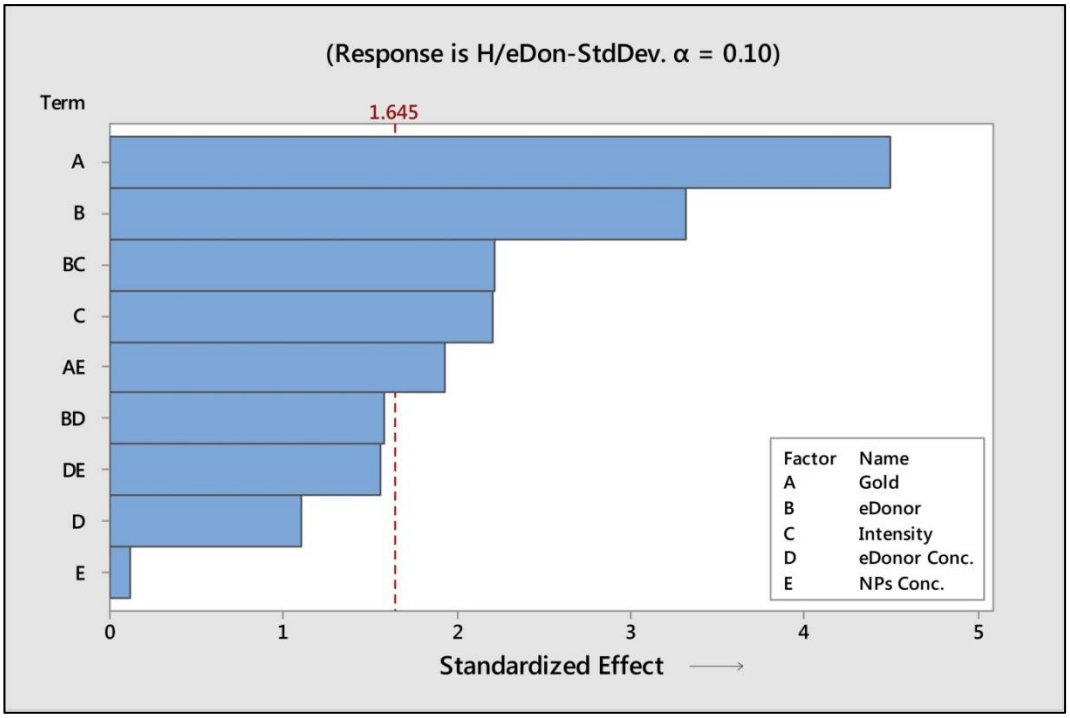

Figure - S 16. Pareto chart of the standardized effects for the variability of H/eDon.

ANNEX III. SUPPORTING INFORMATION FOR PAPER 3

Figure - S 17. Individual value plots with the raw data behind the main effects plots of total formaldehyde generation (F) for each factor under analysis.

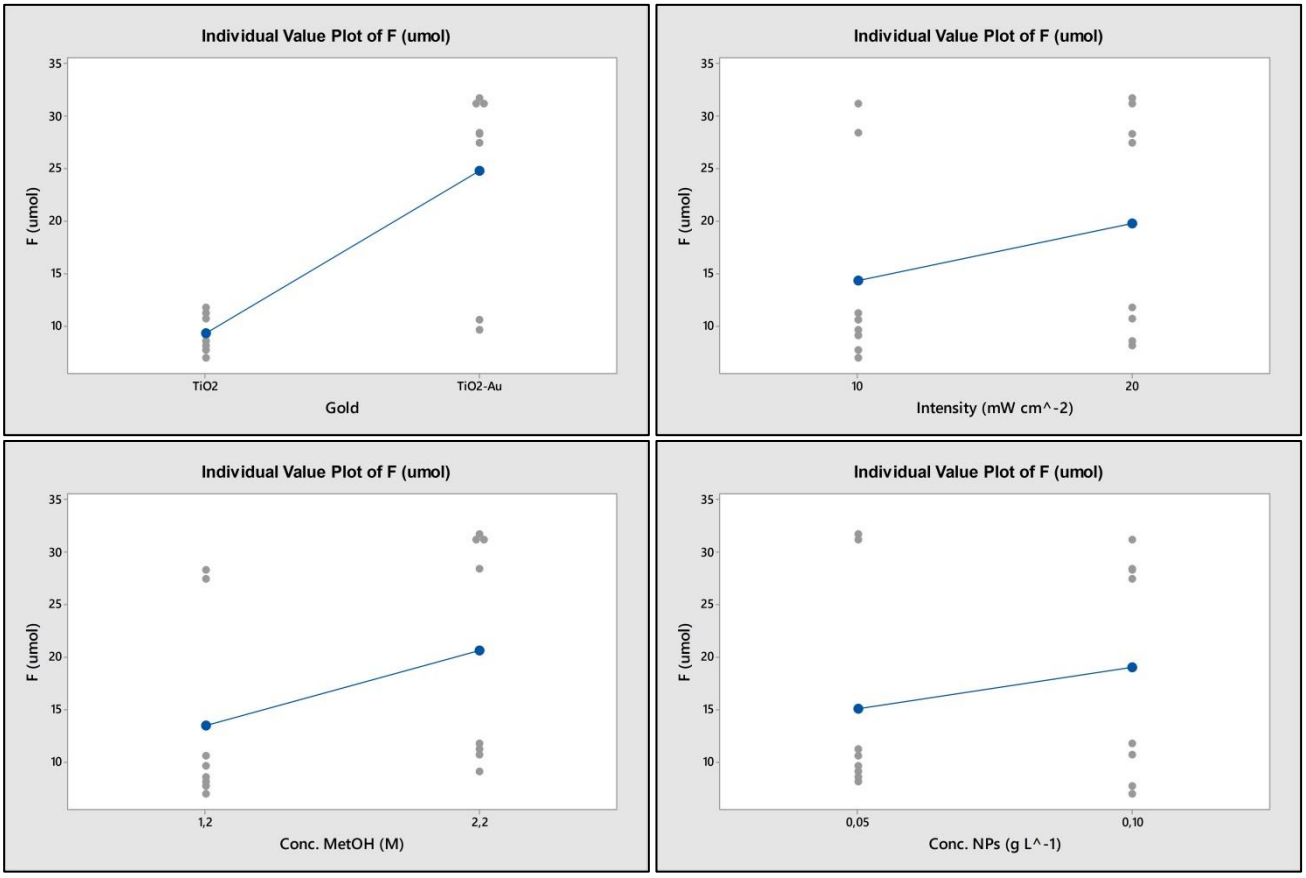

Figure - S 18. Individual value plots with the raw data behind the main effects plots of catalyst productivity of formaldehyde (F/cat) for each factor under analysis.

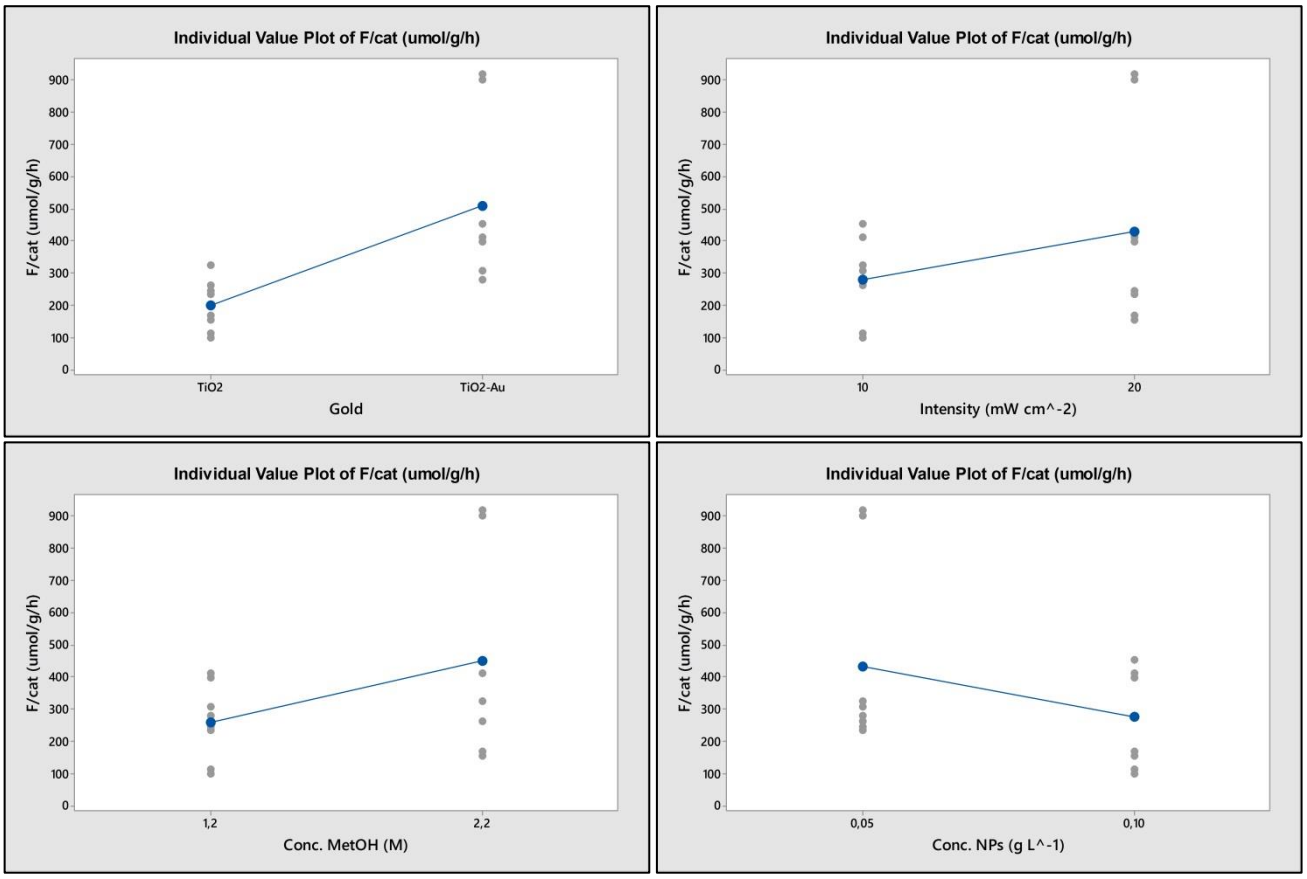

Figure - S 19. Individual value plots with the raw data behind the main effects plots of total formic acid generation (FA) for each factor under analysis.

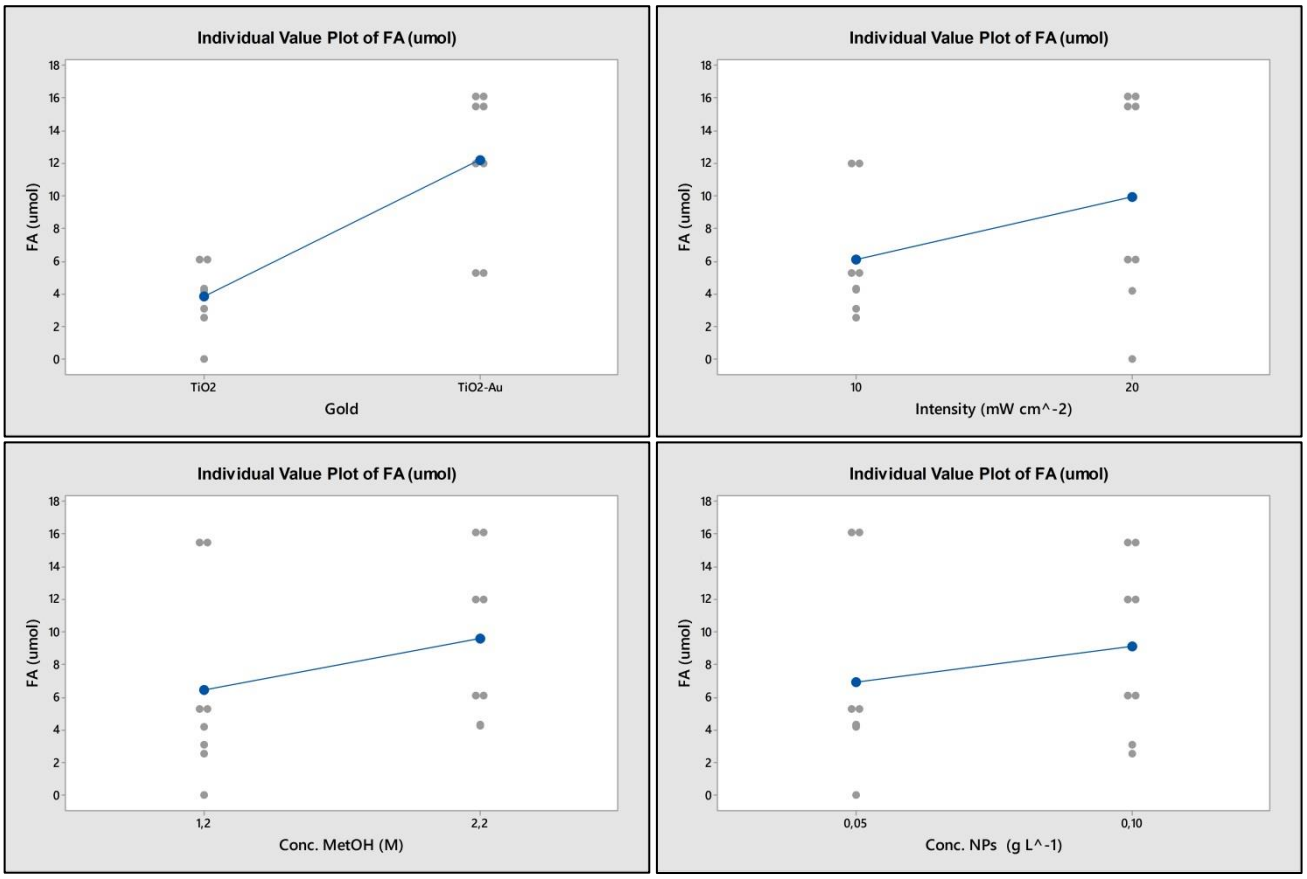

Figure - S 20. Individual value plots with the raw data behind the main effects plots of catalyst productivity of formic acid (FA/cat) for each factor under analysis.